# Millimeter-Wave Quasi-Optical and Spatial Power Combining Techniques

Final Report

by

Kai Chang



August 10, 1992

U. S. Army Research Office

Contract No.: DAAL03-89-K-0085

Department of Electrical Engineering

Texas A & M University

College Station, Texas 77843-3128

APPROVED FOR PUBLIC RELEASE;
DISTRIBUTION UNLIMITED



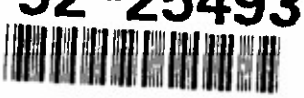

# Millimeter-Wave Quasi-Optical and Spatial Power Combining Techniques

Final Report

by

Kai Chang

August 10, 1992

U. S. Army Research Office

Contract No.: DAAL03-89-K-0085

Department of Electrical Engineering

Texas A & M University

College Station, Texas 77843-3128

# REPORT DOCUMENTATION PAGE

Form Approved
OMB No. 0704-0188



| 1. AGENCY USE ONLY (Leave blank) | 2. REPORT DATE | 3. REPORT TYPE AND DATES COVERED |
|---|---|---|
| | August 10, 1992 | |

**4. TITLE AND SUBTITLE**
Millimeter-Wave Quasi-Optical and Spatial Power Combining Techniques

**5. FUNDING NUMBERS**

**6. AUTHOR(S)**
Kai Chang

**7. PERFORMING ORGANIZATION NAME(S) AND ADDRESS(ES)**
Department of Electrical Engineering
Texas A&M University
College Station, Texas 77843-3128

**8. PERFORMING ORGANIZATION REPORT NUMBER**

**9. SPONSORING/MONITORING AGENCY NAME(S) AND ADDRESS(ES)**
U. S. Army Research Office
P. O. Box 12211
Research Triangle Park, NC 27709-2211

**10. SPONSORING/MONITORING AGENCY REPORT NUMBER**

**11. SUPPLEMENTARY NOTES**
The view, opinions and/or findings contained in this report are those of the author(s) and should not be construed as an official Department of the Army position, policy, or decision, unless so designated by other documentation.

**12a. DISTRIBUTION/AVAILABILITY STATEMENT**
Approved for public release; distribution unlimited.

**12b. DISTRIBUTION CODE**

**13. ABSTRACT** (Maximum 200 words)

This report summarizes the research activities carried out in Electromagnetics and Microwave Laboratory, Department of Electrical Engineering, Texas A&M University. The project was sponsored by the U.S. Army Research Office under contract No. DAAL03-89-K-0085. The topics of investigation included active antenna elements, spatial power combining and injection-locking, quasi-optical components, novel planar slot-line and coplanar waveguide circuits, and other circuit developments and analyses. A list of publications and a report of invention are included.

**14. SUBJECT TERMS**
Quasi-Optical Techniques, Microwaves, Millimeter-Waves, Power Combining, Active Antennas

**15. NUMBER OF PAGES**
65

**16. PRICE CODE**

| 17. SECURITY CLASSIFICATION OF REPORT | 18. SECURITY CLASSIFICATION | 19. SECURITY CLASSIFICATION OF ABSTRACT | 20. LIMITATION OF ABSTRACT |
|---|---|---|---|
| UNCLASSIFIED | UNCLASSIFIED | UNCLASSIFIED | UL |

NSN 7540-01-280-5500

Standard Form 298 (Rev 2-89)
Prescribed by ANSI Std 239-18
298-102

# Millimeter-Wave Quasi-Optical and Spatial Power Combining Techniques

Final Report

by

Kai Chang

August 10, 1992

U. S. Army Research Office

Contract No.: DAAL03-89-K-0085

Department of Electrical Engineering

Texas A & M University

College Station, Texas 77843-3128

# FOREWORD

This report summarizes the research activities carried out in the Electromagnetics and Microwave Laboratory, Department of Electrical Engineering, Texas A & M University. The project was sponsored by the U.S. Army Research Office under contract No. DAAL03-89-K-0085. The period of performance was from April 1, 1989 through June 30, 1992. The topics of investigation included active antenna elements, spatial power combining and injection-locking, quasi-optical components, novel planar slotline and coplanar waveguide circuits, and other circuit developments and analyses.

## Table of Contents

Page

## 1. Introduction and Problems Studied

For the past decade, microwave/millimeter-wave activities have been accelerating for both civil and military applications including telecommunications, radar, sensors, seekers, navigation, remote sensing, electronic warfare and space technology. These applications have created the urgent need for low cost, high performance solid-state integrated systems using planar integrated circuit technology. These integrated systems normally consist of high power transmitters, low noise receivers, antennas, and control devices. To lower the losses and cost, quasi-optical technique is attractive for millimeter-wave frequencies. In many applications, frequency agility is required, and electronic tunability of the system is desirable. The output power from a single active solid-state device is limited by fundamental thermal and impedance problems. To meet the high power requirements for many applications, it is necessary to combine many devices to achieve high power output.

Combining power from many active devices is a difficult task at millimeter-wave frequencies due to the moding and size problems [1]. The maximum number of devices that can be combined in a conventional resonant or hybrid-coupled power combiner decreases as the operating frequency is increased. To overcome these problems, spatial and quasi-optical power combining techniques have been proposed to combine power in free space at high frequencies [2]. In these combiners, the active device is integrated with a radiating element to form an active element. Many of these active elements are then combined in free space or in an open resonator. For efficient power combining, all source elements must be coherent in phase and frequency. Injection-locking through open resonator, space or mutual coupling can be used to achieve the coherency.

In addition to application in active antenna elements and power combiners, quasi-optical techniques can be used for filters, receivers, detector or imaging arrays, power conversion arrays, etc. The techniques are especially attractive for millimeter-wave frequencies due to the advantages of low cost, large size and good performance. Several quasi-optical components were developed with excellence performance under this project.

Along with the research of the quasi-optical components and spatial power combining techniques, work was also carried out on the novel planar slotline and coplanar waveguide

circuit developments. The slotline and coplanar waveguide have the center conductor and ground planes on the same side of the substrate. They are truly uniplanar microwave integrated circuits that have advantage of easy implementation of solid-state devices.

Although most of our experimental work was concentrated at microwave frequencies, the circuits and analyses developed can be applied to millimeter-waves. The problems studied and major accomplishments made are summarized below:

1. A single active radiating element with a Gunn diode mounted directly on the microstrip path antenna has been developed with over 9 percent electronic tuning range.
2. A spatial power combiner has been demonstrated in free space with over 90 percent combining efficiency using two directly integrated Gunn-patch antenna elements.
3. A spatial power combiner has been demonstrated using two aperture coupled microstrip antenna elements.
4. Injection-locking has been achieved for spatial power combiners through space and mutual coupling.
5. An active radiating element using an FET source integrated with a microstrip patch antenna has been developed.
6. Active planar notch antenna elements were invented with a wide electronic tuning bandwidth. A power output of 14.5 $\pm$ 0.8 dBm over a tuning range from 8.9 to 10.2 GHz was achieved. This is equivalent to 14 percent of electronic tuning bandwidth. The circuit is small and can be fabricated at low cost.
7. Power combining of two varactor-tuned active notch antenna elements has achieved over 70% combining efficiency through the 14% tuning range. This is the first varactor tunable power combiner ever reported.
8. An integrated active antenna using annular ring microstrip antenna and Gunn diode was demonstrated with over 70 mW output power at 7 GHz.
9. An integrated image-line steerable active antenna was demonstrated with a 2 percent electronic tuning range corresponding to a frequency steerable range of 4 degrees.
10. A quasi-optical rectifying antenna was developed at 35 GHz with over 39 percent RF to DC conversion efficiency. The device was designed as a large-signal detector.

11. A quasi-optical filter was used to reduce the second harmonic radiation of the rectifying antenna.
12. A low loss quasi-optical open resonator filter was devised using a Fabry-Perot resonator and a narrow slot opening in the coupling waveguide. The filter has an insertion loss of less than 1 dB and should have applications in many millimeter-wave and submillimeter-wave systems.
13. Electronically switchable and tunable coplanar waveguide-slotline bandpass filters were invented with over 20% electronic tuning range. These active filters should have many applications in radar, communications and EW systems.
14. A novel varactor tunable coplanar waveguide Gunn VCO was invented with 300 MHz tuning range at 10 GHz. The circuit is small, lightweight and offers low cost, good reproducibility and excellent performance.
15. A coplanar waveguide fed slotline ring resonator was invented using varactor diodes to create an electronically tunable planar resonator and filter. The resonator has over 23% tuning range and 4.5 $\pm$ 1.5 dB of insertion loss.
16. A multiple dielectric structure was studied for conductor-backed coplanar waveguide to suppress the leakage effects.
17. A simple microstrip to dielectric waveguide transistion has been developed with an insertion loss of less than 1 dB.
18. An optimum dielectric overlay thickness was found for achieving the equal even- and odd- mode phase velocities in coupled microstrip lines. A theoretical analysis based on variational method was developed.
19. An analysis was developed to calculate the susceptance due to a wide inductive strip and a wide resonant strip. The theory was based on a variational method and moment method.
20. A novel resistance measurement technique was devised to characterize high-temperature superconducting materials at microwave frequencies. The method uses a floating resonant strip and the measurement agree very well with the theoretical prediction. The technique can be used for both bulk and thin-film materials.
21. A simple low cost microwave/millimeter-wave impedance measuring technique using

a three-probe microstrip circuit was developed. The method provides good accuracy and ease of calibration.

## 2. Active Antenna Elements

In an active antenna, an active solid-state device is directly integrated with a planar antenna. The circuit can be used as a low cost, small transmitter. Many of these elements can be aligned to form a spatial or quasi-optical power combiner. Under this project, we have developed active antenna elements using path, notch, annular ring, and image-line antennas. The solid-state devices used were Gunn devices and FETs.

### 2.1 Active Patch Antenna Elements

A Gunn diode was integrated with a patch antenna as shown in Figure 1. The placement D of the active device was chosen as such that the device impedance was matched to the input impedance of the patch. The output power was calculated using Friis transmission equation.

At X-band, a 3 dB tuning range of 839 MHz was achieved from 9.278 to 10.117 GHz using bias tuning. This tuning range is equivalent to a 9 percent bandwidth, which is much wider than that of a single passive patch. The results are summarized in the literature [3] (See Appendix 1).

Integration of an FET device with a patch antenna was also demonstrated earlier [4]. The circuit is shown in Figure 2. The circuit consists of a patch antenna, an FET, and matching and bias circuits. The oscillator is formed by placing a frequency selective network, such as a resonator which is a patch antenna, in the feedback loop of an amplifier. If the feedback is positive at the operating frequency, oscillation occurs. The patch acts as both a resonator and radiator.

### 2.2 Active Notch Antennas

The use of a notch antenna has many advantages of broad bandwidth, beamwidth design flexibility, relative high gain, and easy active device integration. Figure 3 shows the varactor-tunable active notch antenna integrated witn a Gunn diode [5]. The circuit exhibits a tuning bandwidth from 8.9 to 10.2 GHz with an output power of 14.5 $\pm$ 0.8

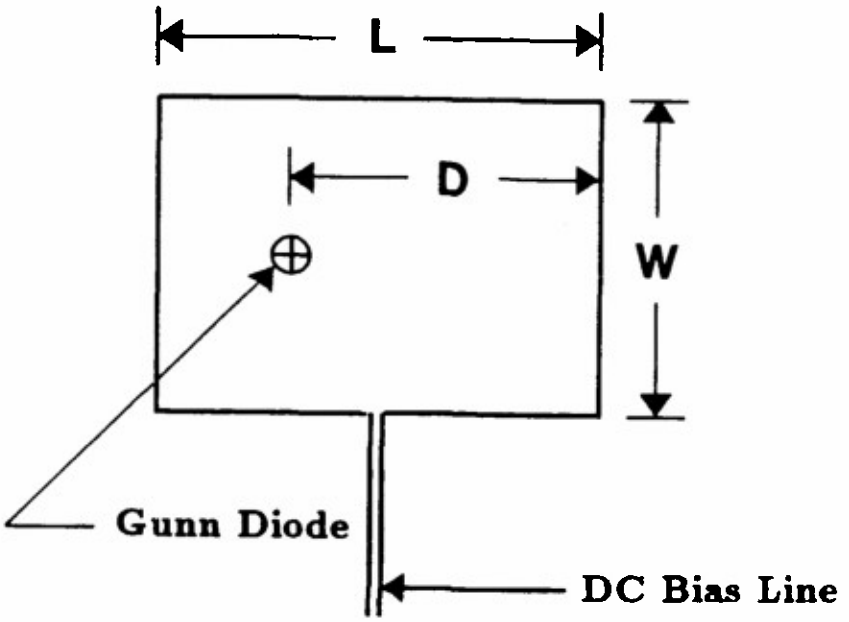


Figure 1. An active patch antenna integrated with a Gunn device

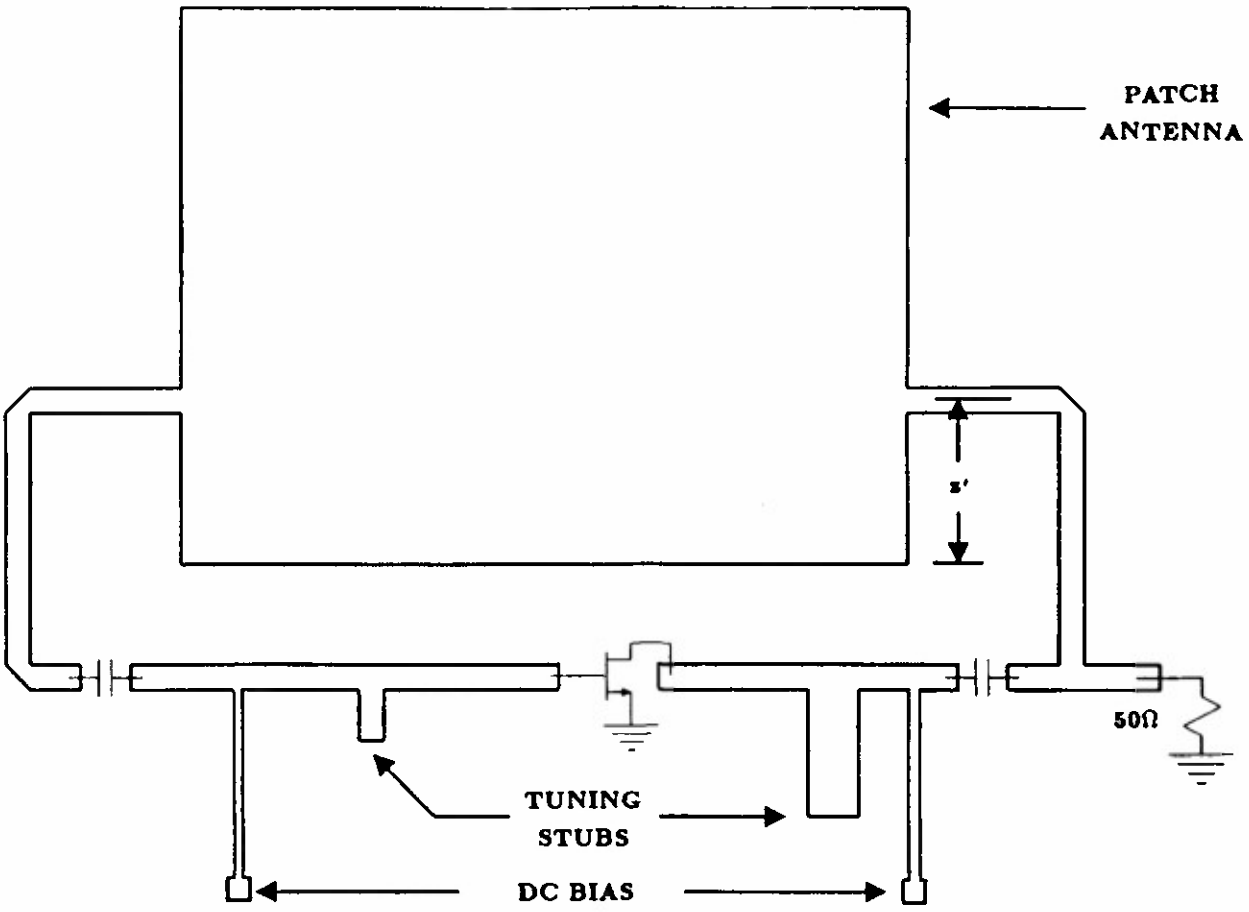


Figure 2. An active patch antenna integrated with an FET device

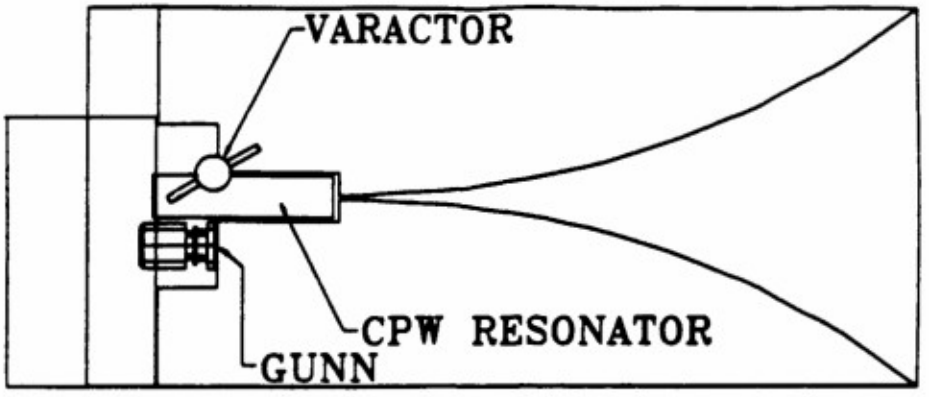


Figure 3. An active notch antenna integrated with a Gunn VCO

dBm. This is equivalent to over 14% tuning bandwidth. The results are given in the literature [5] (See Appendix 2).

### 2.3 Active Annular Ring Microstrip Antennas

The use of an annular ring antenna integrated with a Gunn device was investigated [6]. The circuit is shown in Figure 4. A computer program based on theoretical analysis was used to determined the placement location of the Gunn diode for optimum impedance matching. A passive ring was first built and tested to verify the design procedure. Injection-locking the active antenna was achieved using an external source.

### 2.4 Active Image-Line Antennas

At high frequencies (above 100 GHz), conductor losses become notable and microstrip circuits become so small that using microstrip is difficult. To overcome the radiative and conductor losses, an active image-line grating antenna was proposed. A Gunn diode was placed in an image-line grating antenna with a resonant cap as shown in Figure 5 [7]. A varactor was placed between the Gunn and the shorted end of the oscillator, as close as possible to the Gunn. The varactor gave 1% tuning bandwidth which corresponds to a 4 degrees beam scanning.

## 3. Spatial Power Combining and Injection-Locking

The spatial power combiner utilizes the correct phase relationship of many radiating elements to combine power in free space. For efficient combining, all the source elements must be coherent in phase and frequency. Injection-locking technique can be used for frequency alignment. Feasibility of injection-locking and power combining of using a two-element array has been established.

### 3.1 Combiners Using Active Patch Antenna Elements

Figure 6 shows a two-element power combiner. The two active devices in the two-element array injection-locked each other through mutual coupling. Injection-locking could also be achieved using an external source. A combining efficiency of over 90 percent has been successfully demonstrated [1] (See Appendix 1).

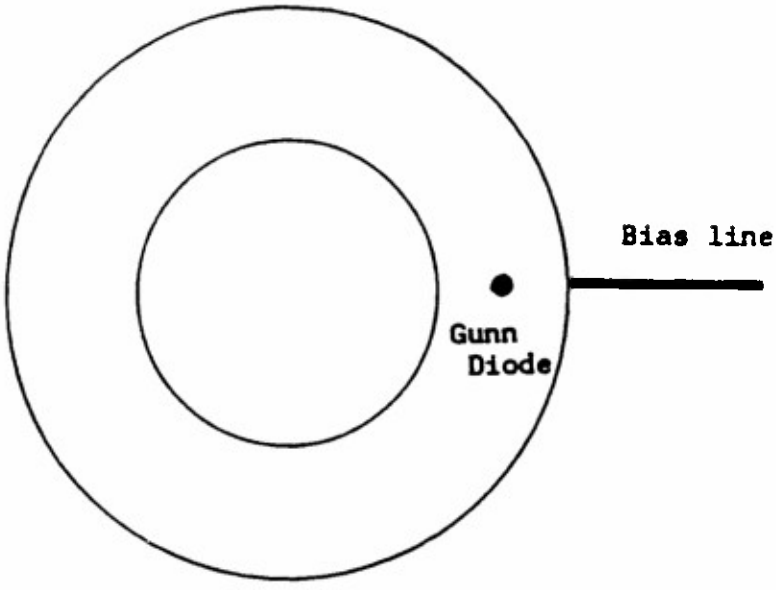


Figure 4. An active annular ring antenna integrated with a Gunn device

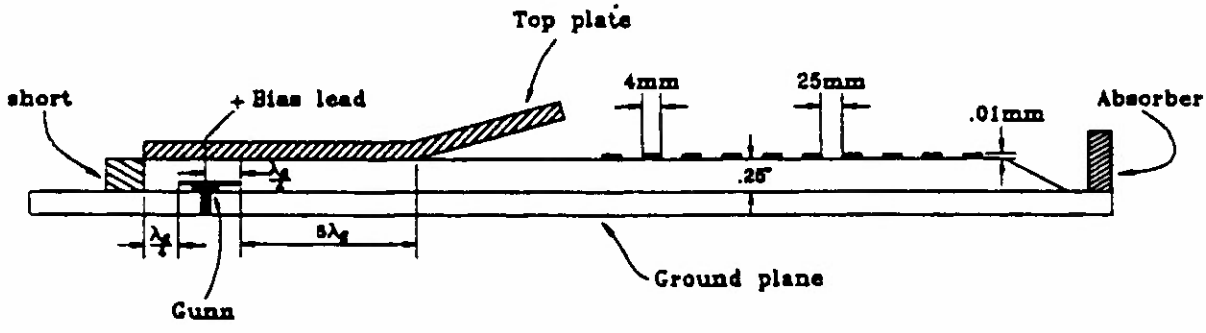


Figure 5. An active image-line grating antenna integrated with a Gunn VCO

### 3.2 Combiners Using Active Notch Antenna Elements

To demonstrate the feasibility of broadband, tunable power combiners, two active notch antennas were set up in a broadside array at $\lambda/4$ separation. The active notch antenna elements were injection-locked to each other through mutual coupling. Power combining experiments of two injection-locked, varactor-tuned active notch antennas were conducted throughout the electronic tuning range at 100 MHz increment over a 1.3 GHz bandwidth at X-band. All power calculations were based on the Friis Transmission Equation. The increase in gain of the notch and the array beam sharpening has been included in the calculation. Over 70% combining efficiency was observed throughout the varactor tuning range. These results represent the first varactor-tunable power combiner over a wide tuning range reported in literature [5] (See Appendix 2).

A four-element and a sixteen-element array using FETs are currently under development. Preliminary results showed good combining efficiency.

## 4. Quasi-Optical Components

Many components can be built using quasi-optical techniques. At millimeter-wave frequencies (above 100 GHz), the quasi-optical components have many advantages of low cost, low losses, high performance, and ease of fabrication.

Under this project, several useful quasi-optical components have been developed. These include a 35 GHz rectifying antenna, a frequency selective surface filter, and a low loss Fabry-Perot resonator.

### 4.1 35 GHz Rectifying Antenna

A quasi-optical rectifying antenna (rectenna) converts the RF power into DC power. It could be used in microwave power transmission or in microwave imaging array.

The basic structure of a rectenna is shown in Fig 7. The low pass filter inserted between the antenna and rectifying circuit is designed so that the fundamental frequency can be passed and a significant portion of the higher order harmonics generated from the nonlinear rectifying circuit be rejected back to the rectifying circuit. The rectifying circuit consists of an single diode shunt-connected across the transmission lines.

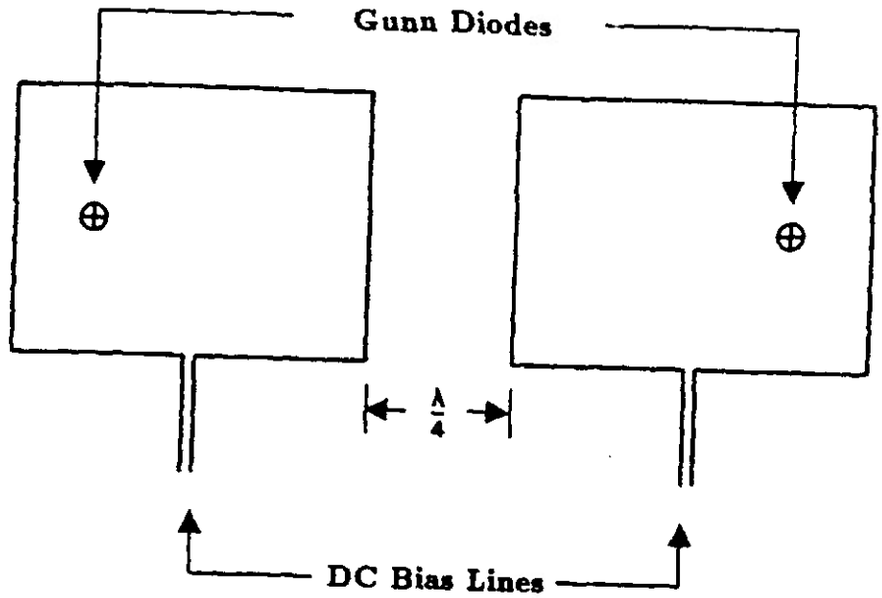


Figure 6. Two-element active antenna array

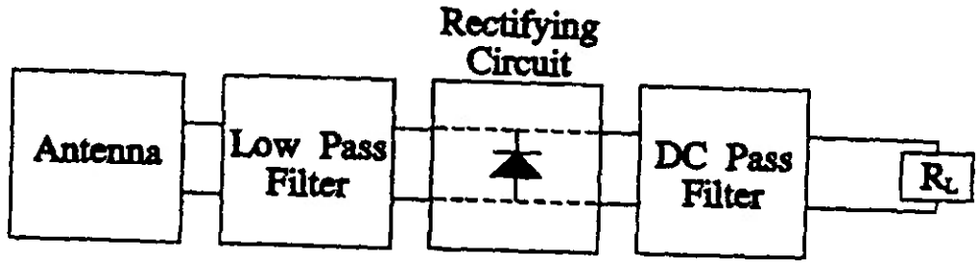


Figure 7. Block diagram of rectenna circuit

The basic principle of the microwave power conversion by this rectifying circuit is analogous to a diode clamping circuit or a large signal mixer at microwave frequencies. The power conversion efficiency is maximized by substantially confining all the higher order harmonics between the low pass filter and the DC pass filter, using an efficient diode and matching the diode's input impedance to antenna's input impedance.

A GaAs Schottky diode (Model DMK6606, Alpha Industries) used in Ka-band mixers was selected for the 35 GHz rectenna. A 35 GHz rectenna was designed using a microstrip dipole as the antenna element. The input impedance of the dipole as an element in an infinite array was calculated using Method of Moment. The impedances calculated from the fundamental frequency to the seventh order harmonic were used as an input data file to LIBRA. The length and the width of a resonant dipole at the fundamental frequency have been determined as 0.46 $\lambda_0$ and 0.02 $\lambda_0$ respectively. The effective impedance of the diode was assumed to be 50 $\Omega$ considering that the output DC voltage should be less than 4.5 volts (half of $V_{br}$) with an operating power level of 100 mW.

Figure 8 shows the circuit layout for the 35 GHz rectenna. Over 39% conversion efficiency was achieved. The results agreed fairly well with the theoretical prediction using a nonlinear circuit analysis [8] (See Appendix 3).

### 4.2 Frequency Selective Surface Filter

Frequency selective surfaces (FSS) have been used for a number of applications including reflector antenna systems and dielectric radome designs. A new application of an FSS is to reject the harmonics produced by a rectifying antenna (rectenna). A rectenna is a receiving antenna that converts a microwave beam into useful DC power. Harmonics of significant power levels are produced by a diode that converts the RF to DC power. This harmonic power is then radiated into free space which may cause potential problems. If the rectenna were placed abroad a satellite, the harmonic radiation could interfere with communication signals. It is desirable to suppress these harmonics by use of an FSS.

A gridded square FSS has been developed to act as a band stop filter. The filter was placed in front of a rectifying antenna array as shown in Figure 9. The filter was designed to pass the fundamental frequency and reject the harmonics.

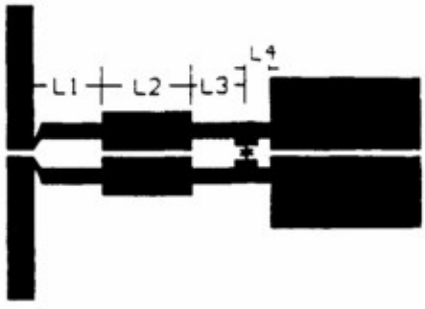


Figure 8. 35 GHz rectenna circuit layout

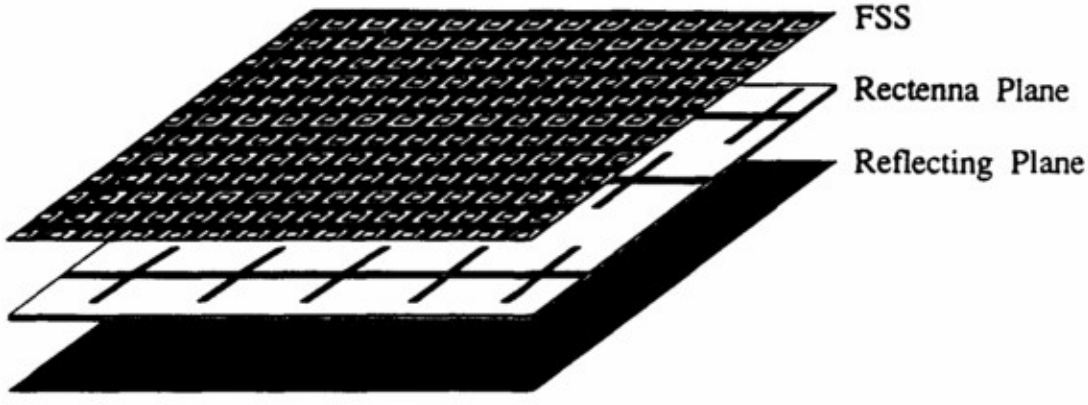


Figure 9. A rectenna array integrated with a frequency selective surface

### 4.3 Low-Loss Open Resonator Coupling and Filters

Fabry-Perot or open resonators have been used at microwave/millimeter-wave frequencies for diplexers, dielectric characterization, antennas, and power combining. Few of these applications have addressed the problem of efficiently coupling power into and out of an open resonator.

For a Fabry-Perot resonator to be made into a useful device, a method of coupling power into and out of the resonator must be devised. Previous methods employed include meshes, small apertures, waveguide apertures, dielectric launchers, and microstrip patch antennas. Most of these methods introduce high losses due to poor coupling efficiencies. To overcome this problem, a novel, simple, and low-loss coupling method using narrow slots was developed. The feed for the antenna is a waveguide opening covered by a thin half-wavelength resonant slot. The results show that the slot is a very efficient method for coupling power into and out of an open resonator and that this coupling method can be used to build a low-loss filter.

Figure 10 shows an open resonator bandpass filter built using this coupling mechanism. An insertion loss of less than 1 dB was achieved for the passband. The filters should have applications in many millimeter-wave and submillimeter-wave systems [9].

## 5. Novel Planar Slotline and Coplanar Waveguide Circuits

In recent years slotline and coplanar waveguide (CPW) have emerged as an alternative to microstrip in microwave and millimeter-wave integrated circuits (MIC). The fact that the center conductor and ground planes are on the same side of the substrate allows series and shunt connections of passive and active solid-state devices. Use of CPW also avoids the need for via holes to connect the center conductor to ground which should help to reduce processing complexity and increase yield in monolithic implementations.

Several novel slotline and CPW components have been developed under this project. These include a tunable filter, a switchable filter, a Gunn VCO, and a tunable ring resonator. The details are given in the following.

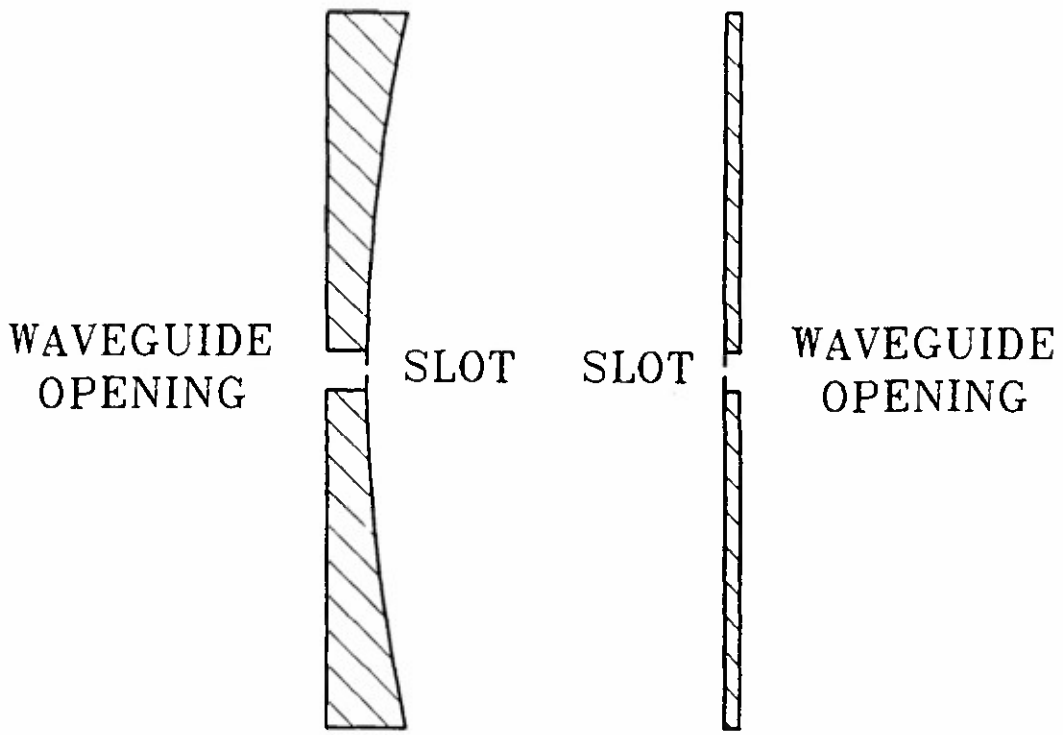


Figure 10 Slot-coupled open resonator filter

## 5.1 Coplanar Waveguide Tunable and Switchable Filters

A novel coplanar waveguide (CPW)-slotline bandpass filter and a microstrip-to-slotline transition has been developed. The circuit is fully planar and allows easy integration of active and passive semiconductor devices in series and in shunt. To test the filter, a new microstrip to slotline transition was designed and two of these transitions exhibited an insertion loss of less than 1.0 dB over the 2.0 to 4.0 GHz range.

Figure 11 shows the schematic diagram of the switchable filter with three sections and three PIN diodes. Each section consists of a CPW resonator. For the tunable filter, the PIN diodes were replaced by varactor diodes.

The three-section CPW-slotline bandpass filter demonstrated an insertion loss of less than 0.2 dB over a 300 MHz bandwidth centered at 2.9 GHz. The three-section CPW-slotline switchable bandpass filter integrated with three PIN diodes was developed with 25.0 dB isolation and 0.7 dB insertion loss. The three-section CPW-slotline varactor-tunable filter integrated with three varactor diodes was demonstrated with a 2.0 dB insertion loss and over 20% electronic tuning range [10] (See Appendix 4).

## 5.2 Coplanar Waveguide Gunn VCO

Considerable effort has been directed toward development of microwave and millimeter-wave receivers in hybrid and monolithic integrated circuit forms. To fully realize the benefits of integration, the local oscillator should be included. This requires a local oscillator in planar form. In addition, for many applications, long-term frequency stability and electronical frequency tunability are also desirable. To achieve these requirements, a high Q resonator, a varactor and a Gunn device are incorporated into a truly planar circuit configuration.

The configuration exhibits a tuning bandwidth from 10.2 to 10.55 GHz with an output power of 16.3 $\pm$ 0.45 dBm. The spectral purity and signal stability are comparable to waveguide and dielectric resonator stabilized microstrip oscillator [11].

Figure 12 shows the novel varactor tunable CPW-slotline Gunn oscillator picture. The circuit consists of a CPW-slotline resonator, a microstrip to slotline transition and a slotline lowpass filter. A Gunn diode is placed on the box at one of the open ends of

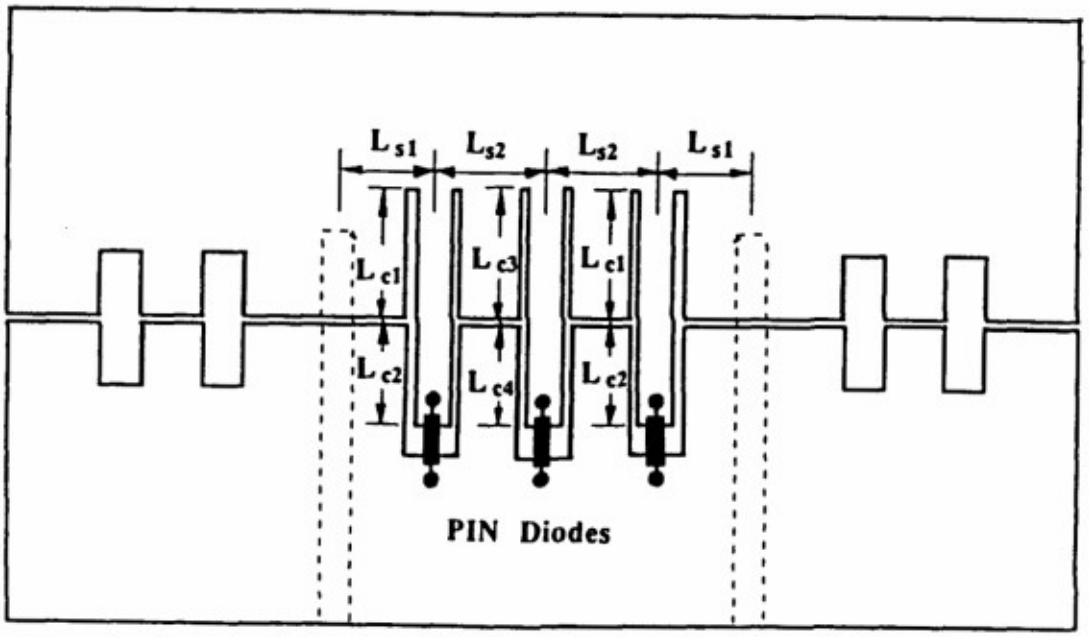


Figure 11. Configuration of the PIN diode switchable CPW-slotline bandpass filter

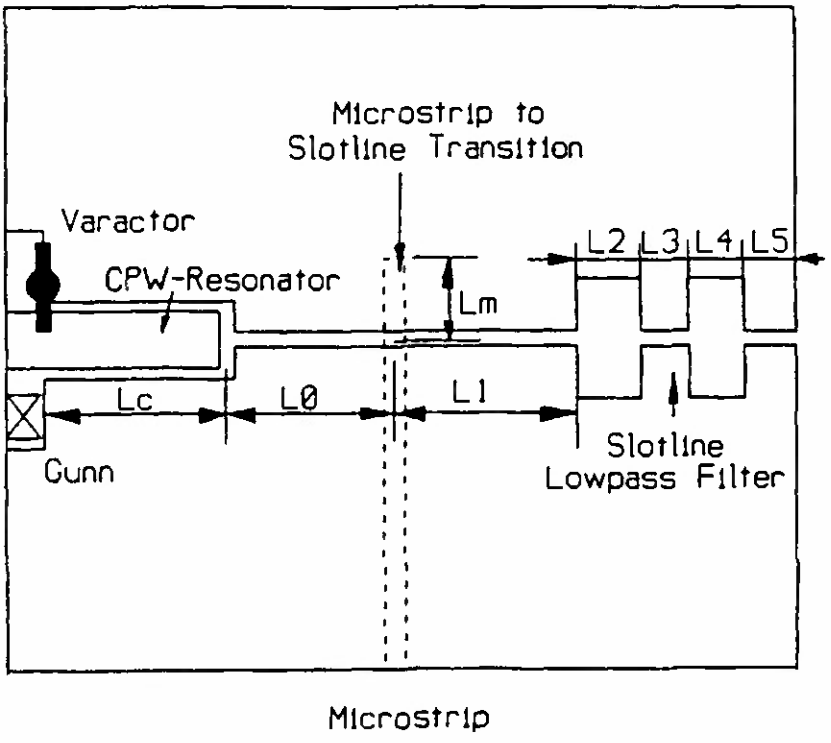


Figure 12. The varactor-tuned CPW-slotline Gunn VCO

the resonator and a varactor at the other end. The circuit offers many advantages of low cost, simplicity, small size, excellent performance, good reproducibility and fully planar configuration. The circuit is amenable to monolithic implementation.

### 5.3 Coplanar Waveguide Fed Slotline Ring Resonators

The search for new uniplanar MIC resonators is of great interest. Microstrip ring resonators can be used for filters and allow easy series insertion of solid-state devices for tuning, switching, and RF power generation. These rings have not been realized in truly planar transmission lines such as slotline or CPW to take advantage of easy shunt device hybrid integration. These truly planar designs should also reduce processing complexity in monolithic applications. Under this project, a CPW fed slotline ring resonator was developed with over 23% varactor tuning range and 4.5 $\pm$ 1.5 dB of insertion loss. A wider tuning range can be obtained for a greater insertion loss variation. The tuning range is wider and the circuit has greater flexibility over the microstrip ring. For instance, the microstrip requires high impedance lines to apply DC biasing and the position of the varactor is fixed at a series gap. Shunt varactor placement on a microstrip ring requires drilling through the substrate. The slotline ring circuit, on the other hand, has inherent DC biasing pads and shunt placement of the varactor can be optimized on the ring. The configuration also lends itself to other device integration for filtering, switching, tuning and RF power generation. Figure 13 shows the circuit configuration of this novel resonator [12].

### 5.4 Conductor-Backed Coplanar Waveguide

CPWs with conductor backing to support the structure (Figure 14) offer an attractive alternative to microstrip as a transmission media for microwave integrated circuit. The usefulness of the conductor backing CPW was questioned due to the mode coupling and energy leakage.

Conventional conductor-backed (grounded) coplanar waveguides (CBCPW) lose energy from its dominant mode in the form of a parallel plate mode (PPM) (leaky wave) propagating in the substrate at all frequencies which can generate undesirable coupling effects (moding problems) and produce an ineffective circuit. A multiple dielectric struc-

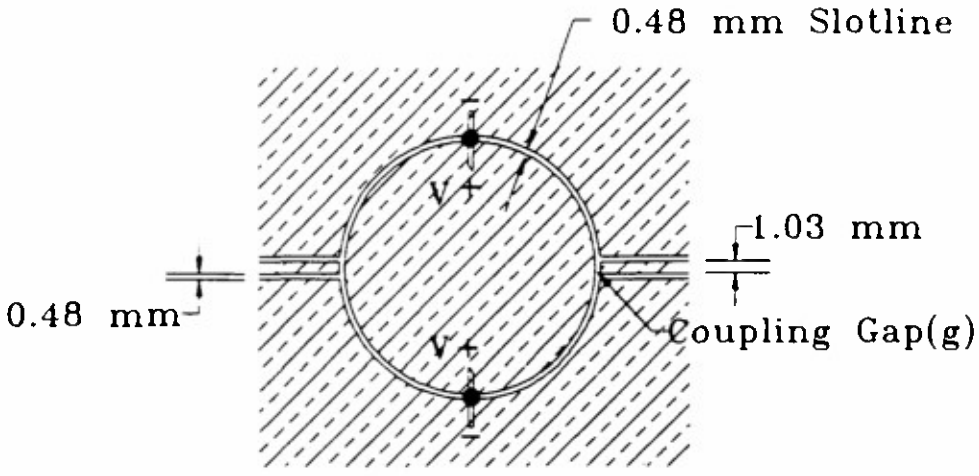


Figure 13. Tunable CPW-fed slotline resonator

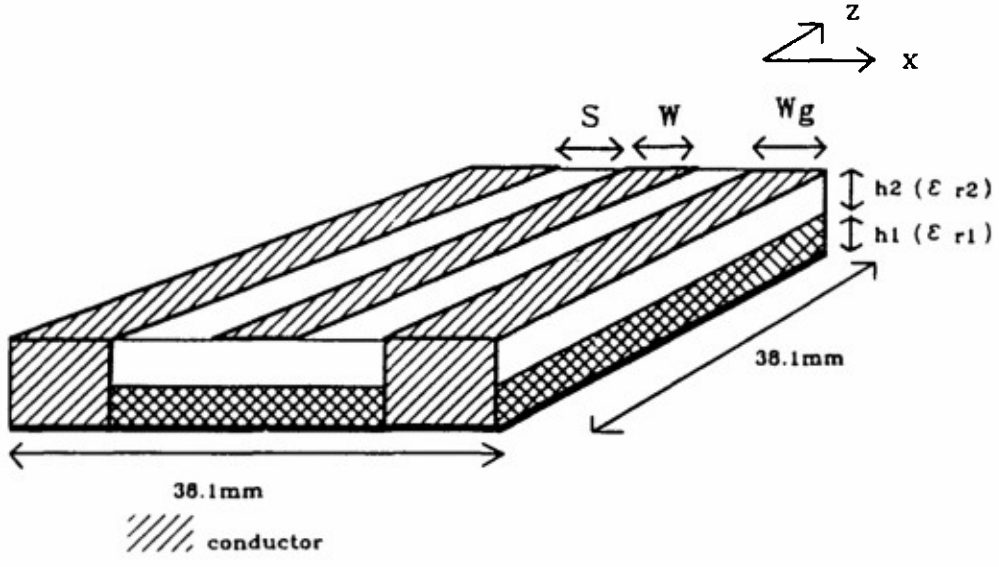


Figure 14. Conductor-backed coplanar waveguide

ture with appropriate dimensions was designed to suppress the leaky wave. The spectral domain method was used to predict the cutoff frequency for the waveguide. Experimental data verifies this procedure and demonstrates the significance of the moding problems. The results should be useful for CBCPW design [13].

## 6. Other Circuits and Analyses

In addition to the research in active antenna elements, spatial power combiners, quasi-optical components, and coplanar waveguide circuits, work was carried out in the analyses and developments of other microwave circuits and components. This section gives a brief summary of these circuits.

### 6.1 Wide Inductive and Capacitive Strip Discontinuities

An analysis based on the variational method and moment method has been developed to calculate the discontinuity susceptance due to a single or multiple inductive strips in a rectangular waveguide as shown in Figure 15(a) and (b). The strips could have wide widths located unsymmetrically on the transverse plane of the waveguide. The current distribution on the strips has been determined by solving a set of linear equations. The theoretical results agree closely with experiments [14].

The analysis was extended to calculate the susceptance of a wide resonant strip on the transverse plane of a rectangular waveguide as shown in Figure 15(c) [15]. Almost any value of susceptance can be obtained at a specified operating frequency by properly choosing the strip depth and strip width.

### 6.2 Superconductive Strip Discontinuities

A two-gap electrically floating resonant strip was used for surface resistance measurements of the high-temperature superconductor, $YBa_2Cu_3O_{7-\delta}$ as shown in Figure 16. The method used has the advantages of simplicity, no electrical contact, operation at various resonant frequencies, and of requiring only a small sample. An analysis was used that allows for the accurate design of the strip dimensions to produce a desired resonant frequency. Experimental measurements on resonant frequencies in X and Ku-band (8-18 GHz) agree well with the calculations. The method allows one to extract the normalized surface

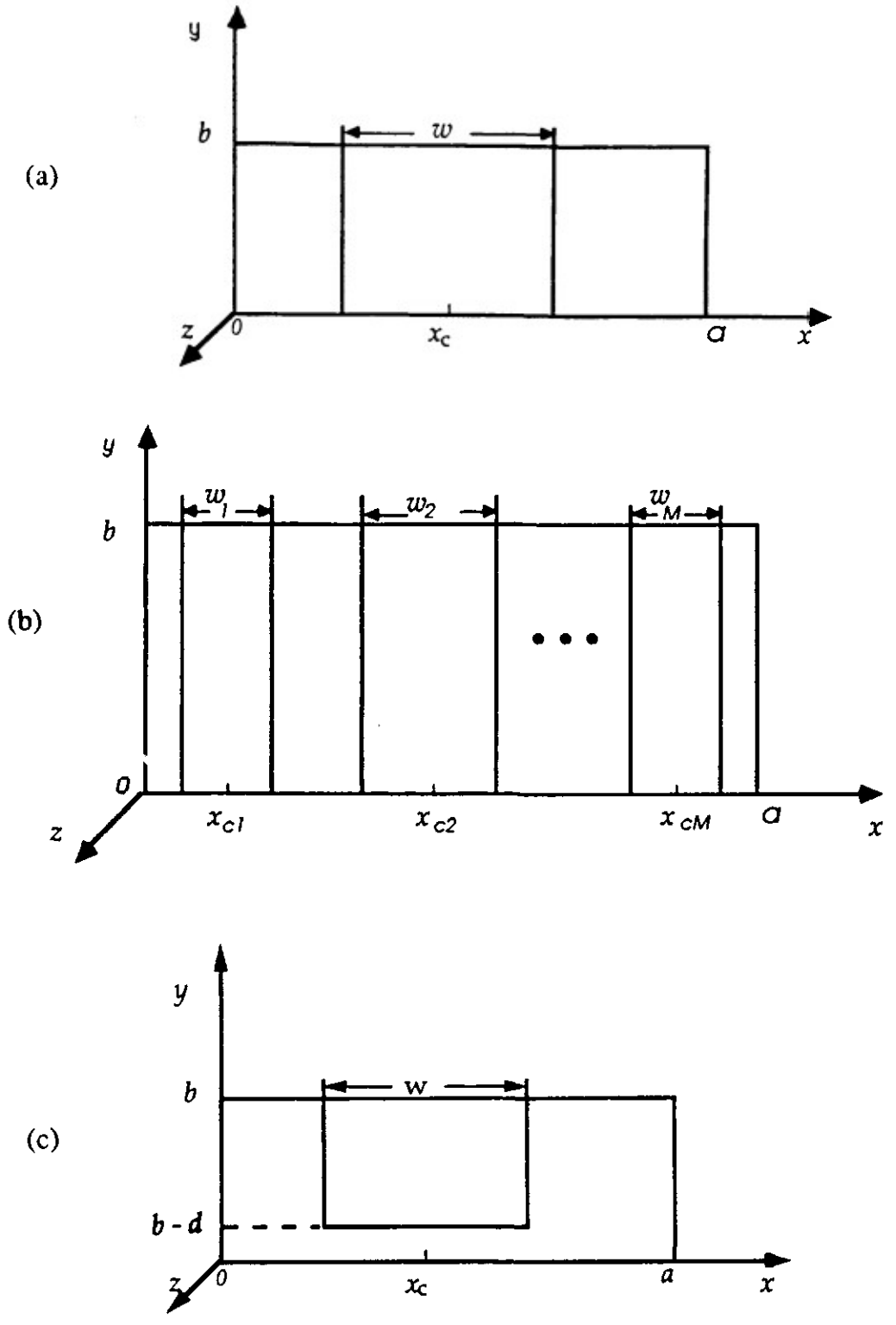


Figure 15. Strip discontinuities in waveguide: (a) a wide inductive strip, (b) multiple inductive strips, (c) a wide resonant strip

resistance of the sample from transmission coefficient measurements at the resonant frequency. These normalized values were found to compare favorably to the Mattis-Bardeen theory taken in the local limit. The resonant strip in waveguide should have applications in high-temperature superconductive material characterization and in the development of waveguide superconductive filters [16].

### 6.3 Microwave/Millimeter-Wave Impedance Measuring Scheme Using a Three-Probe Microstrip Circuit

A simple, compact and low cost three-probe microstrip impedance measuring scheme has been developed. The impedance of an unknown load can be easily determined by measuring the coupling power levels at the three-probes as shown in Figure 17. The coupling coefficients for the three-probes can be unequal and arbitrary, and only one power meter is required by using a single-pole three-throw switch. A prototype device has been built at X-band. The measured results agree very well with those obtained from an HP 8510 automatic network analyzer [17]. The technique has been recently extended to the S-parameter measurements [18].

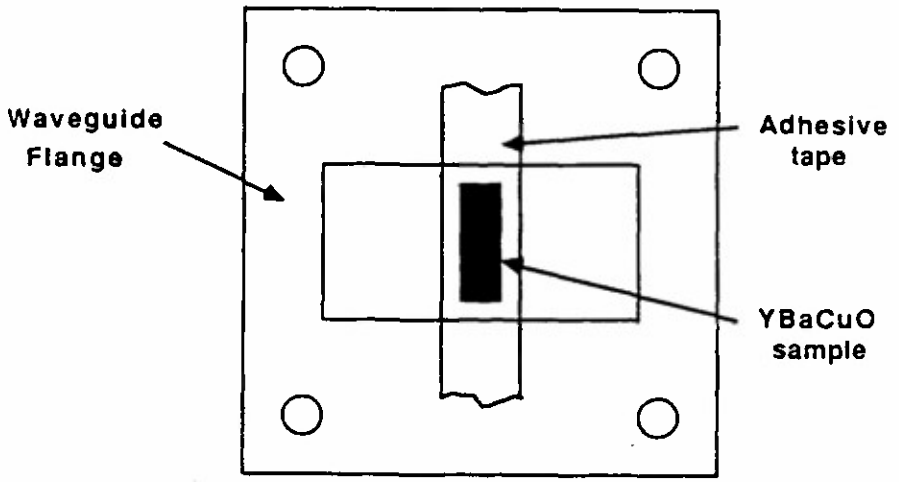


Figure 16. A superconductive strip inside waveguide

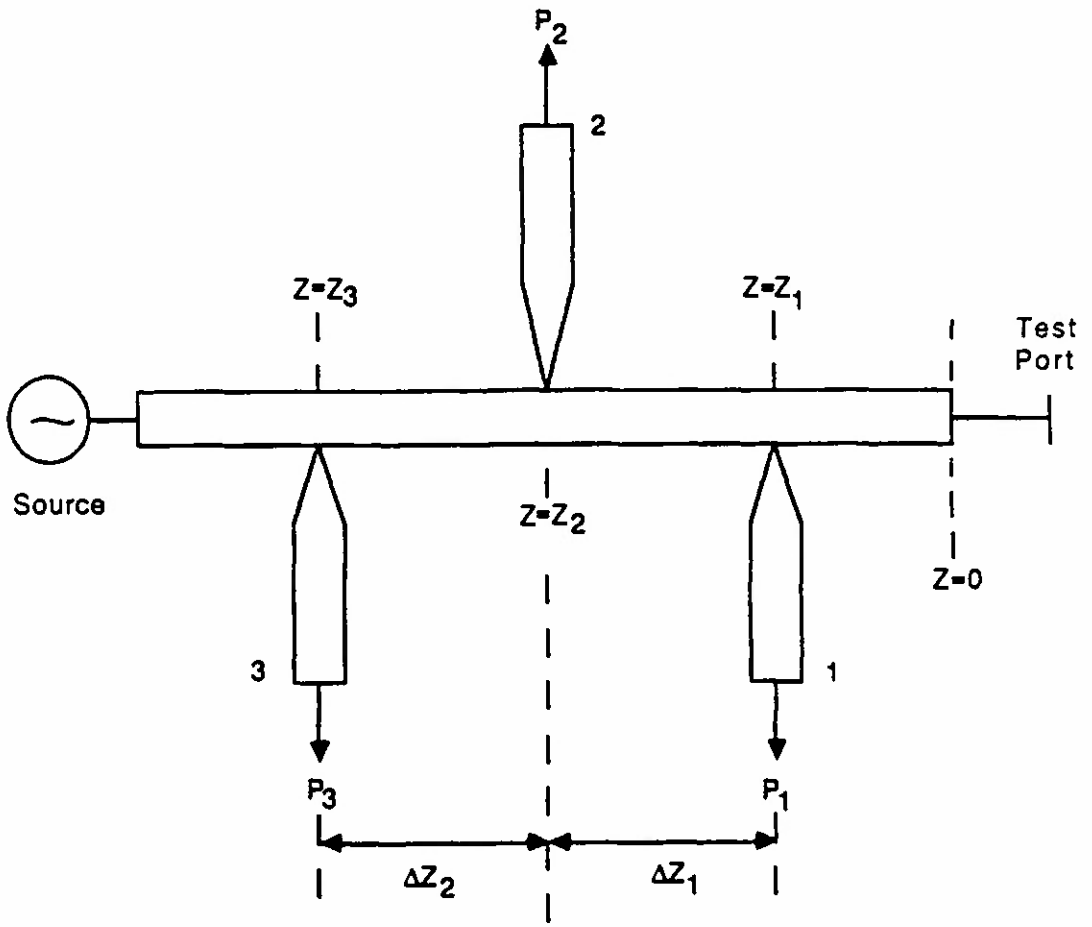


Figure 17. Microstrip three-probe measurement system

## References


1. K. Chang and C. Sun, "Millimeter-Wave Power Combining Techniques," IEEE Trans. on Microwave Theory and Techniques, Vol. MTT-31, Feb. 1983, pp. 91-107.

2. J.W. Mink, "Quasi-Optical Power Combining of Solid-State Millimeter-Wave Sources," IEEE Trans. on Microwave Theory and Techniques, Vol. MTT-34, Feb. 1986, pp. 273-279.

3 K. Chang, K.A. Hummer and J.L. Klein, "Experiments on Injection-Locking of Active Antenna Elements for Active Phased Arrays and Spatial Power Combiners," IEEE Trans. on Microwave Theory and Techniques, Vol. MTT-37, pp. 1078-1084, July 1989.

4. K. Chang, K.A. Hummer, G.K. Gopalakrishnan, "Active Radiating Element Using FET Source Integrated with Microstrip Patch Antenna," Electronics Letters, Vol. 24, No. 21, pp. 1347-1348, Oct. 1988.

5. J.A. Navarro, Y.H. Shu and K. Chang, "Broadband Electronically Tunable Planar Active Radiating Elements and Spatial Power Combiners Using Notch Antennas," IEEE Trans. on Microwave Theory and Techniques, Vol. 40, Feb. 1992, pp. 323-328.

6. R.E. Miller and K. Chang, "Integrated Active Antenna Using Annular Ring Microstrip Antenna and Gunn Diode," Microwave and Optical Technology Letters, Vol. 4, No. 1, Jan. 1991, pp. 72-75.

7. A.M. Kirk and K. Chang, "Integrated Image-Line Steerable Active Antennas," International Journal of Infrared and Millimeter-Waves, Vol. 13, June 1992, pp. 841-850.

8. T. Yoo and K. Chang, "Theoretical and Experimental Development of 10 and 35 GHz Rectennas," IEEE Trans. om Microwave Theory and Techniques, Vol. 40, June 1992, pp. 1259-1266.

9. J.C. McCleary and K. Chang, "Low-Loss Quasi-Optical Open Resonator Filters," 1991 IEEE-MTT Microwave Symposium Digest Technical Papers, Boston, MA., June 1991, pp. 313-316.

10. Y.H. Shu, J.A. Navarro and K. Chang, "Electronically Switchable and Tunable Coplanar Waveguide-Slotline Bandpass Filters," IEEE Trans. on Microwave Theory and Techniques, Vol. 39, Mar. 1991, pp. 548-554.

11. J.A. Navarro, Y.H. Shu and K. Chang, "A Novel Varactor Tunable Coplanar Waveguide-Slotline Gunn VCC," 1991 IEEE-MTT Microwave Symposium Digest Technical Papers, Boston, MA., June 1991, pp. 1187-1190.

12. J.A. Navarro, L. Fan, and K. Chang, "The Coplanar Waveguide-Fed Electronically Tunable Slotline Ring Resonator," 1992 IEEE-MTT Microwave Symposium Digest Technical Papers, Albuquerque, New Mexico, June 1992, pp. 951-954.

13. M.A. Magerko, L. Fan and K. Chang, "Multiple Dielectric Structures to Eliminate Moding Problems in Conductor-Backed Coplanar Waveguide MIC's," IEEE Microwave and Guided Waves Letters, Vol. 2, June 1992, pp. 257-259.

14. B.H. Chu and K. Chang, "Analysis of Wide Transverse Inductive Metal Strips in a Rectangular Waveguide," IEEE Trans. on Microwave Theory and Techniques, Vol. 37, July 1989, pp. 1138-1141.

15. B.H. Chu and K. Chang, "Analysis of a Wide Resonant Strip in Waveguide," IEEE Trans. on Microwave Theory and Techniques, Vol. 40, Mar. 1992, pp. 495-498.

16. M.K. Skrehot and K. Chang, "New Resistance Measurement Technique Applicable to High-Temperature Superconducting Material at Microwave Frequencies," IEEE Trans. on Microwave Theory and Techniques, Vol. 38, Apr. 1990, pp. 434-437.

17. K. Chang, M.Y. Li and T.A. Sauter, "Low Cost Microwave/Millimeter-Wave Impedance Measuring Scheme Using a Three-Probe Microstrip Circuit," IEEE Trans. on Microwave Theory and Techniques, Vol. 38, Oct. 1990, pp. 1455-1460.

18. M.Y. Li and K. Chang, "A Three-Probe Microstrip Measuring System for S-Parameter Measurements," Electronics Letters, Vol. 27, No. 10, May 9, 1991, pp. 836-837.

## List of Personnel

1. Principal Investigator: Kai Chang

2. Research Associates: M. Li, Y. Shu

3. Research Assistants /Students:

| | | |
|---|---|---|
| | B. Chu | J.C. McCleary |
| | G. Gopalakrishnan | J.O. McSpadden |
| | M. Ho | J.A. Miller |
| | K.A. Hummer | R.E. Miller |
| | A.M. Kirk | J.A. Navarro |
| | W.K. Leverich | M.K. Skrehot |
| | G. Luong | T. Yoo |
| | M.A. Magerko | |

4. Degree Awarded

| | | |
|---|---|---|
| Master of Science: | J.A. Miller | August 1989 |
| | R.E. Miller | August 1989 |
| | M.K. Skrehot | August 1989 |
| | J.A. Navarro | December 1990 |
| | A.M. Kirk | May 1991 |
| | J.C. McCleary | December 1991 |
| Ph.D: | G. Gopalakrishnan | December 1990 |
| | B. Chu | August 1991 |

## Report of Invention

A patent application entitled "Planar Active Endfire Radiating Elements and Coplanar Waveguide Filters with Wide Electronic Tuning Bandwidth," has been filed. This patent is now in the final stage of approval by the U.S. Patent Office. K. Chang, J.A. Navarro and Y.H. Shu are co-inventors of this patent.

## List of Publications Under ARO Support

A. Journal Publications


1. B.H. Chu and K. Chang, "Analysis of Wide Transverse Inductive Metal Strips in a Rectangular Waveguide," IEEE Trans. on Microwave Theory and Techniques, Vol. 37, July 1989, pp. 1138-1141.

2 K. Chang, K.A. Hummer and J.L. Klein, "Experiments on Injection-Locking of Active Antenna Elements for Active Phased Arrays and Spatial Power Combiners," IEEE Trans. on Microwave Theory and Techniques, Vol. 37, July 1989, pp. 1078-1084.

3. J.A. Miller, M.Y. Li and K. Chang, "A Simple Microstrip to Dielectric Waveguide Transition," Microwave and Optical Technology Letters, Vol. 2, Nov. 1989, pp. 393-398.

4. J.L. Klein and K. Chang, "Optimum Dielectric Overlay Thickness for Equal Even- and Odd- Mode Phase Velocities in Coupled Microstrip Circuits," Electronics Letters, Vol. 26, No. 5, Mar. 1990, pp. 274-276.

5. M.K. Skrehot and K. Chang, "New Resistance Measurement Technique Applicable to High-Temperature Superconducting Material at Microwave Frequencies," IEEE Trans. on Microwave Theory and Techniques, Vol. 38, Apr. 1990, pp. 434-437.

6. K. Chang, M.Y. Li and T.A. Sauter, "Low Cost Microwave/Millimeter-Wave Impedance Measuring Scheme Using a Three-Probe Microstrip Circuit," IEEE Trans. on Microwave Theory and Techniques, Vol. 38, Oct. 1990, pp. 1455-1460.

7. M.K. Skrehot and K. Chang, "Analysis and Modeling of a High-Temperature Superconducting Floating Resonant Strip in Waveguide," International Journal of Infrared and Millimeter-Waves, Vol. 11, Dec. 1990, pp. 1355-1376.

8. J.A. Navarro, K.A. Hummer and K. Chang, "Active Integrated Antenna Elements," (Invited Paper) Microwave Journal, Vol. 34, Jan. 1991, pp. 115-126.

9. R.E. Miller and K. Chang, "Integrated Active Antenna Using Annular Ring Microstrip Antenna and Gunn Diode," Microwave and Optical Technology Letters, Vol. 4, No. 1, Jan. 1991, pp. 72-75.

10. Y.H. Shu, J.A. Navarro and K. Chang, " Electronically Switchable and Tunable Coplanar Waveguide-Slotline Bandpass Filters," IEEE Trans. on Microwave Theory and Techniques, Vol. 39, Mar. 1991, pp. 548-554.

11. J.A. Navarro, Y.H. Shu and K. Chang, "Broadband Electronically Tunable Planar Active Radiating Elements and Spatial Power Combiners Using Notch Antennas," IEEE Trans. on Microwave Theory and Techniques, Vol. 40, Feb. 1992, pp. 323-328.

12. H.B. Chu and K. Chang, "Analysis of a Wide Resonant Strip in Waveguide," IEEE Trans. on Microwave Theory and Techniques, Vol. 40, Mar. 1992, pp. 495-498.

13. T. Yoo and K. Chang, "Theoretical and Experimental Development of 10 and 35 GHz Rectennas," IEEE Trans. on Microwave Theory and Techniques, Vol. 40, June 1992, pp. 1259-1266.

14. M.A. Magerko, L. Fan and K. Chang, "Multiple Dielectric Structures to Eliminate Moding Problems in Conductor-Backed Coplanar Waveguide MIC's," IEEE Microwave and Guided Waves Letters, Vol. 2, June 1992, pp. 257-259.

15. A.M. Kirk and K. Chang, "Integrated Image-Line Steerable Active Antennas," International Journal of Infrared and Millimeter-Waves, Vol. 13, June 1992, pp. 841-850.

16. G. Luong and K. Chang, "Interconnect of Microstrip Lines Through a Narrow Rectangular Slot in the Common Ground Plane," Microwave and Optical Technology Letters, Vol. 5, July 1992, pp. 388-393.

17. J.O. McSpadden, T. Yoo, and K. Chang, "Theoretical and Experimental Investigation of a Rectenna Element for Microwave Power Transmission," Accepted by IEEE Trans. on Microwave Theory and Techniques, Vol. 40, To appear in Dec. 1992.

18. J.A. Navarro and K. Chang, "Broadband Electronically Tunable Integrated Circuit Active Radiating Elements and Power Combiners," (Invited Paper) Microwave Journal, Vol. 35, To appear in Oct. 1992.

B. Conference Papers

1. J.L. Klein and K. Chang, "Theoretical and Experimental Studies of Dielectric Overlay Microstrip Circuits for Directional Couplers," 14th International Conference on Infrared and Millimeter-Waves, Wurzburg, Germany, Oct. 1989, pp. 145-146.

2. M.K. Skrehot and K. Chang, "Surface Resistance Measurements of High-Tc Superconductors in X and Ku-Bands," 14th International Conference on Infrared and Millimeter-Waves, Wurzburg, Germany, Oct. 1989, pp. 521-522.

3. J.A. Navarro, Y.H. Shu and K. Chang, "Active Endfire Antenna Elements and Power Combiners Using Notch Antennas," 1990 IEEE-MTT Microwave Symposium Digest Technical Papers, May 1990, pp. 793-796.

4. K. Chang, "Recent Developments of Microwave/Millimeter-Wave Integrated Active Antenna Elements," 15th International Conference on Infrared and Millimeter-Waves, Orlando, Florida, Dec. 1990, pp. 520-522.

5. M.Y. Li and K. Chang, "Scattering Parameter Measurements Using a Three-Probe Microstrip Circuit," 15th International Conference on Infrared and Millimeter-Waves, Orlando, Florida, Dec. 1990, pp. 708-710.

6. K. Chang, "Integrated Circuit Active Antenna Elements for Monolithic Implementation," (Invited Paper) SPIE Conference on Monolithic Microwave Integrated Circuits, paper 1475-19, Apr. 1991.

7. J.C. McCleary and K. Chang, "Low-Loss Quasi-Optical Open Resonator Filters," 1991 IEEE-MTT Microwave Symposium Digest Technical Papers, Boston, MA., June 1991.

8. J.A. Navarro, Y.H. Shu and K. Chang, "Wideband Integrated Varactor-Tunable Active Notch Antennas and Power Combiners," 1991 IEEE-MTT Microwave Symposium Digest Technical Papers, Boston, MA., June 1991.

9. J.A. Navarro, Y.H. Shu and K. Chang, "A Novel Varactor Tunable Coplanar Waveguide-Slotline Gunn VCO," 1991 IEEE-MTT Microwave Symposium Digest Technical Papers, Boston, MA., June 1991.

10. J.C. McCleary and K. Chang, "Characterization of Slot-Fed Quasi-Optical Resonators," Progress in Electromagnetics Research Symposium, Boston, MA., July 1991, p. 410.

11. J.A. Navarro, Y.H. Shu and K. Chang, "A Ka-Band Integrated Active Notch Antenna," 16th International Conference on Infrared and Millimeter-Waves, Lausanne, Switzerland, Aug. 1991, pp. 290-291.

12. A.M. Kirk and K. Chang, "Image-Line Voltage Controllable Active Antennas," 16th International Conference on Infrared and Millimeter-Waves, Lausanne, Switzerland, Aug. 1991, pp. 288-289.

13. M.Y. Li and K. Chang, "Techniques for S-Parameter Measurements Using a Three-Probe Circuit," 16th International Conference on Infrared and Millimeter-Waves, Lausanne, Switzerland, Aug. 1991, pp. 362-363.

14. T. Yoo, J.O. McSpadden, and K. Chang, "35 GHz Rectennas Implemented with a Patch and a Microstrip Dipole Antenna," 1992 IEEE-MTT Microwave Symposium Digest Technical Papers, Albuquerque, New Mexico, June 1992, pp. 345-348.

15. J.O. McSpadden, T. Yoo and K. Chang, "Diode Characterization in a Microstrip Measurement System for High Power Microwave Power Transmission," 1992 IEEE-MTT Microwave Symposium Digest Technical Papers, Albuquerque, New Mexico, June 1992, pp. 1015-1018.

16. J.A. Navarro, L. Fan and K. Chang, "The Coplanar Waveguide-Fed Electronically Tunable Slotline Ring Resonator," 1992 IEEE-MTT Microwave Symposium Digest Technical Papers, Albuquerque, New Mexico, June 1992, pp. 951-954.

## Appendices

Appendix 1

K. Chang, K.A. Hummer and J.L. Klein, "Experiments on Injection-Locking of Active Antenna Elements for Active Phased Arrays and Spatial Power Combiners," IEEE Trans. on Microwave Theory and Techniques, Vol. 37, July 1989, pp. 1078-1084.

Appendix 2

J.A. Navarro, Y.H. Shu and K. Chang, "Broadband Electronically Tunable Planar Active Radiating Elements and Spatial Power Combiners Using Notch Antennas," IEEE Trans. on Microwave Theory and Techniques, Vol. 40, Feb. 1992, pp. 323-328.

Appendix 3

T. Yoo and K. Chang, "Theoretical and Experimental Development of 10 and 35 GHz Rectennas," IEEE Trans. on Microwave Theory and Techniques, Vol. 40, June 1992, pp. 1259-1266.

Appendex 4

Y.H. Shu, J.A. Navarro and K. Chang, "Electronically Switchable and Tunable Coplanar Waveguide-Slotline Bandpass Filters," IEEE Trans. on Microwave Theory and Techniques, Vol. 39, Mar. 1991, pp. 548-554.

1078 IEEE TRANSACTIONS ON MICROWAVE THEORY AND TECHNIQUES, VOL. 37, NO. 7, JULY 1989

# Experiments on Injection Locking of Active Antenna Elements for Active Phased Arrays and Spatial Power Combiners

KAI CHANG, SENIOR MEMBER, IEEE, KENNETH A. HUMMER, STUDENT MEMBER, IEEE, AND JAMES L. KLEIN

*Abstract*—Two types of active antenna elements have been studied experimentally. One type uses a microstrip antenna with an active device mounted directly on the antenna. The other uses an active device coupled to a microstrip patch antenna through an aperture. Microstrip active antenna elements and two-element arrays have been demonstrated for both types of circuits. Injection locking of the antenna elements has been achieved through space and mutual coupling. The circuit $Q$ factor was calculated based on the locking gain and the locking bandwidth. The power output from two elements has been successfully combined in free space with a combining efficiency of over 90 percent. For a single active antenna with a Gunn diode mounted directly on the patch, an electronic tuning range exceeding 9 percent has been achieved by varying the dc bias. The results should have many applications in low-cost active arrays, active transmitters, and spatial power combiners.

## I. Introduction and Background

RECENT DEVELOPMENTS in solid-state devices and microwave/millimeter-wave integrated circuits have made it possible to combine the active devices with planar antennas to form active arrays. Many elements can be combined to build an active phased array or a spatial power combiner. These techniques allow monolithic implementation by fabricating both active devices and antennas on a single semiconductor substrate. The circuits can be made at low cost and should have many applications in radar, communication, and EW systems.

Two types of active array configurations have been investigated. The first type uses active devices mounted directly on planar antennas (shown in Fig. 1). The second type uses a transmit–receive (T/R) module mounted directly behind an antenna element (shown in Fig. 9). In these circuits, each element acts as a low-cost transmitter. Many of these elements can be combined to form a spatial power combiner or a quasi-optical power combiner.

Many power-combining approaches have been demonstrated in the microwave and millimeter-wave frequency range [1], [2]. Most of these techniques have serious limitations due to the moding and size problems. Consequently, the maximum number of devices that can be combined is limited. To overcome these problems, spatial or quasi-optical combiners have been proposed to combine the power in free space or in a Fabry–Perot resonator [3]. An active device mounted directly on a planar antenna forms a module for spatial or quasi-optical combiners. In order to achieve coherency and effective combining in free space, the modules will be injection locked to each other through mutual coupling or through an external master source.

This paper reports the design and measurements of a single active patch antenna with a Gunn diode oscillator integrated directly on the patch. The circuit forms an element for spatial or quasi-optical combiners. The output

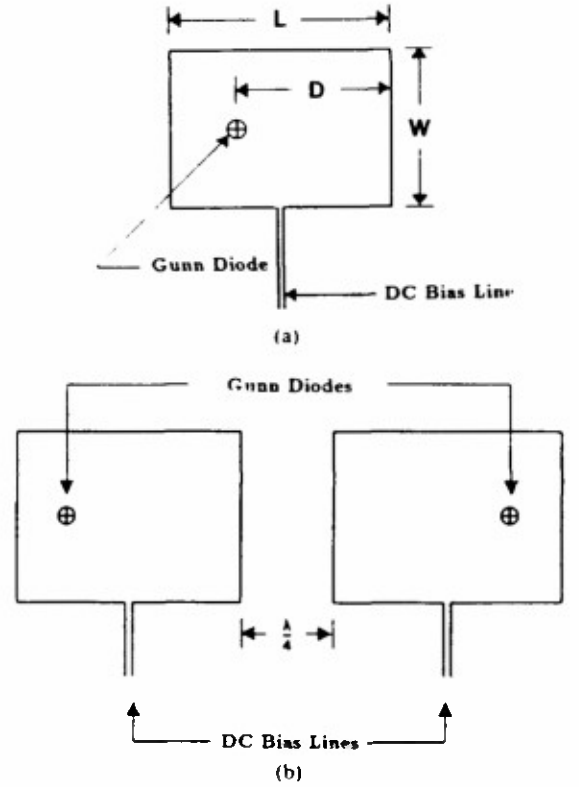


Fig. 1. (a) Single- and (b) two-element active antenna elements with devices mounted directly on antennas.

Manuscript received March 25, 1988; revised January 23, 1989. This work was supported in part by the Army Research Office and by TRW.

K. Chang and K. A. Hummer are with the Department of Electrical Engineering, Texas A&M University, College Station, TX 77843-3128.

J. L. Klein was with the Department of Electrical Engineering, Texas A&M University, College Station, TX. He is now with Texas Instruments Inc., Dallas, TX 75265.

IEEE Log Number 8928198

0018-9480/89/0700-1078$01.00 ©1989 IEEE

power was found comparable to a waveguide circuit using the same Gunn diodes. The active antenna can be made tunable over a 9 percent bandwidth by varying the dc bias. This wider tuning range compared to a passive patch antenna is attributed to a lower loaded $Q$ factor. The loaded $Q$ factor was measured using spatial injection-locking techniques.

Two of these active antennas were successfully combined to form an array. Received output power was approximately doubled, indicating a combining efficiency of over 90 percent. Experimental results also showed that the array antenna pattern broke from a single beam into two separate beams as the dc bias voltage of one of the antennas was varied. This resulted in a tuning range of about 1 percent, which is lower than that of a single active patch antenna.

The second type of circuit configuration (shown in Fig. 9) uses a T/R module mounted directly behind an antenna element. Two commonly used feeding arrangements are the space-feed and corporate-feed techniques. Many T/R modules using FET's have been developed for these applications [4]–[6]. An aperture-coupled microstrip to patch antenna circuit is suitable to connect the T/R module to the antenna element. The circuit can also be used in spatial power combiners if the T/R module is replaced by an oscillator. The design is based upon an analysis using aperture coupling theory and an $S$-parameter matrix [7]. A two-element array was fabricated and tested at about 2.4 GHz. Injection locking through mutual coupling was demonstrated and good power-combining efficiency was achieved.

## II. Patch Antenna with Active Device Mounted Directly on Antenna

Low-cost transmitters and power combiners can be made by mounting the active devices directly on antenna elements. Single-element microstrip active patch antennas have been reported by Thomas *et al.* [8] and Perkins [9] using Gunn and IMPATT diodes. Power combining using an open resonator has also been reported [10]. However, no attempt was made to injection lock two antenna elements through mutual or spatial coupling, to measure the $Q$ factor, or to electronically tune the active antenna element. Furthermore, no attempt was made to combine the output power from two active antennas in free space.

Both the single patch antenna and the two-element array were constructed on Duroid 5870 substrate with a thickness of 1.524 mm. The circuits were designed at $X$-band using Gunn diodes and patch antennas. The circuit configurations are shown in Fig. 1.

The antenna dimensions were determined by equations given by James *et al.* [11]. The placement of the active device was chosen such that the device impedance was matched to the input impedance of the patch. The diode placement location $D$ is given by

$$D = \frac{\lambda_g}{2\pi} \cos^{-1}\left[2Z_{in}G_r\left(1 - \frac{G_m}{G_r}\right)\right]^{1/2} \tag{1}$$

where

$G_r$ = radiation conductance,
$G_m$ = mutual conductance of the two edges of the antenna,
$D$ = distance from either antenna edge to the feed position,
$Z_{in}$ = input impedance of the antenna at the diode location,
$\lambda_g$ = guided wavelength.

For a rectangular patch with width $W = 0.3\lambda_0$ and length $L = \lambda_g/2 - 2\Delta l_{eo}$, $G_r$ and $G_m$ are given by James *et al.* [11]:

$$G_r = \left(\frac{W^2}{90\lambda_0^2}\right) \tag{2}$$

$$\frac{G_m}{G_r} = 0.32. \tag{3}$$

Here $\Delta l_{eo}$ is the equivalent length to account for open-end fringing capacitance. The input impedance $Z_{in}$ was set equal to the magnitude of the active device resistance, assumed to be 8 Ω [12].

The two-element active array is also shown in Fig. 1. Each element was designed to have the same dimensions as the single antenna. Two antenna elements were separated by one quarter of the guided wavelength. The Gunn diode is a packaged pill-type diode from M/A COM. It produced 10–25 mW of output power at 10 GHz in an optimized waveguide circuit.

## III. Results for a Single Active Patch Antenna

To measure the power output from the active antenna, a standard horn antenna was used as a receiver. The active patch antenna has an output power $P_o$ and a gain of $G_1$. A standard horn antenna with a gain of $G_2$ was placed a distance $R$ away from the active antenna. The received power $P_r$ can be measured using a power meter. The output power $P_o$ can be calculated using the following equation:

$$P_o = P_r\left(\frac{4\pi R}{\lambda_0}\right)^2 \frac{1}{G_1 G_2}. \tag{4}$$

Here it is assumed that the two antennas are well aligned and matched, and the polarization loss is neglected.

For a single active patch antenna, the maximum output power is about 15 mW at 10.1 GHz. This power is calculated using (4) based on a 15.4 μW received power. The output power and frequency as a function of dc bias are shown in Fig. 2. A 3 dB tuning range of 839 MHz was achieved from 9.278 to 10.117 GHz. This tuning range is equivalent to a 9 percent bandwidth, which is much wider than that of a single passive patch.

The $E$-plane antenna patterns for several bias voltages are shown in Fig. 3. This shows a beam width of 90°. The large peak present at −60° is most likely due to radiation

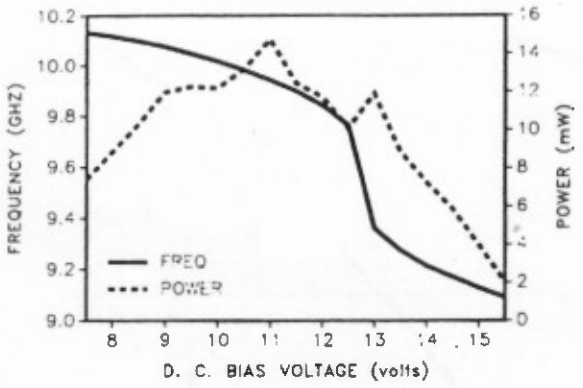


Fig. 2. Output power as a function of frequency and bias voltage for a single active antenna.

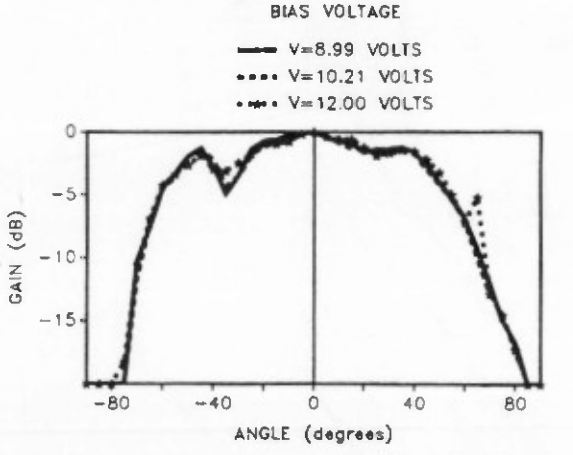


Fig. 3. *E*-plane antenna patterns for several different bias voltage levels for a single active antenna.

from the dc bias line that is required to bias the Gunn diode. The plot also shows that the pattern changes very little as the bias voltage (and thus the frequency and power) is varied.

The single patch antenna can be injection locked by an external signal incident on the patch. Fig. 4 shows the frequency spectrum before and after the injection locking. The frequency stabilization and the noise suppression provided by injection locking are evident. Fig. 5 shows the injection-locking bandwidth versus locking gain (which is defined as $P_o/P_i$). The external $Q$ can be found from Adler [13]:

$$Q_e = \frac{2f_o}{\Delta f}\sqrt{\frac{P_i}{P_o}} \tag{5}$$

where

$Q_e$ = external $Q$ factor,
$f_o$ = operating frequency,
$\Delta f$ = injection-lock bandwidth,
$P_i$ = injection-lock signal power,
$P_o$ = free-running oscillator power.

For the results shown in Fig. 5, the external $Q$ value is about 20. This low $Q$ value explains why a wider tuning range was achieved for a single active patch antenna. The

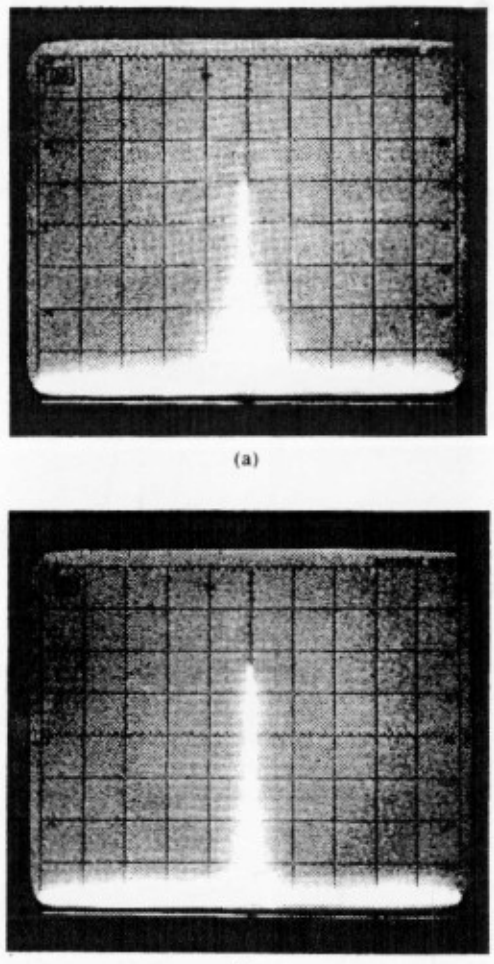

(a)

(b)

Fig. 4. Signal spectra (a) before and (b) after the injection locking. Vertical: 10 dB/div. Horizontal: 500 kHz/Div. Center frequency: 9.967 GHz.

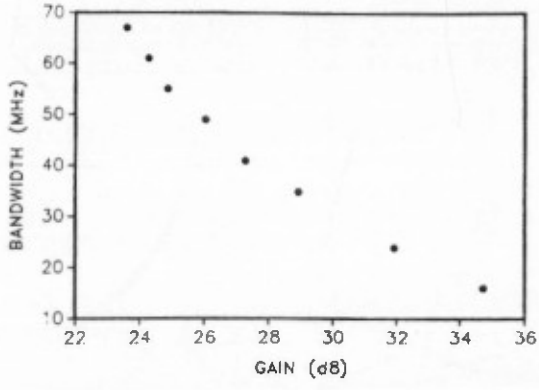


Fig. 5. Injection-locking bandwidth as a function of locking gain.

$Q$ factor measured here compares favorably with those previously reported for microstrip oscillators [14], [15].

## IV. Results for Two-Element Active Array

The two active devices in the two-element array will injection lock each other through mutual coupling. Injection locking may also be obtained by the use of an external source.

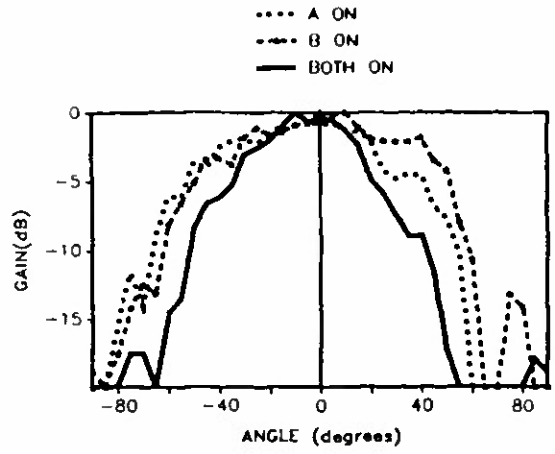


Fig. 6. Measured *E*-plane power pattern for a two-element array.

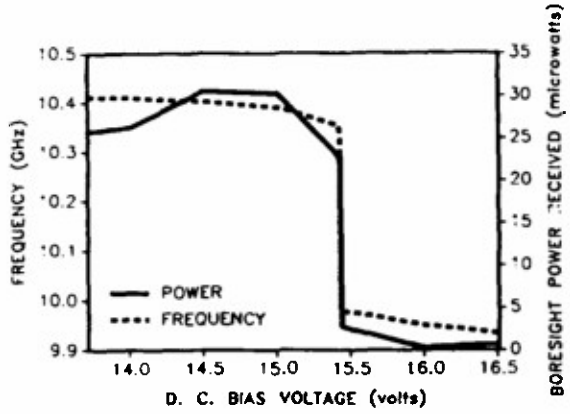


Fig. 7. Frequency and received power as a function of bias voltage of one diode.

The measured *E*-plane pattern for the array is shown in Fig. 6 Also shown are the patterns with either antenna "off." It can be seen that when both antennas are "on," the beam width is narrower and the gain is thus higher. The patterns were normalized to the peak radiation power. The bias to either diode was optimized individually to achieve the maximum output power. The received boresight power and frequency as a function of dc bias on one diode are given in Fig. 7. An output power level of 30 mW was achieved at 10.42 GHz. The power was calculated by using (4) with a two-element array antenna gain. This output power level is about twice that from a single patch active antenna. This demonstrates good combining efficiency. It can be seen that the boresight power and the operation frequency of the array experience a severe drop at a bias voltage of 15.45 V. To investigate this phenomenon, antenna patterns were made for bias voltages above and below 15.45 V. These results are shown in Fig. 8. It was found that the radiation pattern broke from a single beam into two separate beams above this bias voltage. The useful electronic tuning range is about 1 percent due to the breakup phenomenon. It is believed that this breakup is caused by the loss of phase lock. This phenomenon should not pose any serious problem in practical applications for narrow-band systems. A similar breakup

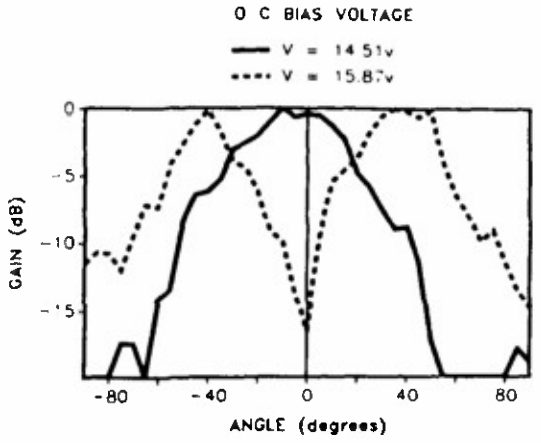


Fig. 8. Pattern broken up above 15.45 V.

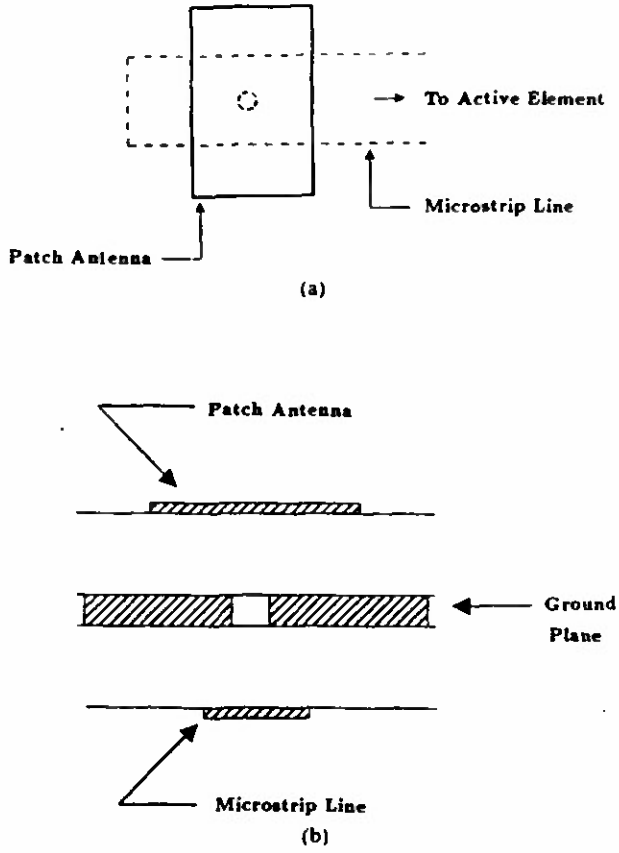


Fig. 9. Aperture-coupled microstrip to patch antenna circuit for active array (a) Top view. (b) Cross-sectional view.

phenomenon has recently been reported by Stephan and Young [16] for a different type of circuit.

## V. Aperture-Coupled Patch Antenna Circuits

One practical difficulty with active arrays using T/R modules is in isolating the input and output signals and maintaining the stability of the array. Another problem is maintaining unidirective radiation and avoiding spurious radiation from feed lines.

To overcome these problems, a two-sided substrate circuit has been proposed [17]. As shown in Fig. 9, the active circuits, which include the oscillators, amplifiers, and phase

TABLE I
DIMENSIONS FOR TWO APERTURE-COUPLED ANTENNAS

| parameter (mm) | Patch A | Patch B |
|---|---|---|
| antenna width | 29.5 | 29.5 |
| antenna length | 39.5 | 39.0 |
| aperture size | 10.25 | 10.0 |
| line length | 50.0 | 50.0 |
| stub length | 19.0 | 19.0 |

Edge separation between elements is 19.5 mm.

shifters, are located on the bottom side of the ground plane. The antenna elements are located on the top side of the ground plane. The ground plane provides a good heat sink for the active devices. The coupling between the two layers is accomplished by circular apertures in the ground plane. The ground plane separates the radiating aperture from the feed network, eliminating the possibility of spurious signal radiation from the source. Because of the good isolation between the radiating antenna and active device, the antenna and active circuits can be optimized separately. Furthermore, since two substrates are used, one can use a low-dielectric-constant substrate for the antennas to increase the efficiency, and a high-dielectric-constant substrate (such as GaAs) for the active circuitry. These features have made aperture-coupled patch antenna circuits a very attractive structure for active array applications.

The design of the aperture-coupled patch antenna was based on the analysis reported by Gao and Chang [7]. A six-port network was used to model the coupling circuit based on the aperture-coupling theory and an $S$-parameter matrix. The input impedance as a function of frequency can be calculated using this analysis.

The spacing between the elements is a prime consideration in the design of the array and is chosen based upon the coupling requirement for injection locking. For the structure considered here, one antenna is to be connected to a sweeper, and the other to a free-running oscillator. The free-running oscillator will be injection locked to the sweeper signal through mutual coupling. The coupling between antennas was designed at 20 dB (thus providing 20 dB of injection-locking gain). Using the data from Jedlicka, Poe, and Carver [18], and assuming $E$-plane antenna coupling, it can be seen that 20 dB coupling corresponds to a one-quarter-wavelength edge separation.

## VI. TWO-ELEMENT ACTIVE ARRAY USING APERTURE-COUPLED PATCH ANTENNAS

To demonstrate the concept, a two-element active array was designed and built on Duroid 5870 substrate operating at around 2.36 GHz. The dimensions for the two aperture-coupled antennas are given in Table I.

Smith charts showing the input impedance for the two antennas are given in Fig. 10. It can be seen that the two antennas have similar impedance characteristics and resonate at almost the same frequency. The coupling between antenna elements was also measured and is given in Fig. 11. It can be seen that maximum coupling is about

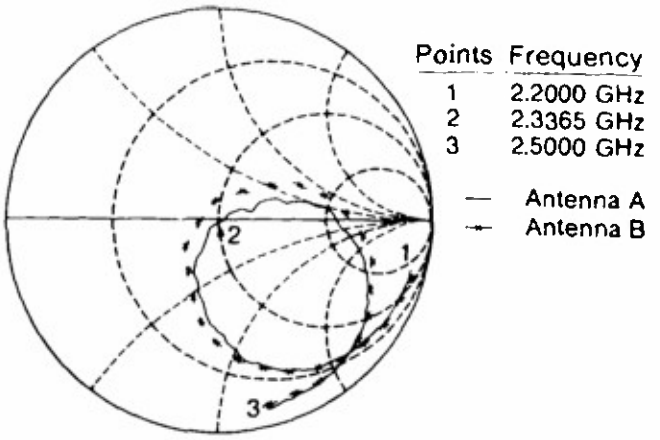


Fig. 10. Input impedance measurements on the two antennas using an HP 8510 network analyzer.

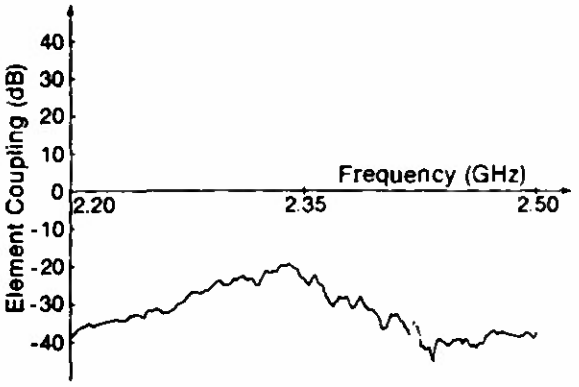


Fig. 11. Mutual coupling between two aperture-coupled antennas.

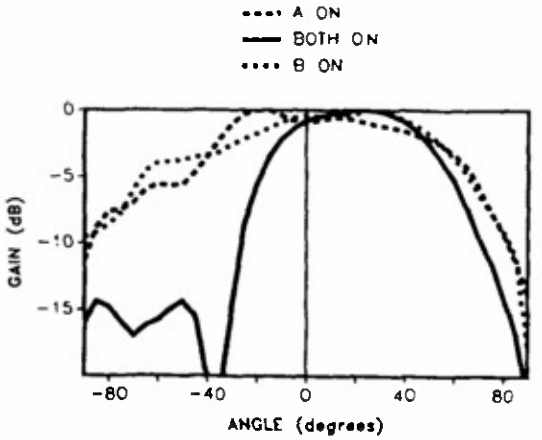


Fig. 12. $E$-plane power pattern of a two-element aperture-coupled active array.

19.4 dB, very close to the desired value of 20 dB. The antenna bandwidth was also measured. The bandwidth for an input $VSWR$ of less than 2.0 is 28.5 MHz for one antenna and 31.5 MHz for the other.

The antenna pattern and injection-locking bandwidth were measured in an anechoic chamber. One antenna was connected to a sweeper and the other to a free-running oscillator. The oscillator was a transistor oscillator manufactured by EMF Systems Inc. The sweeper was used to

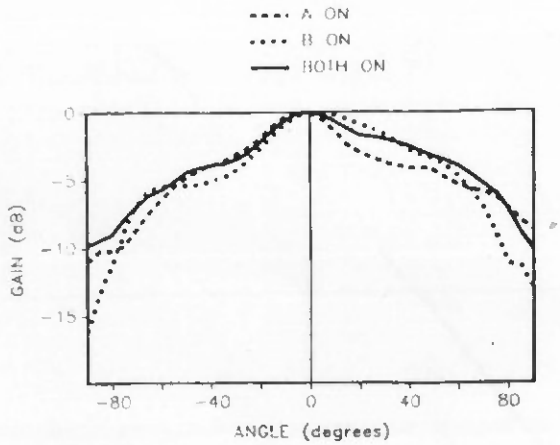


Fig. 13. *H*-plane pattern of a two-element aperture-coupled active array.

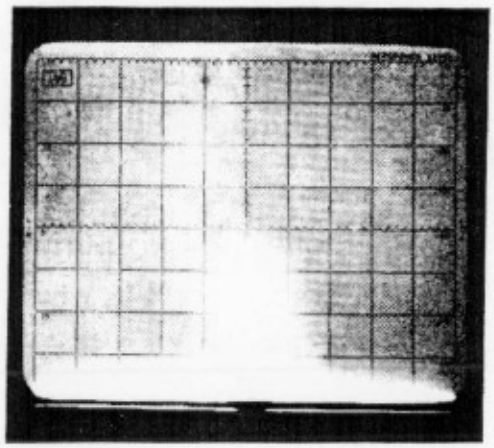

(a)

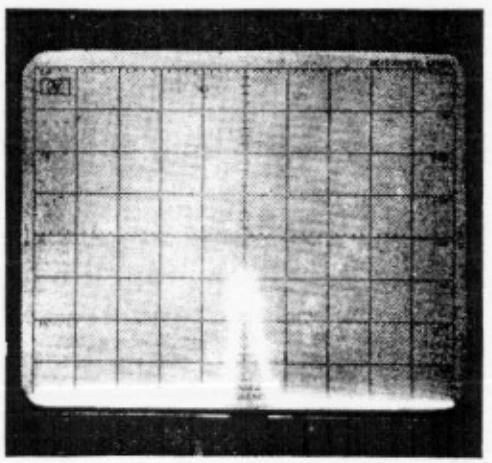

(b)

Fig. 14. Oscillator spectra (a) before and (b) after injection locking. Vertical: 10 dB/div. Horizontal: 100 kHz/div. Center frequency: 2.384 GHz.

injection lock the free-running oscillator by mutual coupling.

Fig. 12 shows the *E*-plane pattern of the active array when only the sweeper is "on," when only the oscillator is "on," and when both sources are "on." When one of the sources was disengaged, a 3 dB beam width of about 90° was measured. This beam width was reduced to 65° when both sources were "on." Furthermore, the power with both sources operating was about 2 dB higher than the power with any single source operating. This shows that the array is exhibiting good power-combining properties. With both sources on, the main lobe is centered at roughly 25°. This off-center condition is due to the different lengths of the transmission lines used to connect antennas and sources. A phase difference thus exists between the two sources. This difference can be adjusted and overcome by the use of a transmission line section or phase shifter.

Fig. 13 shows the *H*-plane pattern of the array. It can be seen that no matter which sources are operating, the antenna pattern remains relatively unchanged. This is to be expected since the antennas are arranged for *E*-plane coupling. Very little *H*-plane coupling can be expected. The antenna *H*-plane beam width was about 120°.

The injection locking through mutual coupling was also demonstrated. Fig. 14 shows the oscillator spectra before and after the injection locking. It can be seen that injection locking has a dramatic effect in reducing oscillator noise. The locking bandwidth was measured to be 2.15 MHz. Assuming an injection-locking gain of 20 dB, the locking bandwidth corresponds to an external $Q$ factor of 217. The narrow locking bandwidth and high $Q$ factor are believed to he due to the high-$Q$ transistor oscillator.

## VII. Conclusions

Two types of active antenna elements have heen investigated. The first type uses active devices directly mounted on thc antennas. The second type uses an aperture-coupled microstrip to patch antenna circuit which can be used to accommodate a transmit–receive module. A two-element array was built and demonstrated in both cases. Injection locking was achieved by using either mutual coupling or an external master source. Good power-combining efficiency was achieved for both circuits. An electronic tuning range of over 9 percent was achieved for the single active antenna element and of about 1 percent for a two-element array.

## Acknowledgment

The authors would like to thank X. Gao and Dr. R. D. Nevels for many helpful discussions.

## References

[1] K. J. Russell, "Microwave power combining techniques," *IEEE Trans. Microwave Theory Tech.*, vol. MTT-27, pp. 472–478, May 1979.

[2] K. Chang and C. Sun, "Millimeter-wave power combining techniques," *IEEE Trans. Microwave Theory Tech.*, vol. MTT-31, pp. 91–107, Feb. 1983.

[3] J. W. Mink, "Quasi-optical power combining of solid-state millimeter-wave sources," *IEEE Trans. Microwave Theory Tech.*, vol. MTT-34, pp. 273–279, Feb. 1986.

[4] H. C. Johnson, R. E. Marx, A. Sanchez, and E. Mykietyn, "A circularly polarized active antenna array using miniature GaAs FET amplifiers," in *1984 IEEE-MTT-S Int. Microwave Symp. Dig.*, pp. 260–262.

[5] C. R. Green *et al.*, "A 2 watt GaAs TX/RX module with integral control circuitry for *S*-band phased array radars," in *1987 IEEE-MTT-S Int. Microwave Symp. Dig.*, pp. 933–936.

[6] J. Pierro and R. Clouse, "An ultraminiature 5-10 GHz, 2-W transmit module for active aperture application," in *1987 IEEE MTT-S Int. Microwave Symp. Dig.*, pp. 941-944.

[7] X. Gao and K. Chang, "Network modeling of an aperture coupling between microstrip line and patch antenna for active array applications," *IEEE Trans. Microwave Theory Tech.*, vol. 36, pp. 505-513, Mar. 1988.

[8] H. J. Thomas, D. L. Fudge, and G. Morris, "Gunn source integrated with a microstrip patch," *Microwave & RF*, pp. 87-89, Feb. 1985.

[9] T. O. Perkins, "Active microstrip circular patch antenna," *Microwave J.*, pp. 110-117, Mar. 1987.

[10] S. Young and K. D. Stephan, "Stabilization and power combining of planar microwave oscillators with an open resonator," in *1987 IEEE MTT-S Int. Microwave Symp. Dig.*, pp. 185-188.

[11] J. R. James, P. S. Hall, and D. Wood, *Microstrip Antenna: Theory and Design*. Stevenage, U.K.: Peregrinus, 1981, ch. 4.

[12] K. Chang *et al.*, "*V*-band low noise integrated receiver," *IEEE Trans. Microwave Theory Tech.*, vol. MTT-31, pp. 146-154, Feb. 1983.

[13] R. Adler, "A study of locking phenomena in oscillators," *Proc. IRE*, vol. 34, pp. 351-357, June 1946.

[14] P. Yen *et al.*, "Millimeter-wave IMPATT microstrip oscillator," in *1983 IEEE MTT-S Int. Microwave Symp. Dig.*, pp. 139-141.

[15] K. Chang *et al.*, "*W*-band (75-110 GHz) microstrip components," *IEEE Trans. Microwave Theory Tech.*, vol. MTT-33, pp. 1375-1382, Dec. 1985.

[16] K. D. Stephan and S. Young, "Mode stability of radiation-coupled injection-locked oscillators for integrated phased arrays," *IEEE Trans. Microwave Theory Tech.*, vol. 36, pp. 921-924, May 1988.

[17] D. Pozar and D. H. Schaubert, "Comparison of architectures for monolithic phased array antennas," *Microwave J.*, pp. 93-104, Mar. 1986.

[18] R. P. Jedlicka, M. T. Poe and K. P. Carver, "Measured mutual coupling between microstrip antennas," *IEEE Trans. Antennas Propagat.*, vol. AP-29, pp. 147-149, Jan. 1981.

✠

**Kai Chang** (S'75-M'76-SM'85) received the B.S.E.E. degree from National Taiwan University, Taipei, Taiwan, the M.S. degree from the State University of New York at Stony Brook, and the Ph.D. degree from the University of Michigan, Ann Arbor, in 1970, 1972, and 1976, respectively.

From 1972 to 1976 he worked for the Microwave Solid-State Circuits Group in the Cooley Electronics Laboratory of the University of Michigan as a research assistant. From 1976 to 1978 he was employed by Shared Applications, Ann Arbor, where he worked in computer simulation of microwave circuits and microwave tubes. From 1978 to 1981, he was with the Electron Dynamics Division, Hughes Aircraft Company, Torrance, CA, where he was involved in the research and development of millimeter-wave devices and circuits. This activity resulted in state-of-the-art IMPATT oscillator and power combiner performance at 94, 140, and 217 GHz. Other activities included silicon and gallium arsenide IMPATT diode design and computer simulation, Gunn oscillator development, and monopulse comparator and phase shifter development. From 1981 to 1985 he worked for TRW Electronics and Defense, Redondo Beach, CA, as a section head in the Millimeter-Wave Technology Department, developing state-of-the-art millimeter-wave integrated circuits and subsystems including mixers, VCO's, transmitters and amplifiers, modulators, up-converters, switches, multipliers, receivers, and transceivers. He joined the Electrical Engineering Department of Texas A&M University in August 1985 as an Associate Professor and was promoted to Professor in 1988. His current interests are in microwave and millimeter-wave devices and circuits, microwave optical interactions, and radar systems.

Dr. Chang serves as the editor of the *Handbook of Microwave and Optical Components*, to be published by Wiley & Sons. He is the editor of *Microwave and Optical Technology Letters*. He has published more than 90 technical papers in the areas of microwave and millimeter-wave devices and circuits.

✠

PII Redacted

**Kenneth A. Hummer** (S'86) [redacted]. He received the B.S. and M.S. degrees in electrical engineering from Texas A&M University, College Station, TX. He is currently pursuing the Ph.D. degree at Texas A&M.

✠

**James L. Klein** received the B.S. and M.S. degrees in electrical engineering from Texas A&M University, College Station, TX, in 1986 and 1988, respectively.

In June 1988, he joined Texas Instruments Inc., Dallas, as a Microwave Design Engineer. He is currently responsible for the design and development of monolithic microwave integrated circuits for use in satellite and airborne phased-array systems.

# Broadband Electronically Tunable Planar Active Radiating Elements and Spatial Power Combiners Using Notch Antennas*

Julio A. Navarro, Yong-Hui Shu, and Kai Chang, *Fellow, IEEE*

*Abstract*—**A Gunn device has been integrated with two types of active planar notch antennas. The first type uses a coplanar waveguide (CPW) resonator and a stepped-notch antenna with bias tuning to achieve a bandwidth of 275 MHz centered at 9.33 GHz with a power output of 14.2 ± 1.5 dBm. The second type uses a CPW resonator with a varactor for frequency tuning to achieve a bandwidth of over 1.3 GHz centered at 9.6 GHz with a power output of 14.5 ± 0.8 dBm. This is equivalent to over 14% electronic tuning bandwidth. Both configurations exhibit a very clean and stable output signal. A theoretical circuit model was developed to facilitate the design. The model agrees well with experimental results. Injection-locking experiments on the second configuration show a locking gain of 30 dB with a locking bandwidth of 30 MHz at 10.2 GHz. Power combining experiments of two varactor-tuned CPW active notch antenna elements in a broadside configuration have achieved well over 70% combining efficiency throughout the wide tuning range. The circuits have advantages of small size, low cost, and excellent performance.**

## I. Introduction

CONSIDERABLE effort has been directed toward the development of microwave and millimeter-wave hybrid and monolithic integrated circuits. Recent developments have made it possible to combine active devices with planar antennas to create active radiating elements or active quasi-optical transmitters. Due to the power limitations of active solid-state radiating elements, quasi-optical and spatial power combining techniques have been used by [1]–[6]. The general power combining techniques have been reviewed in [6]. The spatial power combining techniques create a single, coherent and higher-power signal from many low-power radiating sources. Furthermore, spatial or quasi-optical power combining is not limited by size or moding problems and allows the combination of a greater number of active radiating elements.

The microstrip patch antenna has been used for an active, planar, integrated, low-cost radiating element [1], [2], [7]–[10]. The microstrip patch antenna provides a resonant structure for the Gunn diode to oscillate, a ground plane for efficient heat sinking, and an inexpensive method to create a microwave source. However, the active patch antenna has exhibited very narrow tuning ranges with high cross-polarization levels, and wide power output deviations. Futhermore, the structure has inherent deficiencies for active millimeter-wave operation due to its small patch dimensions, and it does not allow easy integration of other solid-state devices, such as the varactor, for wideband electronic frequency tuning. Previously, varactor tuning has been accomplished using waveguide and microstrip Gunn oscillators [11], [12], but no attempt has been made to integrate the varactor-tuned Gunn oscillator directly into the antenna. An alternative approach for active element integration can be accomplished by sing the notch antenna.

The notch antenna has many desirable characteristics which include broad impedance matching bandwidth and planar nature, as well as good reproducibility, and ease of integration to passive and active devices. Furthermore, the length of the notch can be increased to create a travelling-wave antenna like the linear-tapered slot antenna (LTSA) [13]. The main design parameter of the notch antenna is the flare of the slot as given by the exponentially-tapered Vivaldi antenna [14]. Other important work has been reported in the characteristics of the antenna impedance and radiation [15]–[17]. The flexibility of this type of antenna makes it ideal for many diverse applications.

An FET has been integrated with a notch antenna [18] using slotline and CPW to create a 20 GHz receiver front-end. No other attempt has been made to use the advantages of the notch for an active quasi-optical transmitter. This paper presents two novel configurations for the integration of a Gunn oscillator to a notch antenna:

1) Biased-tuned Gunn oscillator in the CPW resonator using a stepped-notch antenna. The notch is coupled to the center of a CPW resonator which is physically perpendicular to the slotline.

2) Varactor-tuned Gunn oscillator in a CPW resonator using a smooth-tapered notch antenna. The notch is coupled to one end of a CPW resonator which is physically in colinear to the slotline.

The first configuration exhibits a clean, stable bias-tuned signal from 9.2 to 9.47 GHz with a power output of 14.2 ± 1.5 dBm. However, bias tuning creates a wide deviation in power output and the resonator orientation

Manuscript received November 29, 1990; revised September 18, 1991. This work was supported in part by the U.S. Army Research Office.

Y. Shu is with Epsilon Lambda Electronics Corporation, Geneva, IL.
J. Navarro and K. Chang are with the Department of Electrical Engineering, Texas A&M University, College Station, TX 77843-3128.

IEEE Log Number 9104775

*Patent pending

may introduce a strong cross-polarization component. For most active antenna applications, a low-cost method of providing a clean, stable signal with moderate and constant power output over a wider electronic tuning bandwidth is needed. This can be accomplished by introducing a varactor in the oscillating circuit. The second configuration, with varactor tuning, exhibits a tuning bandwidth from 8.9 and 10.2 GHz with an output power of 14.5 ± 0.8 dBm. The spectral purity and tuning range are comparable to state-of-the-art results achieved in waveguide and microstrip oscillators. The theoretical tuning curve obtained from a circuit model agrees fairly well with experimental results.

Injection-locking experiments were also conducted showing a locking gain of 30 dB with a locking bandwidth of 30 MHz at 10.2 GHz. Power combining experiments of two varactor-tuned active notch antenna elements, in a broadside configuration at a distance of 8 mm ($\lambda/4$ at 9.6 GHz) apart, have achieved well over 70% combining efficiency throughout the tuning range with a maximum of 129.2% at 9.7 GHz. To the best of the authors' knowledge, this is the first varactor tunable power combiner ever reported.

The circuits offer many advantages of low cost, simplicity, small size, wide electronic tuning range, good stability, and excellent performance. Although Gunn and varactor diodes were used here, other active devices can also be used. Due to their planar nature, these circuits are amenable to monolithic implementation and offer many applications in radar, communications, and electronic warfare systems.

## II. The Active CPW Stepped-Notch Antenna

Fig. 1 shows the active CPW stepped-notch antenna configuration. The circuit consists of a stepped-notch antenna coupled to a CPW resonator via slotline. A Gunn diode is placed in a heat-sink at the open terminals of the resonator. The notch is formed by many step transformers which match the slotline impedance to free space.

The resonator is the essential design element for improved oscillation and stability. Considering the planar nature, $Q$-factor, and ease of integration with active devices, CPW was chosen for the resonator. The CPW slots were designed to be 0.3 mm with a 3.5 mm separation. This arrangement provides a 50 Ω characteristic impedance and mates well with the 3.5 mm cap of the Gunn diode. The length of the resonator is about 0.5λ at 10 GHz. A DC block was incorporated at the shorted end for biasing purposes. The circuit is mounted on an L-shaped metal block which serves as a heat-sink and holder.

The notch antenna design was accomplished by using cascading slotlines which act as impedance transformers from the coupling point to free space. The low dielectric constant of 2.3 allows efficient antenna radiation. The input impedance of the notch was matched to the resonator at the coupling point.

Matching from free space to the resonator was optimized using a transmission line equivalent circuit model. The lengths of the transformer sections were optimized for minimum return-loss throughout $X$-band. The circuit was fabricated on a 60 mil thick, RT-Duroid 5870 substrate. To test the passive circuit, an SMA connector was soldered on to the CPW resonator and the measurements were performed on an HP-8510 Network Analyzer. The stepped-notch antenna gain was measured at 9.3 and 9.6 GHz and found to be 7.1 and 7.7 dBi, respectively. Integration of an active device may change the antenna efficiency and introduce degenerate modes at the oscillating frequency. However, one can use this method to approximate the oscillator power output. The gain measurements were used to calculate the oscillator power output with the Friis transmission equation:

$$P_t = P_r \left(\frac{4\pi R}{\lambda}\right)^2 \left(\frac{1}{G_{ot} G_{or}}\right) \tag{1}$$

where

$P_r$ = Power received.
$P_t$ = Power transmitted from the active notch antenna.
$\lambda$ = Wavelength of operation.
$R$ = Antenna range length.
$G_{ot}$ = Gain of the transmit antenna.
$G_{or}$ = Gain of the receive antenna.

A Gunn device from M/A COM was integrated with the stepped-notch antenna. This Gunn diode produces 72 mW in an optimized waveguide circuit. The bias voltage vs. frequency and power output is shown in Fig. 2.

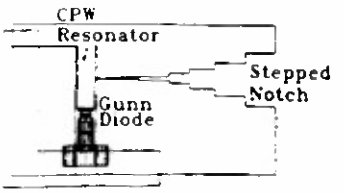


Fig. 1. CPW Stepped-notch antenna circuit configuration.

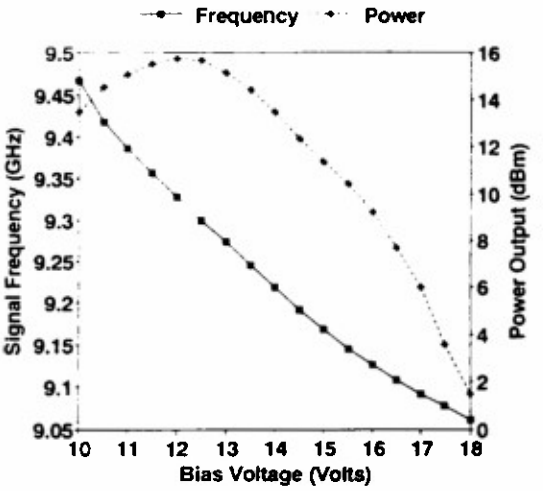


Fig. 2. Frequency and power output versus bias voltage of the active CPW stepped-notch antenna.

The 3 dB bias-tuning bandwidth was 275 MHz centered at 9.33 GHz with a maximum power output of 37.5 mW at 9.328 GHz.

## III. The Varactor-Tunable CPW Active Notch Antenna

Fig. 3(a) shows the varactor-tunable CPW active notch antenna configuration. The circuit consists of a notch antenna integrated with a varactor-tuned CPW resonator. The notch antenna couples to the resonator via slotline. A Gunn and a varactor diode are placed at either end of the CPW resonator. This arrangement provides strong coupling between the Gunn diode and the varactor diode for increased tuning bandwidth.

The CPW resonator allows multiple dc-biased devices to be integrated due to its inherent dc blocks used for separate biasing. The input impedance of the antenna was matched at the coupling point with the resonator and the flare of the notch antenna was modified from the stepped to a smooth taper for improved bandwidth performance.

A theoretical model was developed to facilitate the design. The equivalent circuit can be represented as shown in Fig. 3(b). The modeling of the CPW junction is based on reference [19]. Neglecting the junction discontinuity effects, the transformer ratio n is set equal to 1. The flare of the notch antenna was approximated by 24 sections of slotlines of different widths and impedances. The equivalent circuits of the Gunn and varactor diodes used for calculations are shown in Fig. 4. The diode parasitics for the Gunn and varactor are given by the vendor. The following conditions were used to determine the oscillating frequencies at various varactor bias levels:

$$|\mathrm{Re}\,(Z_{\mathrm{diode}})| \geq |\mathrm{Re}\,(Z_{\mathrm{circuit}})| \qquad (2)$$

$$\mathrm{Im}\,(Z_{\mathrm{diode}}) + \mathrm{Im}\,(Z_{\mathrm{circuit}}) = 0 \qquad (3)$$

where Re $(Z_{\mathrm{diode}})$ is assumed to be $-8\ \Omega$ [20] and the oscillations occur when condition 1 is satisfied. The oscillating frequencies are found from condition 2.

The overall dimensions of the circuit board are 1 × 2 inches. The circuit was etched on a 60 mil thick RT-Duroid 5870 substrate. To test the passive circuit, a coaxial connection was soldered on to the notch and measured on an HP-8510 Network Analyzer. The measured SWR was less than 2:1 throughout the *X*-band range (8–12.4 GHz). The passive notch was then tested in an anechoic chamber for the field patterns and relative gain. The relative gain ($G_o$) of the passive notch antenna measured at 9.0, 9.6, and 10.2 GHz were 8.0, 8.2, and 9.0 dBi, respectively. The gain was later used in (1) to determine the active notch output power.

A Gunn and varactor diode from M/A COM were integrated into the resonator and coupled to the notch antenna via slotline. This Gunn diode (MA49106) produces 80 mW in an optimized waveguide circuit while the varactor (MA46602F) is rated for 1.6 pF at 0 V. Theoretical results were calculated using the circuit model shown in Fig. 3(b) and (2) and (3). Fig. 5 shows the theoretical

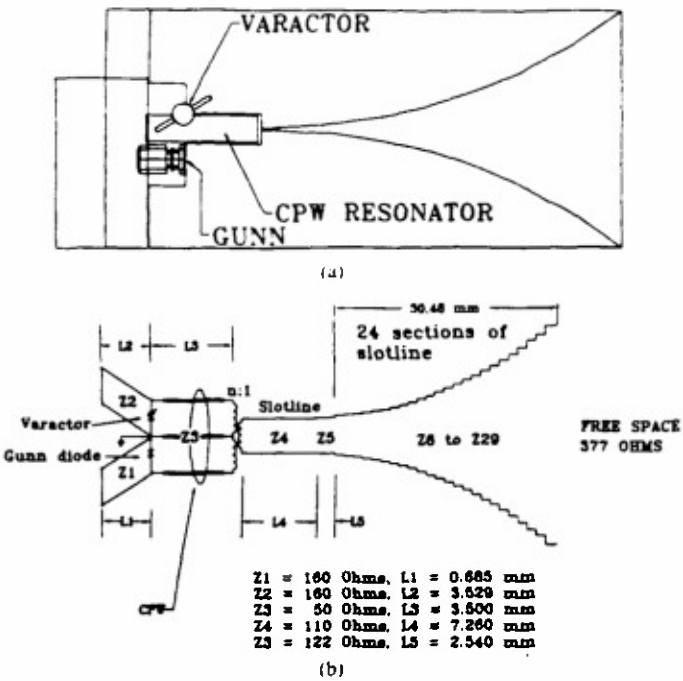


Fig. 3. The varactor-tunable CPW notch antenna. (a) Circuit configuration. (b) Equivalent circuit.

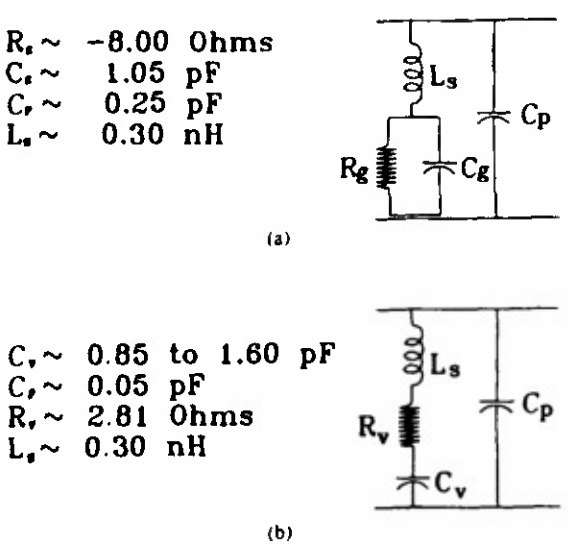


Fig. 4. Device Equivalent Circuits. (a) Gunn diode. (b) Varactor diode.

tuning curve obtained for varying varactor bias levels from 0 to 30 V. Experimental results are shown in the same figure for comparison. Considering the large deviation of active device modelling parameters, the theoretical model agrees fairly well with the experimental results. A frequency tuning range of 8.9 to 10.2 GHz was achieved for varactor voltages of 0 to 30 V. This is equivalent to over 14% electronic tuning bandwidth. There are no mode jumps and the signal spectrum remains clean and very stable, with an output power variation of ±0.8 dBm throughout the frequency tuning range. The spectrum of the received signal from the varactor-tunable notch antenna is comparable to the spectrum of the active stepped-notch. The *E* and *H*-field patterns as well as the cross-

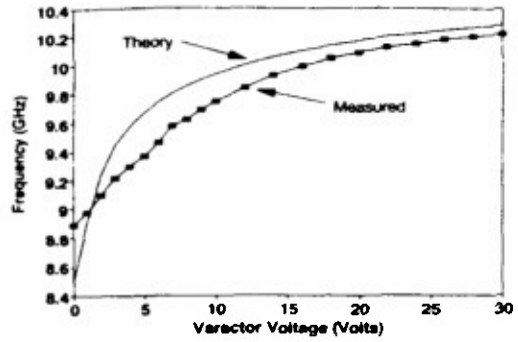


(a)

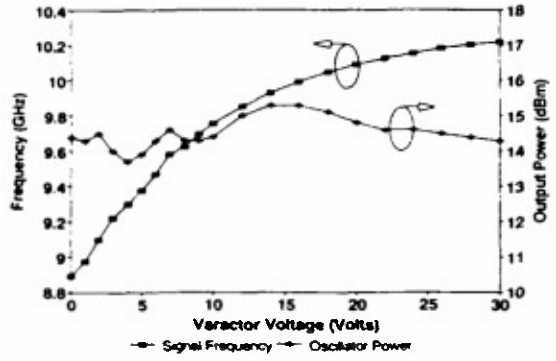


(b)

Fig. 5. Active varactor-tunable CPW notch antenna results. (a) The theoretical and experimental varactor tuning frequency versus voltage (b) The experimental power output of the active varactor-tunable CPW notch antenna

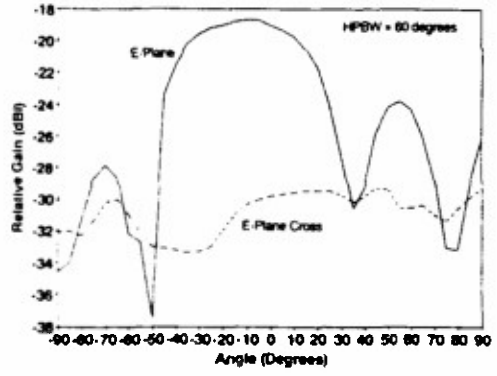


(a)

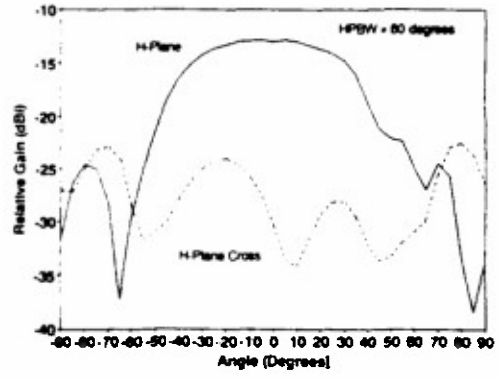


(b)

Fig. 6. Field patterns of the active varactor-tunable CPW notch antenna at 10.2 GHz. (a) $E$-plane pattern and cross-polarization measurements. (b) $H$-plane pattern and cross-polarization measurements.

polarization patterns are shown in Fig. 6 for the varactor-tunable active notch antenna at 10.2 GHz. The back radiation remains below $-10$ dB throughout the tuning bandwidth.

## IV. Injection-Locking and Power-Combining Experiments

Injection-locking experiments with an external HP-8690B Sweep Oscillator source were performed to determine the locking-gain and locking-bandwidth of the active notch antenna configuration. The test measurement set-up is shown in Fig. 7. Equation (1) was used to determine the $P_i$ from $P_t$ and $P_o$ from $P_r$. Injection-locking experiments were performed throughout the electronic tuning range. The locking-gain ($P_o/P_i$) vs. locking bandwidth ($\Delta F$) results are shown in Fig. 8 and they are comparable to previous patch antenna experiments [1]. A locking gain of 30 dB with a locking bandwidth of 30 MHz was obtained at 10.2 GHz. The $Q$-factor of the circuit is found to be 21.5 and can be calculated with [21]

$$Q_e = \frac{2F_o}{\Delta F}\sqrt{\frac{P_i}{P_o}} \tag{4}$$

The locking gain in dB is defined as

$$G_L = 10 \log \frac{P_o}{P_i} \tag{5}$$

where

$Q_e$ = External $Q$-factor.
$F_o$ = Operating frequency.
$\Delta F$ = Injection-locking bandwidth.
$P_i$ = Injection-lock signal power.
$P_o$ = Free-running oscillator power.

Quasi-optical combiners using Fabry-Perot resonators and spatial power combiners have the potential of combining many solid-state devices at millimeter-wave frequencies. To demonstrate the feasibility of the spatial power combiner, two notch antennas were set up in a broadside array at 8 mm separation. To achieve efficient power-combining, the active notch antenna elements must injection-lock to each other through mutual coupling. Power combining experiments of two injection-locked, varactor-tuned active notch antennas were conducted throughout the electronic tuning range at 100 MHz increments. The power combining efficiency is defined by

$$\text{Efficiency} = \left(\frac{P_{\text{combiner}}}{P_1 + P_2}\right) \times (100)\% \tag{6}$$

where

$P_1$ = Power of active notch #1 (Use $G_{o1} = G_o$, $G_o$ is the antenna gain of a single passive notch antenna).
$P_2$ = Power of active notch #2 (Use $G_{o2} = G_o$).
$P_{\text{combiner}}$ = Power of injection-locked, power-combined signal (Use $G_{oc} = 2G_o$).

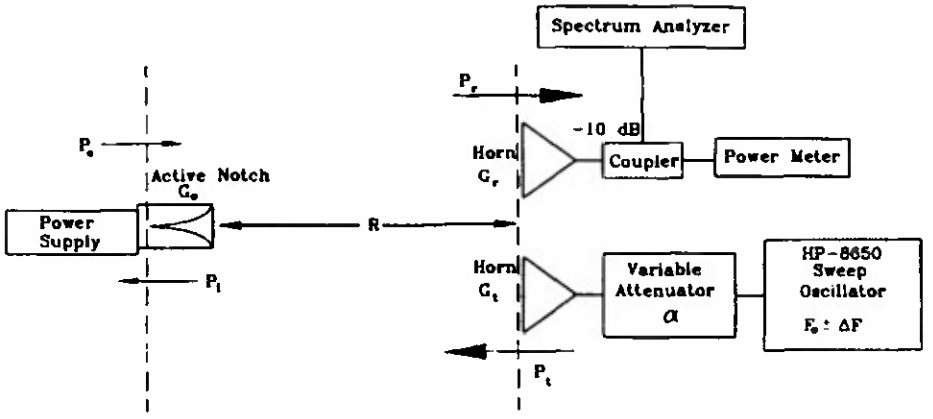


Fig. 7. The measurement set-up for injection-locking experiments using an external source.

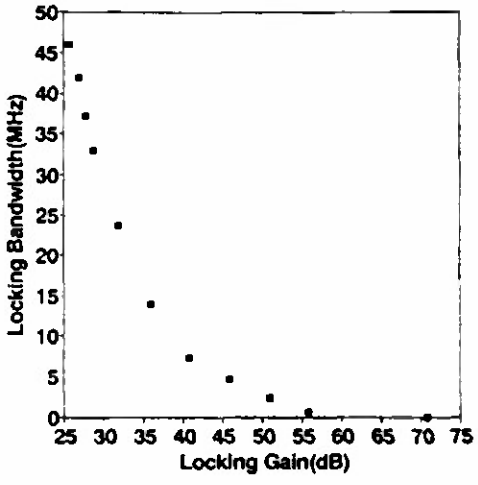


Fig. 8. The injection locking-gain versus locking-bandwidth at 10.2 GHz.

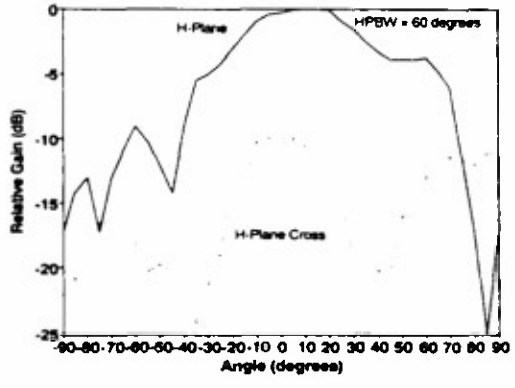


Fig. 9. The *H*-plane and cross-polarization meausurements of two mutually-coupled injection-locked, power combined active notch antennas at 9.6 GHz.

All power calculations are calculated from (1). For the $P_1$ and $P_2$ calculations, the gain of a single passive antenna was used for the transmitting active antenna gain $G_{at}$. For the $P_{combiner}$ calculations, the array gain was assumed to have twice the gain of a single passive antenna. The power combining efficiencies measured at 9.4, 9.7, and 10 GHz were 90.0, 129.2, and 75.0%, respectively. The combining efficiency of over 100% at certain frequencies can be attributed to improved impedance matching in two mutually-coupled oscillators as compared to a single oscillator which is not fully optimized. Similar results have been reported by another power combiner [22]. The *H*-plane field pattern and cross-polarization measurements at 9.6 GHz are shown in Fig. 9 for the combiner. The 3 dB beamwidth of the array was 53 degrees compared to 78 degrees for a single element. To the best of our knowledge, these results represent the first wideband varactor-tunable power combiner reported in literature.

## V. Conclusion

The Gunn device has been integrated with a stepped-notch antenna using a CPW resonator. The configuration was modified to incorporate a varactor diode and form a varactor-turned active antenna element. Over 14% electronic tuning range was achieved with a fairly constant power output. Two of these varactor-tuned active antenna elements were successfully injection-locked to each other via mutual coupling and power combined throughout the wide electronic tuning range with over 70% combining efficiency.

These circuits offer a small, simple, lightweight, low-cost, reproducible, and truly planar active wideband tunable source for many microwave applications. Using these elements in planar arrays with injection-locking and power combining techniques will enable higher power levels. The wide varactor tuning range should prove useful for frequency modulated communication links, radar, and electronic warfare applications. The circuits are amenable to monolithic circuit integration for mass production and should have many applications in frequency-agile transmitters at microwave and millimeter-wave bands.

## Acknowledgment

The authors would like to thank Mr. R. C. Waits for his instruction and use of the fabrication facilities. The

authors would also like to thank Mr. J. C. McCleary and Mr. K. A. Hummer for many valuable discussions and suggestions.

## REFERENCES


[1] K. Chang, K. A. Hummer, and J. L. Klein, "Experiments on injection locking of active antenna elements for active phased arrays and spatial power combiners," *IEEE Trans. Microwave Theory Tech.*, vol. 37, no. 7, pp. 1078-1084, July 1989.

[2] R. A. York and R. C. Compton, "Quasi-optical power combining using mutually synchronized oscillator arrays," *IEEE Trans. Microwave theori Tech.*, vol. 39, no. 6, pp. 1000-1009, June 1991.

[3] Z. B. Popovic, R. M. Weikle II, M. Kim, K. A. Potter, and D. B. Rutledge, "Bar-grid oscillators," *IEEE Trans. Microwave Theory Tech.*, vol. 38, no. 3, pp. 225-230, Mar. 1990.

[4] J. W. Mink, "Quasi-optical power combining of solid-state millimeter-wave sources," *IEEE Trans. Microwave Theory Tech.*, vol. MTT-34, pp. 273-279, Feb. 1986.

[5] S. Young and K. D. Stephan, "Stabilization and power combining of planar microwave oscillators with an open resonator," in *1987 IEEE MTT-S Int. Microwave Symp. Dig.*, pp. 185-188.

[6] K. Chang and C. Sun, "Millimeter-wave power-combining techniques," *IEEE Trans. Microwave Theory Tech.*, vol. MTT-31, no. 2, pp. 91-107, Feb. 1983.

[7] H. J. Thomas, D. L. Fudge, and G. Morris, "Gunn source integrated with a microstrip patch," *Microwave and RF*, vol. 24, pp. 87-89, Feb. 1985.

[8] T. O. Perkins, "Active microstrip circular patch antenna," *Microwave J.*, vol. 30, pp. 110-117, Mar. 1987.

[9] J. Birkeland and T. Itoh, "Planar FET oscillators using periodic microstrip patch antennas," *IEEE Transactions on Microwave Theory and Techniques*, vol. 37, no. 8, pp. 1232-1236, Aug. 1989.

[10] K. Chang, K. A. Hummer, and G. Gopalakrishnan, "Active radiating element using FET source integrated with microstrip path antenna," *Electron. Lett.*, vol. 24, no. 21, pp. 1347-1348, Oct. 13, 1988.

[11] J. S. Joshi, "Wide-band varactor-tuned X-Band Gunn Oscillators in full-height waveguide cavity," *IEEE Trans. Microwave Theory Tech.*, vol. MTT-21, no. 3, pp. 137-139, Mar. 1973.

[12] D. Rubin, "Varactor-tuned millimeter-wave MIC oscillator," *IEEE Trans. Microwave Theory Tech.*, vol. MTT-24, no. 11, pp. 866-867, Nov. 1976.

[13] K. S. Yngvesson, T. L. Korzeniowski, Y. S. Kim, E. L. Kollberg, and J. F. Johansson, "The tapered slot antenna-a new integrated element for millimeter-wave applications," *IEEE Trans. Microwave Theory Tech.*, vol. 37, no. 2, pp. 364-374, Feb. 1989.

[14] P. J. Gibson, "The Vivaldi Aerial," in *Proc. 9th European Microwave Conf.*, Brighton, UK, 1979, pp. 101-105.

[15] R. Janaswamy, D. H. Schaubert, and D. M. Pozar, "Analysis of the Transverse Electromagnetic Mode Linearly Tapered Slot Antenna," *Radio Science*, vol. 21, no. 5, pp. 797-804, Sept.-Oct. 1986.

[16] H. Jingxi and F. Zhibo, "Analysis of Vivaldi antennas," in *Proc. IEE 6th Int. Conf. on Antennas and Propagation*, pt. 1, 1989, pp. 206-208.

[17] R. Janaswamy and D. H. Schaubert, "Characteristic impedance of a wide slot-line on low permittivity substrates," *IEEE Trans. Microwave Theory Tech.*, vol. MTT-34, pp. 900-902, Aug. 1989.

[18] U. Guttich, "Planar integrated 20 GHz receiver in slotline and coplanar waveguide technique," *Microwave and Optical Technology Letters*, vol. 2, no. 11, pp. 404-406, Nov. 1989.

[19] K. C. Gupta, R. Garg, and I. J. Bahl, Microstrip Lines and Slotlines Norwood, MA: Artech House, 1979, p. 294.

[20] K. Chang, K. Louie, A. J. Grote, R. S. Tahim, M. J. Mlinar, G. M. Hayashibara, and C. Sun, "V-band low-noise integrated circuit receiver," *IEEE Trans. Microwave Theory Tech.*, vol. MTT-31, pp. 146-154, Feb. 1983.

[21] R. Adler, "A study of locking phenomena in oscillators," in *Proc. IRE*, vol. 34, pp. 351-357, June 1946.

[22] A. Mortazawi and T. Itoh, "A periodic planar Gunn diode power combiner oscillator," *IEEE Trans. Microwave Theory Tech.*, vol. 38, pp. 86-87, Jan. 1990.


**Julio A. Navarro** [redacted]

B.S.E.E. and M.S.E.E. from Texas A&M University in 1988 and 1990, respectively.

He was a Co-op Student with General Dynamics-Fort Worth from May 1985 to February 1991. At General Dynamics, he worked in Avionic Systems Design, Advanced Technology and Systems Engineering, Emitters and Intelligence, Antenna Systems and Radar Cross Section Research. He is presently a Teaching and Research Assistant at Texas A&M. As a Research Assistant, he has designed varactor tunable endfire radiating elements, switchable and tunable uniplanar filters and varactor tunable Gunn VCOs. He has also developed Ka-band aperture-coupled circular path antennas for a NASA-Lewis-Texas Instruments project. His current research interests include high-Q uniplanar resonators and quasi-optical power combiners. He holds an NSF Engineering Fellowship and is currently pursuing the Ph.D. degree under the direction of Dr. Kai Chang.

**Yonghui Shu** [redacted]. He received the B.S. and M.S. degrees in electrical engineering from the Nanjing Institute of Technology, Nanjing, China in 1982 and 1985, respectively.

From March 1985 to July 1989, he worked for the Department of Radio Engineering of Nanjing Institute of Technology (current name, Southeast University) as a Lecturer. From August 1989 to July 1990, he was with the Department of Electrical Engineering of Texas A&M University as a Research Associate. In August 1990, he joined Epsilon Lambda Electronics Corporation, Geneva, IL, as a Microwave Design Engineer. His current interests are in microwave and millimeter-wave devices, circuits and subsystems.

Mr. Shu has published 20 technical papers in microwave and millimeter-wave areas.

**Kai Chang** (S'75-M'76-SM'85-F'91) received the B.S.E.E. degree from the National Taiwan University, Taipei, Taiwan; the M.S. degree from the State University of New York at Stony Brook; and the Ph.D. degree from the University of Michigan, Ann Arbor, in 1970, 1972, and 1976, respectively.

From 1972 to 1976, he worked for the Microwave Solid-State Circuits Group, Cooley Electronics Laboratory of the University of Michigan as a Research Assistant. From 1976 to 1978, he was employed by Shared Applications, Inc., Ann Arbor, where he worked in computer simulation of microwave circuits and microwave tubes. From 1978 to 1981, he worked for the Electron Dynamics Division, Hughes Aircraft Company, Torrance, CA., where he was involved in the research and development of millimeter-wave solid-state devices and circuits, power combiners, oscillators and transmitters. From 1981 to 1985, he worked for the TRW Electronics and Defense, Redondo Beach, CA., as a Section Head, developing state-of-the-art millimeter-wave integrated circuits and subsystems including mixers, VCO's, transmitters, amplifiers, modulators, upconverters, switches, multipliers, receivers, and transceivers. He joined the Electrical Engineering Department of Texas A&M University in August 1985 as an Associate Professor and was promoted to a Professor in 1988. In January 1990, he was appointed E-Systems Endowed Professor of Electrical Engineering. His current interests are in microwave and millimeter-wave devices and circuits, microwave integrated circuits, microwave optical interactions, and antennas.

Dr. Chang served as the editor of the four-volume "Handbook of Microwave and Optical Components" published by John Wiley & Sons, Inc. in 1989 and 1990. He is the editor of the Microwave and Optical Technology Letters and the Wiley Book Series in Microwave and Optical Engineering. He has published over 130 technical papers and several book chapters in the areas of microwave and millimeter-wave devices and circuits. Dr. Chang received the Special Achievement Award from TRW in 1984, the Halliburton Professor Award in 1988 and the Distinguished Teaching Award in 1989 from the Texas A&M University.

# Theoretical and Experimental Development of 10 and 35 GHz Rectennas

Tae-Whan Yoo and Kai Chang, *Fellow, IEEE*

*Abstract*—**A 35 GHz rectenna has been developed with 39% conversion efficiency. The rectenna uses a microstrip dipole antenna and a commercially available mixer diode. Over 60% conversion efficiency was demonstrated using this diode at 10 GHz. A theoretical analysis was derived to predict the performance of the rectenna. The analysis is a useful tool for device and circuit design. The theoretical and experimental results should have many applications in microwave power transmission and detection.**

## I. Introduction

THE AVAILABILITY of power for use in space is a key requirement for future space activities. The current method of power generation with solar panels or batteries on board of each satellite has many difficulties in packaging the power system, unfolding them in space, and achieving a high output power. Power becomes a limiting factor in the design of most systems. To overcome these problems, a potential method may be to deploy a Utility Power Satellite (UPS) in space. The UPS will generate power using solar, nuclear or other techniques. The power would then be converted into microwave or laser beams, transmitted through a free space and converted back into a useful form of energy for users.

The laser beam has an advantage of the small beam divergency. However, the efficiencies in generating the laser beam and converting it back into electrical energy are low compared with those of microwave. Therefore, the development of power transmission system by microwave beams is attracting new attention in space application.

The rectenna (rectifier + antenna) which receives and converts microwave power into dc power is a key element of this power transmission system. Since the rectenna was invented [1] it has been improved through studies [2], [3] and used for various applications such as the microwave powered helicopter [4], the receiving array for Solar Power Satellite [5], and the experiment on the microwave powered aircraft which was recently conducted by Canada under the project name of SHARP (Stationary High Altitude Relay Platform) [6]. As a result, the structure of rectenna has been evolved from a bulky bar-type to a planar thin-film type greatly reducing the weight to power output ratio [7]. The typical power conversion efficiency achieved is 85% at 2.45 GHz.

The rectifying process is a nonlinear process. It is difficult to figure out how the rectenna circuit is optimized for the maximum conversion efficiency. There were several theoretical analyses to solve this problem. These analyses can be divided into two methods. One is to directly simulate the rectenna circuit in time domain [8]. The other is to find a closed-form equation which can explain the relationship between diode parameters and the conversion efficiency [9], [10]. A computer simulation in [8] sucessfully showed the conversion efficiency lager than 80% at 2.5 GHz. A mathematical model in [9] was derived to relate the power conversion efficiency with the conduction period of diode. A fixed relationship between the dc output voltage and the RF input voltage was assumed and the conduction period was unknown. A closed-form for efficiency in [10] was derived by expanding the current-voltage ($I$–$V$) equation of diode with the diode voltage. But this is valid only for a high-efficiency rectenna since short turn-on period was assumed.

All these studies were concentrated on 2.45 GHz. Considering that the frequencies below 3 GHz are not strongly attenuated by the atmosphere even under a severe weather condition [11], 2.45 GHz is thought of as a proper frequency for the application of power transmission between ground-to-ground, ground-to-space, and space-to-ground. However, for the space-to-space application the operating frequency can be increased to allow power transmission over much longer distances with the smaller antenna and rectenna. Although the efficiencies of rectenna and generator are low at 35 GHz, the advantages of size reduction and longer transmission distance overcome the low device conversion efficiencies. The overall system efficiency is thus higher at 35 GHz than 2.45 GHz for long distance transmission using the same size of antenna and rectenna [12].

In this paper we report theoretical analysis and experimental results on 10 and 35 GHz rectenna. A closed-form equation for the conversion efficiency has been derived to analyze the diode for the high frequency rectenna. To derive the closed-form equation we assumed that the effects of harmonics higher than or equal to the second order were small and the forward voltage drop of the diode didn't change during the turn-on period. The closed-form equation was validated by comparing it with a nonlinear circuit

Manuscript received May 22, 1991; revised October 24, 1991. This work was supported in part by the NASA Center for Space Power and the Army Research Office.

The authors are with the Department of Electrical Engineering, Texas A&M University, College Station, TX 77843-3128.

IEEE Log Number 9107446.

simulation computer program called LIBRA developed by EEsof Inc.. The maximum efficiency limited by the parasitic series resistance and the junction capacitance of a diode has been calculated using the closed-form equation. It was possible to interpret the cutoff frequency of a diode as a parameter to limit the highest operating frequency of the diode in the power conversion circuit as a result of this calculation. This result of closed-form equation will be useful to select or design a diode for rectenna at any arbitrary frequency.

A 35 GHz dipole rectenna has been designed with the closed-form equation and LIBRA which uses a Harmonic Balance method to solve a nonlinear circuit. The overall conversion efficiency of rectenna was measured using the waveguide array simulator. The dc power was 39% of the input power of 51 mW and the reflected power was 12% of the incident power. The incident power includes both the input power to the rectenna diodes and the reflected power. The power conversion efficiency of the diode at 10 GHz was measured by sending the power through a coaxial line. The highest efficiency was measured as 60%, which was consistent with the simulation result with LIBRA. The devices used were commerically available mixer diodes which are not optimized for this application. It is believed that higher efficiency could be achieved with optimized devices.

## II. Closed-Form Equation for the Conversion Efficiency

### A. Basic Circuit Structure of Rectenna

The basic structure of a rectenna is shown in Fig. 1. The low pass filter inserted between the antenna and rectifying circuit is designed so that the fundamental frequency can be passed and a significant portion of the higher order harmonics generated from the nonlinear rectifying circuit be rejected back to the rectifying circuit. The rectifying circuit consists of a single diode shunt-connected across the transmission lines.

The basic principle of the microwave power conversion by ths rectifying circuit is analogous to a diode clamping circuit or a large signal mixer at microwave frequencies. The power conversion efficiency is maximized by substantially confining all the higher order harmonics between the low pass filter and the dc pass filter, using an efficient diode and matching the diode's input impedance to antenna's input impedance.

The power conversion efficiency of a diode changes as the operating power level changes. The power conversion efficiency of a rectenna generally changes with the input power as shown in Fig. 2. $V_j$, $V_{br}$, and $R_L$ are the forward voltage drop (junction voltage), the breakdown voltage of the diode, and the dc load resistance of the rectenna, respectively. The efficiency is small in the low power region because the voltage swing at the diode is below or comparable with the forward voltage drop of the diode. The efficiency increases as the power increases and levels off with the generation of strong higher order harmonics.

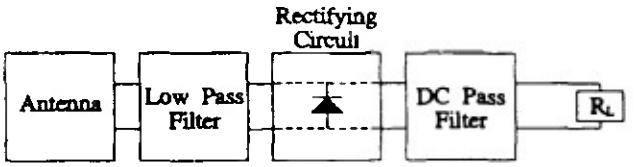


Fig. 1. Block diagram of a rectenna circuit.

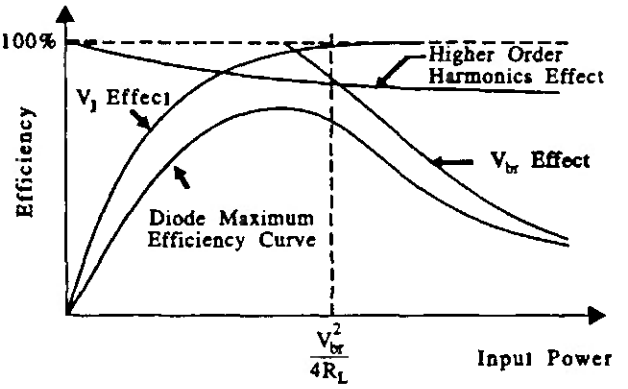


Fig. 2. General relationship between microwave to dc power conversion efficiency and input power.

The efficiency sharply decreases as the voltage swing at the diode exceeds the breakdown voltage ($V_{br}$) of the diode. The critical input power where the breakdown effect becomes dominant is expressed as $V_{br}^2/4R_L$ in Fig. 2.

The three parameters of diode such as $V_{br}$, zero-biased junction capacitance ($C_{jo}$), and series resistance ($R_S$) determine the power conversion efficiency of rectenna. These parameters are related with each other due to the diode material properties [13]. The breakdown voltage of a diode used for a 2.45 GHz rectenna is on the order of 60 V. The $C_{jo}$ and $R_S$ with this breakdown voltage are several pF and less than 1 Ω respectively which are small enough to operate at 2.45 GHz. The breakdown voltage is much larger than the junction voltage of the diode which is about 0.8 V. Therefore the efficiency of the efficiency vs input power curve in Fig. 2 can increase nearly to 100% before reaching at the region where the breakdown effect is dominant. For 35 GHz rectenna, $C_{jo}$ should be reduced to the order of 0.1 pF. But this reduction results in the increase of $R_S$ and the decrease of $V_{br}$. The typical value of $V_{br}$ of a *Ka*-band mixer diode is 10 V with $R_S$ of 4–8 Ω and $C_{jo}$ of 0.1 pF. The efficiency would be low with this small value of $V_{br}$ because the junction voltage effect is still not negligible even at the maximum efficiency point of the efficiency vs input power curve as illustrated in Fig. 2. Consequently, it is important to have a good trade-off between the diode parameters in designing a diode. The closed-form equation derived in the next subsection will be useful to design a diode for a high frequency rectenna.

### B. Derivation of Closed-form Equation for Conversion Efficiency

The equivalent circuit of the Schottky diode is shown in Fig. 3. The diode consists of a series resistor ($R_S$), a

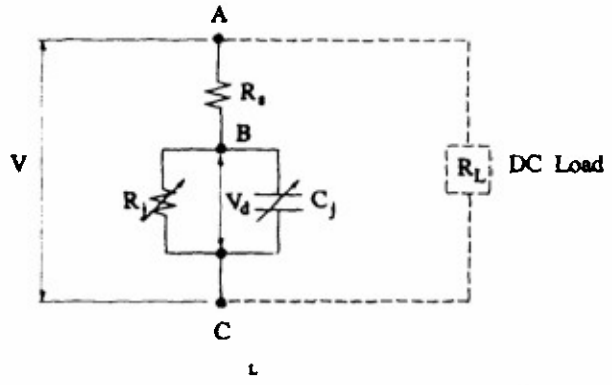


Fig. 3. Equivalent circuit of a *Ka*-band beamlead Schottky diode used for the derivation of a closed-form equation. $R_j$ and $C_j$ model the intrinsic junction for the diode. $R_S$ is the parasitic series resistance of the diode and $R_L$ is the dc load.

nonlinear resistor ($R_j$) described by the $I$–$V$ relationship of a diode at dc, and a nonlinear junction capacitance ($C_j$). The reactive parasitic elements of the physical diode are excluded from this model because they can be tuned out without affecting the rectifying efficiency. The closed-form expressions for the rectifying efficiency and the effective microwave impedance of the diode are derived with the following assumptions:

1) The voltage $V$ applied between node $A$ and $C$ consists of the dc term and the fundamental frequency only.
2) The current due to the junction capacitance is negligible when the diode is forward biased.
3) The forward voltage drop across the intrinsic diode junction is constant during the forward-bias period.

The first assumption is reasonable considering that the magnitude of the higher order harmonics is usually small compared to those of the dc and fundamental components. The second assumption is based on the fact that the change of $V_d$ in Fig. 3 is small during the forward-bias period.

Under these assumptions, the voltage waveform of $V$ and $V_d$ can be expressed as follows:

$$V = -V_0 + V_1 \cos(\omega t) \tag{1}$$

$$V_d = \begin{cases} -V_{d0} + V_{d1} \cos(\omega t - \phi), & \text{if diode is off} \\ V_f & \text{if diode is on.} \end{cases} \tag{2}$$

The voltage $V_0$ in (1) is the output dc voltage and the voltage $V_1$ is the peak voltage of an incident microwave. $V_{d0}$ and $V_{d1}$ are the dc and the fundamental frequency components of diode junction voltage $V_d$, respectively, when the diode is off. $V_f$ is the forward voltage drop of the diode when the diode is on. $V_0$ is known by specifying the output dc power. The efficiency and the diode effective impedance are calculated by relating the other variables such as $V_1$, $V_{d0}$, $V_{d1}$, and $\phi$ to the known variable of $V_0$.

By applying Kirchoff's voltage law along the dc-pass loop shown as a dotted line in Fig. 3, the dc voltage ($-V_{d\,DC}$) of $V_d$ is related to the dc component of $V$ according to

$$V_0 = \frac{V_{d,DC}}{1 + r} \tag{3}$$

where $r = R_s/R_L$ and $R_L$ is the dc load resitance as shown in Fig. 3. $V_{d,DC}$ introduced here is the average value of the waveform $V_d$, and $V_{d0}$ in (2) is the dc component of the waveform $V_d$ in turn-off period. Therefore, $V_{d,DC}$ is derived by taking an average of $V_d$ over one full period as

$$V_{d,DC} = V_{d0}\left(1 - \frac{\theta_{off}}{\pi}\right) + \frac{V_{d1}}{\pi} \sin\theta_{off} - V_f \frac{\theta_{off}}{\pi} \tag{4}$$

where $\theta_{off}$ is the phase angle where the diode is turned off as shown in Fig. 4. The phase variable $\theta$ is defined as $\theta = \omega t - \phi$. Since the switching of the diode occurs when $V_d$ is equal to the forward voltage drop $V_f$ of the diode, $\theta_{off}$ is calculated by

$$\cos\theta_{off} = \frac{V_f + V_{d0}}{V_{d1}}. \tag{5}$$

On the other hand, the equation for the current flowing through $R_S$ is written as follows when the diode is off:

$$R_S \frac{d(C_j V_d)}{dt} = V - V_d. \tag{6}$$

Since $C_j$ is a monotonic increasing funtion of $V_d$, $C_j$ can be expanded as follows:

$$C_j = C_0 + C_1 \cos(\omega t - \phi) + C_2 \cos(2\omega t - 2\phi) + \cdots. \tag{7}$$

Substituting $C_j$ into (6) with a Fourier series of (7) and neglecting the terms higher than the second harmonic, the equation becomes

$$\omega R_S(C_1 V_{d0} - C_0 V_{d1}) \sin(\omega t - \phi) = V_{d0} - V_0 + (V_1 \cos\phi - V_{d1}) \cos(\omega t - \phi) - V_1 \sin\phi \sin(\omega t - \phi). \tag{8}$$

Since the above equation should hold during the off period of the diode, each term should separately zero:

$$V_{d0} = V_o \tag{9a}$$

$$V_{d1} = V_1 \cos\phi \tag{9b}$$

$$V_1 \sin\phi = \omega R_S(C_0 V_{d1} - C_1 V_{d0} + C_2 V_{d1}). \tag{9c}$$

The phase delay is obtained from (9) as follows:

$$\phi = \arctan\left[\omega R_S\left(C_0 - \frac{C_1 \cos\theta_{off}}{1 + v_f} + C_2\right)\right] = \arctan(\omega R_S C_{eff}) \tag{10}$$

where $v_f = V_f/V_0$. From (3), (4), (5), and (9a), the relationship between $\theta_{off}$ and $r$ is derived as

$$\frac{\pi r}{1 + v_f} = \tan\theta_{off} - \theta_{off}. \tag{11}$$

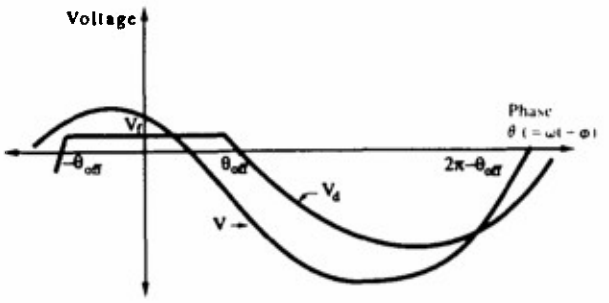


Fig. 4. Simplified time-domain waveform of voltage V and $V_d$. $V_d$ is the voltage between intrinsic diode. V is the voltage between A and C of Fig. 3. Variable $\theta$ is defined as $\theta = \omega t - \phi$.

$\theta_{off}$ is determined by the ratio of $R_S$ to $R_L$ and the ratio of the forward voltage drop $V_f$ to the dc output voltage $V_0$. $V_f$ is solved with the $I$–$V$ relation of the diode:

$$I_s\left(\exp\left(\frac{eV_f}{nkT}\right) - 1\right) = \frac{-V_0 + V_1 - V_f}{R_S} \tag{12}$$

$V_1$ in (12) is a function of $\theta_{off}$ and therefore $V_f$ cannot be solved without first knowing $\theta_{off}$. However, since the left term is of exponential form $V_f$ does not vary significantly from the cut-in voltage of the diode which is about 0.6 to 0.8 V for a GaAs-Pt Schottky diode. Therefore, $\theta_{off}$ is solved from (11) substituting $V_f$ with a typical value of the cut-in voltage of the diode.

Once $\theta_{off}$ is solved from a given $V_0$, $R_S$, and $R_L$, the efficiency and the input impedance can be calculated from the time domain waveform $V$ and $V_d$. These waveforms are expressed as a function of $\theta_{off}$, diode parameters, and $V_0$ or $V_1$.

$$P_{DC} = \frac{V_0^2}{R_L}$$

$$P_{loss} = \mathrm{LOSS}_{on,R_S} + \mathrm{LOSS}_{on,diode} + \mathrm{LOSS}_{off,R_S} + \mathrm{LOSS}_{off,diode}$$

$$\mathrm{LOSS}_{on,R_S} = \frac{1}{2\pi}\int_{-\theta_{off}}^{\theta_{off}} \frac{(V - V_f)^2}{R_S}\, d\theta$$

$$\mathrm{LOSS}_{on,diode} = \frac{1}{2\pi}\int_{-\theta_{off}}^{\theta_{off}} \frac{(V - V_f)V_f}{R_S}\, d\theta$$

$$\mathrm{LOSS}_{off,R_S} = \frac{1}{2\pi}\int_{\theta_{off}}^{2\pi-\theta_{off}} \frac{(V - V_d)^2}{R_S}\, d\theta$$

$$\mathrm{LOSS}_{off,diode} = \frac{1}{2\pi}\int_{-\theta_{off}}^{2\pi-\theta_{off}} \frac{(V - V_d)V_d}{R_S}\, d\theta$$

$$efficiency = \frac{P_{DC}}{P_{loss} + P_{DC}} \tag{13}$$

where the variable $\theta$ is substituted for $\omega t - \phi$. The current ($I$) flowing through $R_S$ can be expressed as follows:

$$I = I_0 + I_{1r}\cos(\omega t) + I_{1i}\sin(\omega t)$$

$$I_0 = \frac{1}{2\pi R_S}\left\{\int_{-\theta_{off}}^{\theta_{off}} (V - V_f)\, d\theta + \int_{\theta_{off}}^{2\pi-\theta_{off}} (V - V_d)\, d\theta\right\}$$

$$I_{1r} = \frac{1}{\pi R_S}\left\{\int_{-\theta_{off}}^{\theta_{off}} (V - V_f)\cos(\theta + \phi)\, d\theta + \int_{\theta_{off}}^{2\pi-\theta_{off}} (V - V_d)\cos(\theta + \phi)\, d\theta\right\}$$

$$I_{1i} = \frac{1}{\pi R_S}\left\{\int_{-\theta_{off}}^{\theta_{off}} (V - V_f)\sin(\theta + \phi)\, d\theta + \int_{\theta_{off}}^{2\pi-\theta_{off}} (V - V_d)\sin(\theta + \phi)\, d\theta\right\}. \tag{14}$$

The input admittance of the diode at the fundamental frequency is calculated as

$$Y = \frac{I_{1r} - jI_{1i}}{V_1}. \tag{15}$$

If the susceptance part resonates with the dc pass filter in Fig. 1, the input impedance to be matched to the antenna becomes the inverse of real part of $Y$.

To validate the closed-form equation the conversion efficiency calculated with the closed-form equation was compared with the results simulated by a nonlinear circuit computer program (LIBRA). The efficiency of the diode as defined by the ratio of output dc power to the net power transmitted to the rectenna is compared in Fig. 5 for 10 and 35 GHz. The diode parameters used for the calculation are summarized in Table I. Since the effect of $V_{br}$ was not included in the closed-form equation, the efficiency calculation using the closed-form equation terminated when the negative peak of the diode junction voltage reached $V_{br}$. At 10 GHz the efficiency calculated with the closed-form equation is close to the efficiency calculated with LIBRA. At 35 GHz there is relativly big difference in efficiency showing approximatly 10% of difference in the region where the efficiency calculated with LIBRA is not affected by the finite $V_{br}$. Increase of the difference at 35 GHz is considered to be caused by the effect of nonlinear junction capacitance which becomes dominant at the high frequency. The closed-form equation is not accurate enough to be used for the design of the high frequency rectenna. However, it can be used to estimate the preliminary efficiency of rectenna with any kind of diode at any arbitrary frequency. This is important because it predicts the efficiency level achievable through the nonlinear circuit optimization which usually takes a long time. It also explains how the efficiency is decreased by breaking down the power dissipation mechanism in the diode. In the next subsection we calculated the power conversion efficiency of an ideal diode using the closed-form equation.

### C. Power Conversion Efficiency of Ideal Diode

The power conversion efficiency of an ideal diode with a finite $R_S$ and $C_j$ was calculated using the closed-form

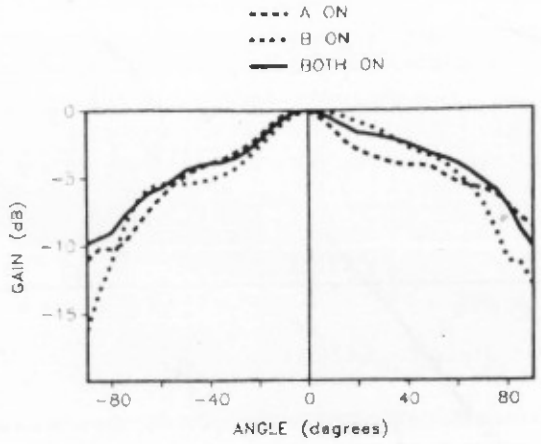


Fig. 13. *H*-plane pattern of a two-element aperture-coupled active array.

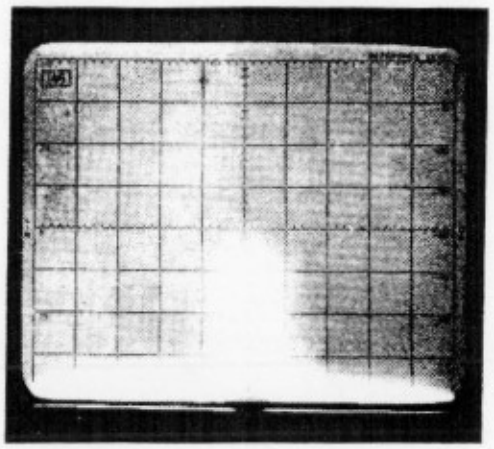

(a)

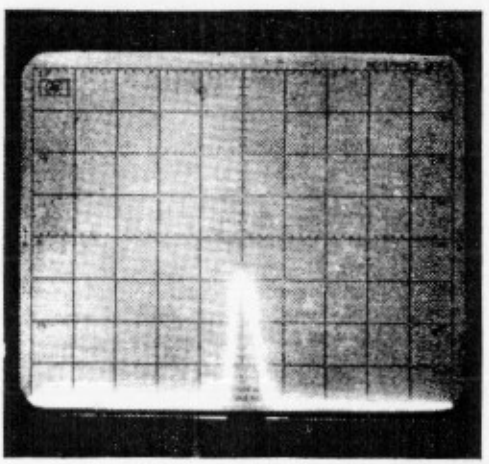

(b)

Fig. 14. Oscillator spectra (a) before and (b) after injection locking. Vertical: 10 dB/div. Horizontal: 100 kHz/div. Center frequency: 2.384 GHz.

injection lock the free-running oscillator by mutual coupling.

Fig. 12 shows the *E*-plane pattern of the active array when only the sweeper is "on," when only the oscillator is "on," and when both sources are "on." When one of the sources was disengaged, a 3 dB beam width of about 90° was measured. This beam width was reduced to 65° when both sources were "on." Furthermore, the power with both sources operating was about 2 dB higher than the power with any single source operating. This shows that the array is exhibiting good power-combining properties. With both sources on, the main lobe is centered at roughly 25°. This off-center condition is due to the different lengths of the transmission lines used to connect antennas and sources. A phase difference thus exists between the two sources. This difference can be adjusted and overcome by the use of a transmission line section or phase shifter.

Fig. 13 shows the *H*-plane pattern of the array. It can be seen that no matter which sources are operating, the antenna pattern remains relatively unchanged. This is to be expected since the antennas are arranged for *E*-plane coupling. Very little *H*-plane coupling can be expected. The antenna *H*-plane beam width was about 120°.

The injection locking through mutual coupling was also demonstrated. Fig. 14 shows the oscillator spectra before and after the injection locking. It can be seen that injection locking has a dramatic effect in reducing oscillator noise. The locking bandwidth was measured to be 2.15 MHz. Assuming an injection-locking gain of 20 dB, the locking bandwidth corresponds to an external $Q$ factor of 217. The narrow locking bandwidth and high $Q$ factor are believed to be due to the high-$Q$ transistor oscillator.

## VII. Conclusions

Two types of active antenna elements have been investigated. The first type uses active devices directly mounted on the antennas. The second type uses an aperture-coupled microstrip to patch antenna circuit which can be used to accommodate a transmit–receive module. A two-element array was built and demonstrated in both cases. Injection locking was achieved by using either mutual coupling or an external master source. Good power-combining efficiency was achieved for both circuits. An electronic tuning range of over 9 percent was achieved for the single active antenna element and of about 1 percent for a two-element array.

## Acknowledgment

The authors would like to thank X. Gao and Dr. R. D. Nevels for many helpful discussions.

## References

[1] K. J. Russell, "Microwave power combining techniques," *IEEE Trans. Microwave Theory Tech.*, vol. MTT-27, pp. 472–478, May 1979.

[2] K. Chang and C. Sun, "Millimeter-wave power combining techniques," *IEEE Trans. Microwave Theory Tech.*, vol. MTT-31, pp. 91–107, Feb. 1983.

[3] J. W. Mink, "Quasi-optical power combining of solid-state millimeter-wave sources," *IEEE Trans. Microwave Theory Tech.*, vol. MTT-34, pp. 273–279, Feb. 1986.

[4] H. C. Johnson, R. E. Marx, A. Sanchez, and E. Mykietyn, "A circularly polarized active antenna array using miniature GaAs FET amplifiers," in *1984 IEEE-MTT-S Int. Microwave Symp. Dig.*, pp. 260–262.

[5] C. R. Green *et al.*, "A 2 watt GaAs TX/RX module with integral control circuitry for *S*-band phased array radars," in *1987 IEEE-MTT-S Int. Microwave Symp. Dig.*, pp. 933–936.

The low pass filter which consists of three transmission line sections was optimized using TOUCHSTONE. The cutoff frequency of the low pass filter was located between the fundamental and the second order harmonic. Because the coplanar strip line was not available in TOUCHSTONE, an ideal transmission line was substituted for the optimization. The ideal transmission line was converted to the physical transmission line using the closed-form equation in [15]. The dimensions of the transmission lines are shown in Table II. The Duroid substrate was 10 mils thick with a 2.2 dielectric constant.

The efficiency and the reflected power have been calculated through the nonlinear circuit simulation (LIBRA). The circuit model for the simulation is shown in Fig. 7. The efficiency was maximized by adjusting $L4$ of the dc pass filter. The optimum length of $L4$ was 0.022 $\lambda_o$. The circuit configuration and the photograph of the actual circuit are shown in Fig. 8. The circuit was fabricated on a substrate having a thin (10 $\mu$m) copper layer because the smallest gap of the circuit was 100 $\mu$m. This thickness is still 30 times larger than the substrate skin depth at 35 GHz. The circuit was etched using the conventional method and a beamlead diode was mounted on the circuit with a silver epoxy.

### C. 35 GHz Rectenna Measurements

The overall efficiency is defined as the ratio of the output dc power to the incident power. The incident power includes both input power to the rectenna diode and reflection power. A waveguide array simulation technique [16] was used to measure the overall efficiency. This technique permits the generation of high power densities and the accurate measurement of efficiency. The measurement setup is shown in Fig. 9. A special waveguide expander was fabricated to appropriately simulate the rectenna array. The smaller side of a *Ka*-band waveguide (WR-28) was enlarged to make the cross section at the end of the waveguide expander be square. The longer side was not expanded in order for the mainlobe of the simulated array to be located in the same direction as that of two plane waves constructing the $TE_{10}$ mode. The area of the expanded cross section was 0.28 inch by 0.28 inch. This area is 40% larger than the effective area of a dipole antenna located a quarter wavelength above a ground plane. Therefore, the actual reflection of the rectenna might be smaller than the value measured with this setup. A photo of waveguide expanded section, a quarter wavelength spacer and a reflecting ground plane are shown in Fig. 10. The quarter wavelength spacer was placed between the rectenna and the reflecting plane.

The measured data is plotted in Fig. 11. The circles show the measured efficiencies which are defined as the ratio of the dc output power to the input power into the diode. The simulated results have been plotted together for comparison. The theoretical efficiency with 100 Ω dc loads are better than those with 400 Ω loads. The highest

TABLE II
OPTIMIZED LENGTHS OF COPLANAR STRIP LINES OF 35 GHz RECTENNA

| L1 (mm) | L2 (mm) | L3 (mm) | L4 (mm) |
|---|---|---|---|
| 0.92 | 1.19 | 0.58 | 0.18 |

$Z_{high}$: 245 Ω Width: 0.2 mm Gap: 0.4 mm
$Z_{low}$: 130 Ω Width: 0.5 mm Gap: 0.1 mm

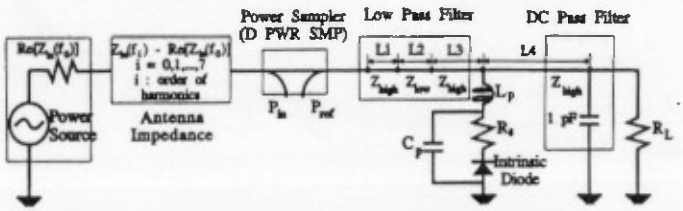


Fig. 7. Circuit model of 35 GHz dipole rectenna for the nonlinear circuit computer simulation (LIBRA). $Z_{in}(f_i)$: Antenna input impedance at the $i$th harmonic frequency. The real part of the antenna input impedance is used as a source resistance for the power source. The dual port power sampler (DPWRSMP) is used to measure the input and the reflected power.

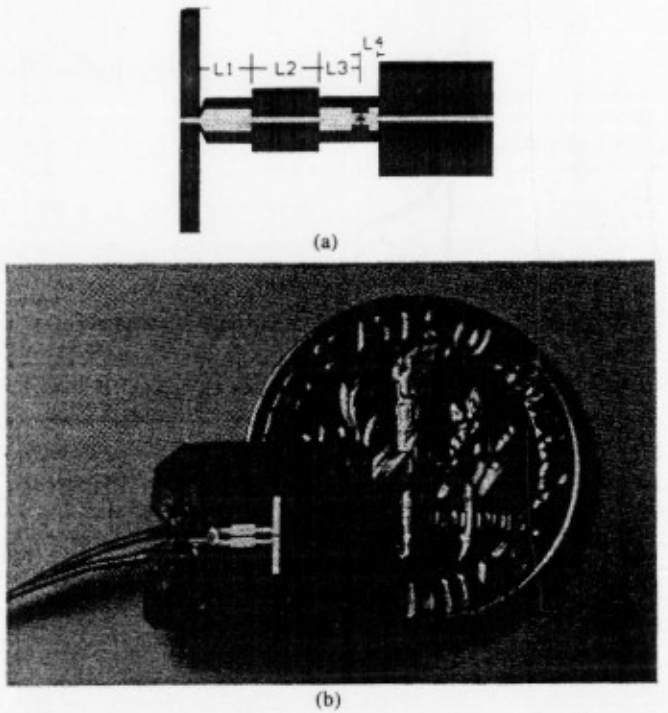


Fig. 8. 35 GHz dipole retenna. (a) Circuit configuration. (b) Photograph of an actual circuit.

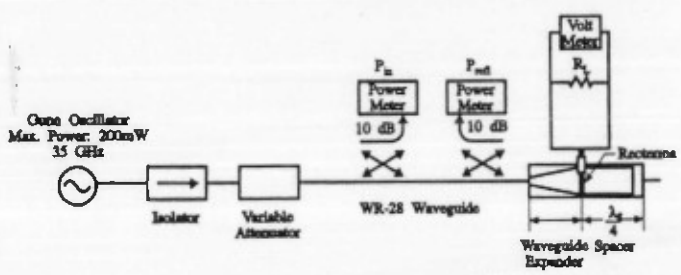


Fig. 9. Experimental setup for the measurement of the overall efficiency and the reflected power of a 35 GHz rectenna.

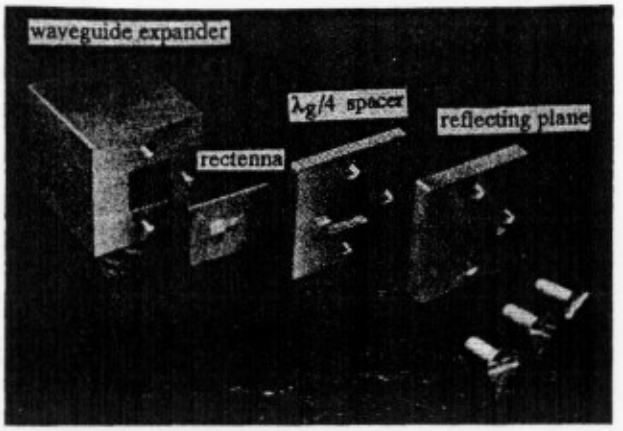


Fig. 10. A waveguide expanded section assembly consisting of a waveguide expander, a quarter wavelength spacer, and a reflecting plane.

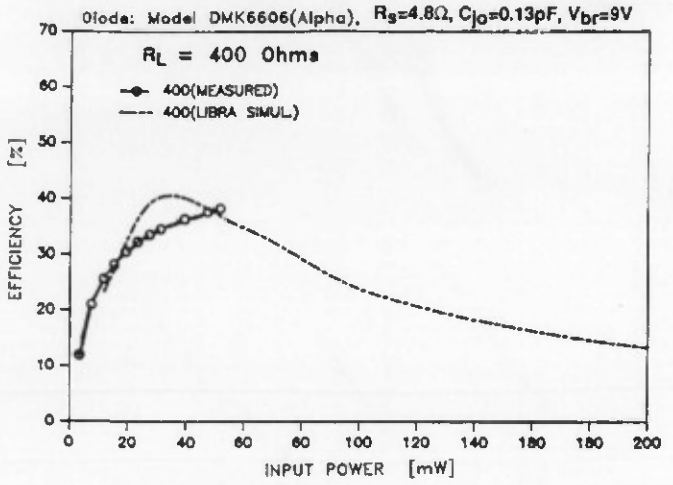


(a)

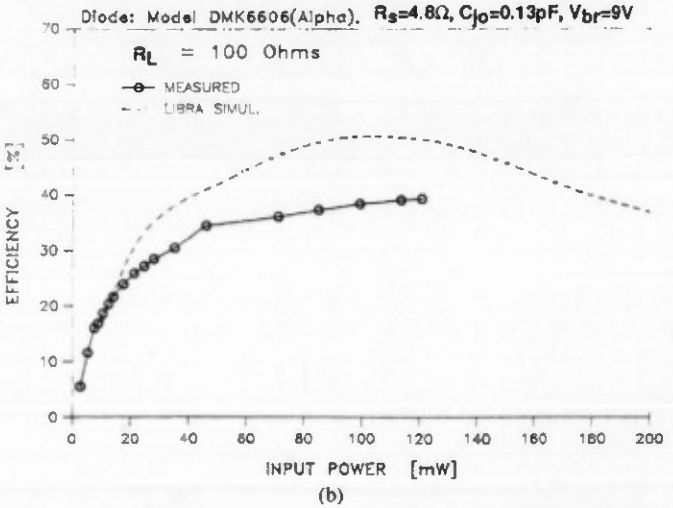


(b)

Fig. 11. 35 GHz to dc power conversion efficiency. (a) With a 400 Ω dc load. (b) With a 100 Ω dc load. The efficiencies calculated by LIBRA are plotted together to compare with the measured result. The diode parameters used for simulation are listed in Table I.

efficiency measured was 39%. The measured maximum efficiencies for 100 and 400 Ω loads are about the same. But the reflection power is 12% of the incident power at

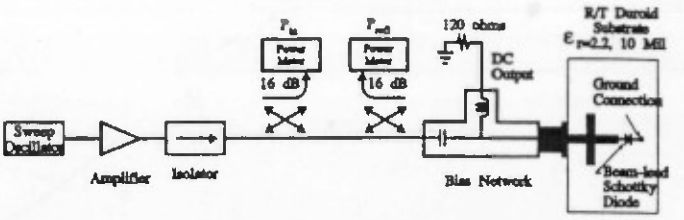


Fig. 12. Experimental setup for the measurement of the conversion efficiency of a *Ka*-band beam-lead diode at 10 GHz.

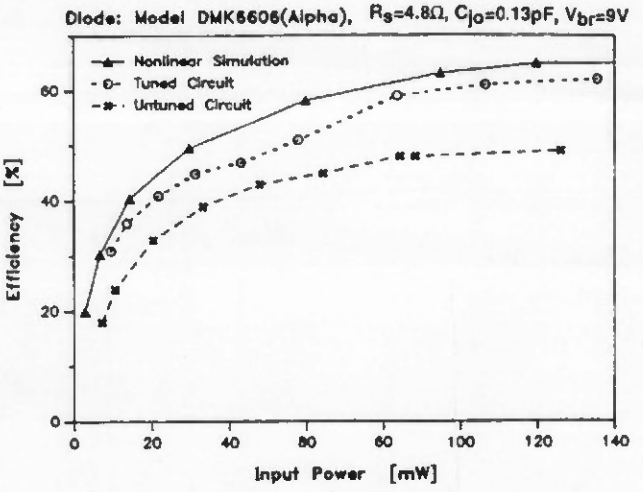


Fig. 13. 10 GHz to dc conversion efficiency of a *Ka*-band diode measured with 120 Ω dc load.

400 Ω load and 21% of the incident power at 100 Ω load. The reflection can be reduced in the array environment.

### *D. Measurement of Power Conversion Efficiency at 10 GHz*

The power conversion efficiency of a *Ka*-band diode (Model DMK6606, Alpha Industries) was measured at 10 GHz. A coaxial cable directional coupler and 50 Ω coaxial cables were used in the measurement as shown in Fig. 12. The circuit consisted of a 50 Ω microstrip transmission line and a beam-lead diode. One end of the beam-lead diode is connected to the end of microstrip line and the other end is connected to the ground plane through a hole. The dc output power was extracted using a bias-T network. The efficiency was measured with and without the open stub tuner illustrated in Fig. 12. The measured efficiencies are plotted in Fig. 13. There was approximatly 10% of improvement with the open stub tuner. The efficiency with the open stub tuner approaches 60% which is agreed with the results from nonlinear computer simulation results.

## IV. Conclusion

A 35 GHz rectenna has been developed with 39% of power conversion efficiency. The rectenna used a microstrip dipole and a *Ka*-band mixer diode. A computer program LIBRA was used to optimize the rectenna for the

high conversion efficiency. The net power conversion efficiency of the same diode was measured at 10 GHz using a simple rectifying circuit. The net conversion efficiency was 60%. If the impedance of a antenna is matched to a rectifying circuit, 60% efficiency would be possible at GHz with this diode. A closed-form equation was derived for the analysis of the high frequency rectenna by neglecting the higher order harmonics. In order to estimate the maximum efficiency limited by a finite $R_S$ and $C_{jo}$, a net conversion efficiency of an ideal diode with the same $R_S$ and $C_{jo}$ was calculated using the closed-form equation. With the *Ka*-band diode used for 35 GHz rectenna, the maximum efficiency was calculated to be approximatly 60% at 35 GHz. The actual maximum efficiency is smaller than this efficiency due to the effect of the finite forward voltage drop and the breakdown voltage.

## Acknowledgment

The constant encouragement of Dr. A. D. Patton is acknowledged. The authors would like to thank Mr. J. McSpadden for many helpful suggestions and reviewing the manuscript, Mr. W. C. Brown of Raytheon Company for useful discussion, Mr. Y. Shu and Mr. L. Fan for machining the hardware, and Dr. S. M. Wright for allowing us to use his computer program for antenna input impedance. The authors would also like to thank reviewers for making many useful suggestions.

## References

[1] W. C. Brown *et al.*, U.S. Patent 3 434 678, Mar. 25, 1969.
[2] W. C. Brown, "Experiment in the transport of energy by microwave beam," in *IEEE Int. Conv. Rec.*, vol. 12, pt. 2, Mar. 1964, pp. 8–18.
[3] ——, "The history of power transmission by radio waves," *IEEE Trans. Microwave Theory Tech.*, vol. 32, no. 9, pp. 1230–1242, Sept. 1984.
[4] ——, "Experiments involving a microwave beam to power and position a helicopter," *IEEE Trans. Aerosp. Electron. Syst.*, vol. AES-5, no. 5, pp. 692–702, Sept. 1969.
[5] ——, "Solar Power Satellite Program Rev. DOE/NASA Satellite Power System Concept Develop. Evaluation Program," Final Proc. Conf. 800491, July 1980.
[6] J. Schlesak, A. Alden and T. Ohno, "A microwave powered high altitude platform," in *IEEE MTT-S Int. Microwave Symp. Dig.*, 1988, pp. 283–286.
[7] W. C. Brown, "Performance characteristics of the thin-film, etched-circuit rectenna," in *IEEE MTT-S Int. Microwave Symp. Dig.*, 1984, pp. 365–367.
[8] J. J. Nahas, "Modeling and computer simulation of a microwave-to-dc energy conversion element," *IEEE Trans. Microwave Theory Tech.*, vol. 23, no. 12, pp. 1030–1035, Dec. 1975.
[9] W. C. Brown and E. E. Eves, "A microwave beam power transfer and guidance system for use in an orbital astronomy support facility," Final Report (Phase II) to NASA, NAS-8-25374, Sept. 1972.
[10] G. P. Boyakhchyan *et al.*, "Analytical calculation of a high-efficiency microwave rectifier employing a Schottky-barrier diode," *Telecom. Radio Engin.* (English Translation of Elaktrosvyaz, and Radiotekhnika) vol. 37-38, no. 10, pp. 64–66, Oct. 1983.
[11] W. C. Brown, "All electronic propulsion key to future space ship design," presented at *AIAA/ASME/SAE/ASEE 24th Joint Propulsion Conf.*, Boston, July 1988.
[12] K. Chang, J. C. McCleary, and M. A. Pollock, "Feasibility study of 35 GHz microwave power transmission in space," *Space Power*, vol. 8, no. 3, pp. 365–370, June 1989.
[13] S. M. Sze, *Physics of Semiconductor Devices*. New York: Wiley, 1981, ch. 2 and 5.
[14] S. M. Wright, "Efficient analysis of infinite microstrip arrays on electrically thick substrate," Ph.D. dissertation, University of Illinois at Urbana-Champaign, 1984.
[15] I. J. Bahl, "Transmission lines," in *Handbook of Microwave and Optical Components*, K. Chang Ed., vol. 1, New York: Wiley, 1989, p. 35.
[16] P. W. Hannan and M. A. Balfour, "Simulation of a phase-array antenna in a waveguide," *IEEE Trans. Antennas Propagat.*, vol. AP-13, pp. 342–353, May 1965.

**Taewhan Yoo** received the B.S. degree in nuclear engineering from Seoul National University at Seoul, Korea in 1981, the M.S. degree in physics from Korea Advanced Institute of Science and Technology at Seoul, Korea in 1983. He is currently working on his doctoral dissertation at Texas A&M University, College Station, on microwave power transmission.

From 1983 to 1988 he was with Electronics and Telecommunication Research Institute at Taejon, Korea. His research area was the development of opto-electronic devices for fiber optic communication. His interests include microwave integrated circuit and its CAD design, wireless communication, and optoelectronic devices.

**Kai Chang** (S'75-M'76-SM'85-F'91) received the B.S.E.E. degree from the National Taiwan University, Taipei, Taiwan, the M.S. degree from the State University of New York at Stony Brook, and the Ph.D. degree from the University of Michigan, Ann Arbor, in 1970, 1972, and 1976, respectively.

From 1972 to 1976, he worked for the Microwave Solid-State Circuits Group, Cooley Electronics Laboratory of the University of Michigan as a Research Assistant. From 1976 to 1978, he was employed by Shared Applications, Inc., Ann Arbor, where he worked in computer simulation of microwave circuits and microwave tubes. From 1978 to 1981, he worked for the Electron Dynamics Division, Hughes Aircraft Company, Torrance, CA, where he was involved in the research and development of millimeter-wave solid-state devices and circuits, power combiners, oscillators and transmitters. From 1981 to 1985, he worked for the TRW Electronics and Defense, Redondo Beach, CA, as a Section Head, developing state-of-the art millimeter-wave integrated circuits and subsystems including mixers, VCO's, transmitters, amplifiers, modulators, upconverters, switches, multipliers, receivers and transceivers. He joined the Electrical Engineering Department of Texas A&M University in August 1985 as an Associate Professor and was promoted to Professor in 1988. In January 1990, he was appointed E-Systems Endowed Professor of Electrical Engineering. His current interests are in microwave and millimeter-wave devices and circuits, microwave integrated circuits, microwave optical interactions, and antennas.

He served as the Editor of the four-volume *Handbook of Microwave and Optical Components*, published by John Wiley & Sons, Inc. in 1989 and 1990. He is the Editor of the *Microwave and Optical Technology Letters* and the *Wiley Book Series in Microwave and Optical Engineering*. He has published over 150 technical papers and several book chapters in the areas of microwave and millimeter-wave devices and circuits. Dr. Chang received the Special Achievement Award from TRW in 1984, the Halliburton Professor Award in 1988 and the Distinguished Teaching Award in 1989 from the Texas A&M University.

# Electronically Switchable and Tunable Coplanar Waveguide–Slotline Band-Pass Filters

Yong-Hui Shu, Julio A. Navarro, and Kai Chang, *Fellow, IEEE*

*Abstract*—A novel coplanar waveguide (CPW) slotline band-pass filter has been developed. The circuit allows planar integration of active and passive semiconductor devices both in series and in shunt. To test the filter, a new microstrip to slotline transition was designed and two of these transitions exhibited an insertion loss of less than 1.0 dB over the 2.0 to 4.0 GHz range. A three-section CPW–slotline band-pass filter demonstrated an insertion loss of less than 0.2 dB over the passband centered at 2.9 GHz. A three-section CPW–slotline switchable band-pass filter integrated with three p-i-n diodes was developed with a 0.7 dB insertion loss in the passband when the p-i-n diodes are OFF and 25.0 dB isolation across the entire band when the p-i-n diodes are ON. A three-section CPW–slotline varactor-tunable filter integrated with three varactor diodes was demonstrated with a 2.0 dB insertion loss and over 20% electronic tuning range. Simple transmission line circuit models were used to optimize the design.

## I. Introduction

THERE is an increasing demand to use microwave and millimeter-wave hybrid and monolithic integrated circuits for many system applications. Because of their planar nature, these circuits offer cost, weight, reliability, and reproducibility advantages when combined with photolithographic techniques. Microstrip has been the main transmission line used in microwave circuit design, partly because of the vast amount of design information available. Although semiconductor devices can be readily integrated in series, shunt devices must be mounted by drilling through the substrate. Drilling adds cost and discontinuities which make the design more difficult and degrade the performance, especially at millimeter-wave frequencies. Furthermore, the microstrip impedance and guided-wavelength characteristics are very sensitive to substrate thickness, which further increases design problems at higher frequencies.

Coplanar waveguide (CPW) is an alternative transmission line that is truly planar and allows easy series and shunt device mounting. CPW is not very sensitive to substrate thickness and allows a wide range of impedance values on relatively thick substrates. The radiation loss in the CPW odd mode is low for an open transmission line. These characteristics make CPW important for millimeter-wave circuits and have aroused considerable interest in microwave and millimeter-wave integrated circuit design [1]–[3]. Although several papers [4]–[6] analyze the characteristics and advantages of CPW, there are only a limited number of CPW components available for circuit design. These components include directional couplers [6]–[7], mixers [8], [9], diplexers [10], [11], and end-coupled resonant CPW filters [12]. This paper describes the integration of microstrip, slotline, and CPW to create a novel CPW slotline band-pass filter and a new microstrip-to-slotline transition.

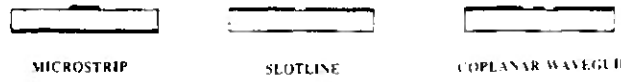


Fig. 1. Cross-sectional view of microstrip line, slotline, and coplanar waveguide.

Fig. 1 shows a cross-sectional view of each of these transmission lines. The filter uses CPW resonators interconnected via slotline. The filter is planar and allows easy series and shunt device mounting. Transmission line models were developed to design the filters. To test the filters, a new microstrip-to-slotline transition was developed. This transition is unique and differs from previous transitions [3] due to the advantage of providing dc blocks required for device biasing and low-pass filters to reduce the transition loss.

A pair of microstrip-to-slotline transitions was developed with a 1.0 dB loss throughout the 2.0 to 4.0 GHz band. A three-section CPW–slotline filter was developed with less than 0.2 dB insertion loss in the passband and over 30.0 dB isolation in the stopbands. Integrating three p-i-n diodes in the three-section filter created a switchable filter. When the p-i-n diodes were reversed-biased, the switchable filter exhibited a 0.7 dB insertion loss in the passband and over 30.0 dB in the stop bands. When the p-i-n diodes were forward-biased, the switchable filter exhibited over 25.0 dB insertion loss. Integrating three varactor diodes in the three-section filter created a tunable band-pass filter. The varactor-tunable filter exhibited a 20% electronic tuning range with 2.0 dB insertion loss in the passband and over 20.0 dB isolation in the stopbands.

The circuit design was based on simple transmission line models. The insertion loss of the microstrip, slotline, and CPW was included. The discontinuity effects between the slotline and coplanar resonator were not included. The parasitics of the devices were obtained from the vendor catalog,

Manuscript received June 12, 1990; revised October 3, 1990. This work was supported in part by the U.S. Army Research Office and the Texas Higher Education Coordinating Board's Advanced Technology Program.

Y.-H. Shu was with the Department of Electrical Engineering, Texas A&M University, College Station, TX. He is now with the Epsilon Lambda Electronics Corporation, Geneva, IL 60134.

J. A. Navarro and K. Chang are with the Department of Electrical Engineering, Texas A&M University, College Station, TX 77843-3128.

IEEE Log Number 9041958.

0018-9480/91/0300-0548$01.00 ©1991 IEEE

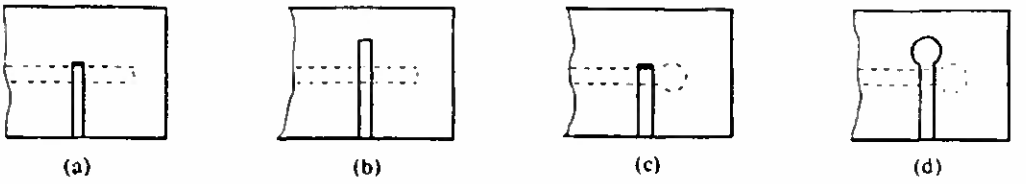


Fig. 2. Different microstrip-to-slotline transitions. (Solid line: microstrip line. Dashed line: slotline.) (a) Soldered microstrip short and uniform $\lambda/4$ slotline. (b) Virtual short with uniform $\lambda/4$ open microstrip and uniform $\lambda/4$ slotline. (c) Soldered microstrip short and slotline open circuit through nonuniform circular slotline. (d) Virtual short with nonuniform circular microstrip and slotline open circuit through nonuniform circular slotline.

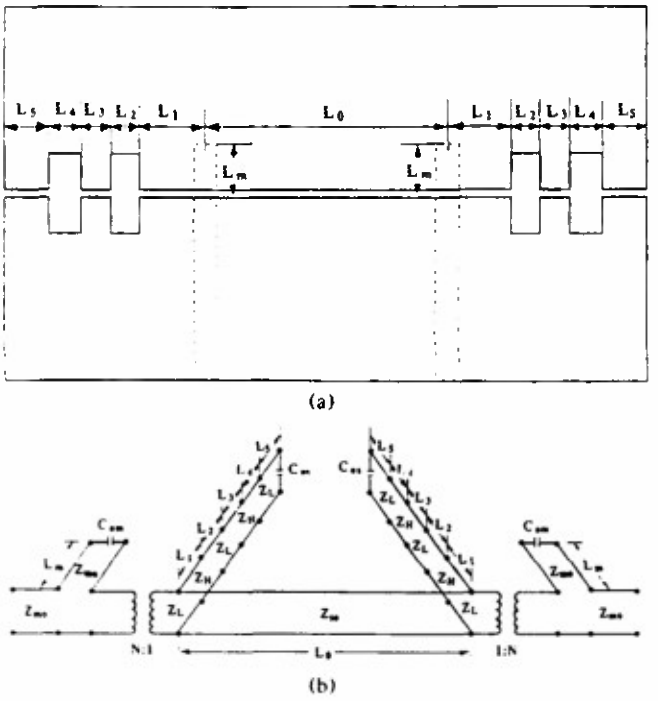


Fig. 3. The novel microstrip-to-slotline transition: (a) configuration; (b) equivalent circuit.

which gives typical values only. Even with these uncertainties, the analysis did predict the performance of the transitions and filters. Better agreement between theory and experiment could be achieved with more accurate information and analysis.

These new filters offer low passband insertion loss and high stopband isolation. The theoretical and experimental results agree well. These filters are amenable to monolithic implementation. The circuit configurations should have many applications in microwave and millimeter-wave systems.

## II. Microstrip-to-Slotline Transition

Low-loss, wide-band microstrip-to-slotline transitions have been reported in the literature. Schuppert [13] reviews the different transitions shown in Fig. 2. These transitions offer good performance and are widely used for circuit design. Owing to the requirements of device biasing, we developed a new microstrip-to-slotline transition which incorporates a dc block and a slotline low-pass filter for an RF choke.

Fig. 3(a) shows the microstrip-to-slotline transition circuit. The circuit consists of two microstrip-to-slotline transitions, two slotline low-pass filters, and two dc blocks for device biasing. Fig. 3(b) shows the equivalent circuit for the transition. $C_{om}$ and $C_{os}$ represent the open circuit capacitance for microstrip and slotline, respectively. The transmission line characteristic impedance of microstrip and slotline are defined by $Z_{m0}$ and $Z_{s0}$, respectively. $Z_{m0}$ is equal to 50 $\Omega$ while $Z_{s0}$ is equal to 60 $\Omega$, respectively. $Z_L$ and $Z_H$ are the low and high impedance values used in the slotline low-pass filter design, respectively. The transformer ratio, $N$, is reported by [14] to be

$$N = \frac{V(h)}{V_0} \tag{1}$$

where

$$V(h) = -\int_{-b/2}^{b/2} E_y(h)\, dy \tag{2}$$

where $h$ is the thickness of the substrate, $b/2$ is the length of the microstrip feed to the slotline, $V_0$ is the voltage across the slot, and $E_y(h)$ is the electric field of the slotline on the dielectric surface on the opposite side. From Cohn's analysis [15],

$$E_y(h) = -\frac{V_0}{b}\left(\cos\left(\frac{2\pi U}{\lambda_0}h\right) - \cot(q_0)\sin\left(\frac{2\pi U}{\lambda_0}h\right)\right) \tag{3}$$

where

$$q_0 = \frac{2\pi U}{\lambda_0}h + \arctan\left(\frac{U}{V}\right) \tag{4}$$

$$U = \sqrt{\epsilon_r - \left(\frac{\lambda_0}{\lambda_{gs}}\right)^2} \tag{5}$$

$$V = \sqrt{\left(\frac{\lambda_0}{\lambda_{gs}}\right)^2 - 1} \tag{6}$$

where $\lambda_{gs}$ is the guided wavelength of the slotline.

A computer program based on the equivalent circuit of Fig. 3(b) was developed and used to analyze and optimize the transition's performance. The lengths of the microstrip open stubs ($L_m$), each section of the slotline low-pass filter ($L_1, L_2, L_3, L_4, L_5$) and interconnecting slotlines ($L_0$) were optimized at fixed characteristic impedance values for the required reflection ($S_{11}$) and insertion ($S_{21}$) characteristics. The program was optimized for maximum insertion loss ($S_{21}$) of $-0.5$ dB with a minimum return loss ($S_{11}$) of $-20$ dB throughout the 2.0 to 4.0 GHz range. Closed-form equations for microstrip [16], [17] and slotline [18] transmission lines were used to analyze the circuit parameters. The transitions were fabricated on a 50-mil-thick RT-Duroid 6010.5 sub-

TABLE I
OPTIMIZED LENGTHS OF TRANSMISSION LINES OF MICROSTRIP-TO-SLOTLINE TRANSITION SHOWN IN FIG. 3(a)
$Z_H = 245\ \Omega$, $Z_L = 60\ \Omega$, $Z_{m0} = 50\ \Omega$, $Z_{s0} = 60\ \Omega$

| Variable | $L_0$ | $L_1$ | $L_2$ | $L_3$ | $L_4$ | $L_5$ | $L_m$ |
|---|---|---|---|---|---|---|---|
| mm | 26.70 | 4.90 | 0.90 | 0.76 | 2.53 | 15.90 | 9.70 |

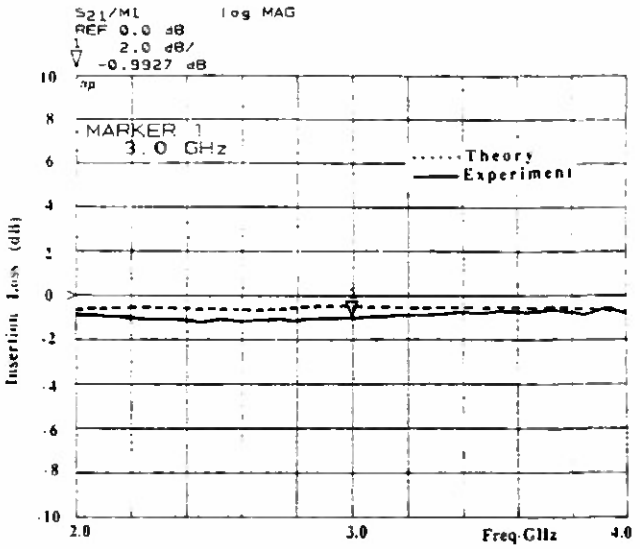


Fig. 4. Theoretical and experimental insertion loss of the transition.

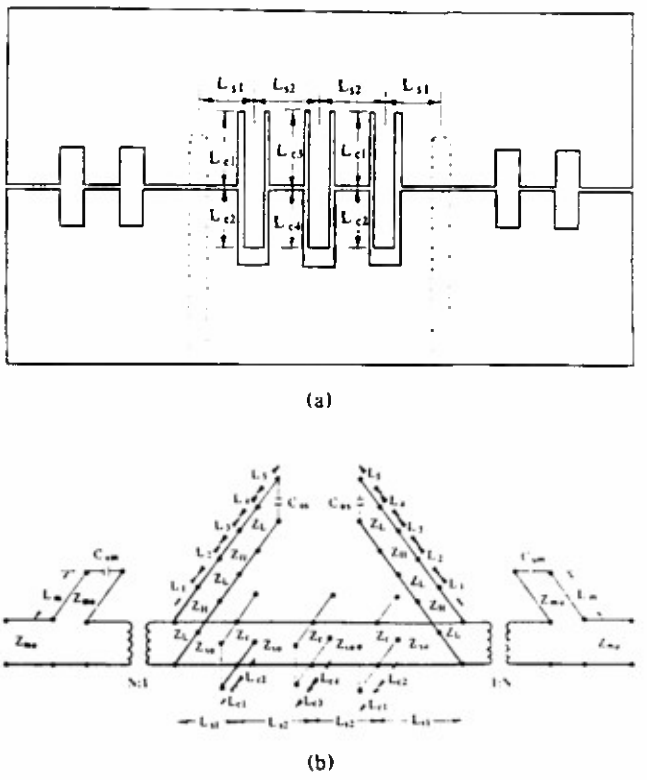


Fig. 5. The novel CPW–slotline band-pass filter: (a) configuration; (b) equivalent circuit.

strate and the $S$ parameters were tested using standard SMA connectors with an HP-8510 network analyzer. Table I lists the optimized circuit dimensions and Fig. 4 shows the theoretical and experimental insertion loss of the transitions, respectively. The experimental insertion loss of two transitions is less than 1.0 dB in the 2.0 to 4.0 GHz frequency range. This loss performance is considered very good since it includes two coaxial-to-microstrip transitions, two microstrip-to-slotline transitions, and a 26 mm length of slotline. Overall, the theoretical and experimental results agree well. This circuit was used to test the CPW–slotline filters.

## III. THE CPW–SLOTLINE BAND-PASS FILTERS

Fig. 1 shows a cross-sectional view of the CPW transmission line. CPW allows the easy integration of series and shunt devices on a planar transmission line. Previous CPW band-pass filters [1] used end-coupled resonators. Although these circuits show good performance, device mounting and biasing are difficult to incorporate. This section describes the use of CPW resonators coupled via slotlines to create a new CPW–slotline band-pass filter.

The most basic design element of a band-pass filter is the resonator. Resonators can be designed with a combination of open and short terminations. Because of the ease of device integration, our filter uses CPW resonators with an open and a shorted end interconnected via slotline. Fig. 5 shows the novel CPW–slotline band-pass filter configuration and its equivalent circuit. The microstrip-to-slotline transition is used to test the filter. The insertion loss through a pair of transitions is about 1.0 dB across the 2.0 to 4.0 GHz range, as described in Section II.

TABLE II
OPTIMIZED LINE LENGTHS OF CPW–SLOTLINE BAND-PASS FILTER SHOWN IN FIG. 5
$Z_H = 245\ \Omega$, $Z_L = 60\ \Omega$, $Z_{m0} = 50\ \Omega$, $Z_{s0} = 60\ \Omega$, $Z_c = 50\ \Omega$

| Variable | $L_{c1}$ | $L_{c2}$ | $L_{c3}$ | $L_{c4}$ | $L_{s1}$ | $L_{s2}$ |
|---|---|---|---|---|---|---|
| mm | 18.70 | 16.23 | 18.26 | 17.00 | 3.00 | 10.35 |

From the equivalent circuit, a computer model using cascading transmission lines was developed. The model accounts for all open and short termination effects. The model optimized the CPW resonators and interconnecting slotline lengths to achieve at least 30.0 dB insertion loss in the stopbands (2.0–2.5; 3.3–4.0 GHz) and less than 0.2 dB in the passband (2.75–3.05 GHz). The closed-form equations for CPW in [18] were used to analyze the circuit parameters. The characteristic impedances of the CPW resonators and interconnecting slotlines are 50 Ω and 60 Ω, respectively. To minimize optimization variables and form a symmetrical configuration, the lengths of the first and third resonators are equal to each other. The optimization variables $L_{s1}$, $L_{s2}$, $L_{c1}$, $L_{c2}$, $L_{c3}$ and $L_{c4}$ are shown in Fig. 5 and the optimized dimensions are given in Table II.

The filter and transitions were fabricated on a 50-mil-thick RT-Duroid 6010.5 substrate and the $S$ parameters were measured using standard SMA connectors with an HP-8510 network analyzer. Fig. 6 shows the theoretical and experimental insertion loss of the filter with the transitions, respectively. In the passband, the theoretical insertion loss (including transition loss) is around 0.7 dB at a center frequency of 2.9 GHz. The experimental results of the CPW–slotline filter with two microstrip-to-slotline transitions show a center fre-

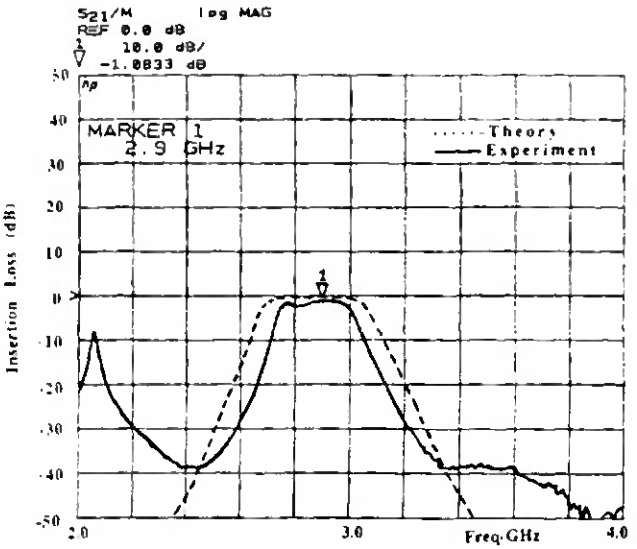


Fig. 6. Theoretical and experimental insertion loss of the novel CPW–slotline band-pass filter.

quency of 2.9 GHz with an insertion loss of less than 1.2 dB. The actual loss due to filter excluding the transition loss is only 0.2 dB. The stopband isolation is greater than 30.0 dB except for a microstrip feedline stub resonance from the transition at 2.1 GHz. The feedline resonance is due to the quarter-wavelength stub ($L_m$ in Fig. 3(a)) resonating at 2.1 GHz. The effect could be eliminated by using a $\frac{1}{4}\lambda$ stub. The stub resonance was verified using the HP-8510 time-domain functions. The filter was isolated to show that the spike at 2.1 GHz was not due to the filter. The theoretical model generally predicts the experimental performance. The design can be easily modified for different frequencies and passband characteristics.

## IV. P-I-N Diode Switchable CPW Slotline Band-Pass Filters

Switchable band-pass filters have many applications in microwave systems. Martin *et al.* [19] integrated p-i-n diodes into a ring resonator to form a switchable ring resonator. This section describes the integration of p-i-n diodes into the planar CPW–slotline filter to create a switchable microwave filter. The p-i-n diodes are mounted over the open end of the CPW resonators. Fig. 7 shows the circuit configuration and equivalent circuit of the three-section, three-diode switchable filter. The p-i-n diode has the equivalent circuit shown in Fig. 8. $R_f$ is the forward-biased series resistance of the diode while $R_r$ is the reversed-biased series resistance. $C_j$ represents the junction capacitance and $L_p$ and $C_p$ represent the package parasitics. $L_s$ accounts for the inductance of the bonding wire to the semiconductor material in the diode. The p-i-n diodes used are M/A COM 47047's with $L_p = 2.0$ nH, $C_p = 0.1$ pF, $L_s = 0.2$ nH, and $C_j = 0.3$ pF at $-50$ V and $R_f = 1.3\ \Omega$ at 100 mA. Although $R_r$ is not quoted, similar reversed-biased devices show a resistance of 2 Ω. These values were used in the computer model analysis and optimization.

In the design procedure, while the p-i-n diodes are reversed-biased (OFF state), the lengths of the resonators and

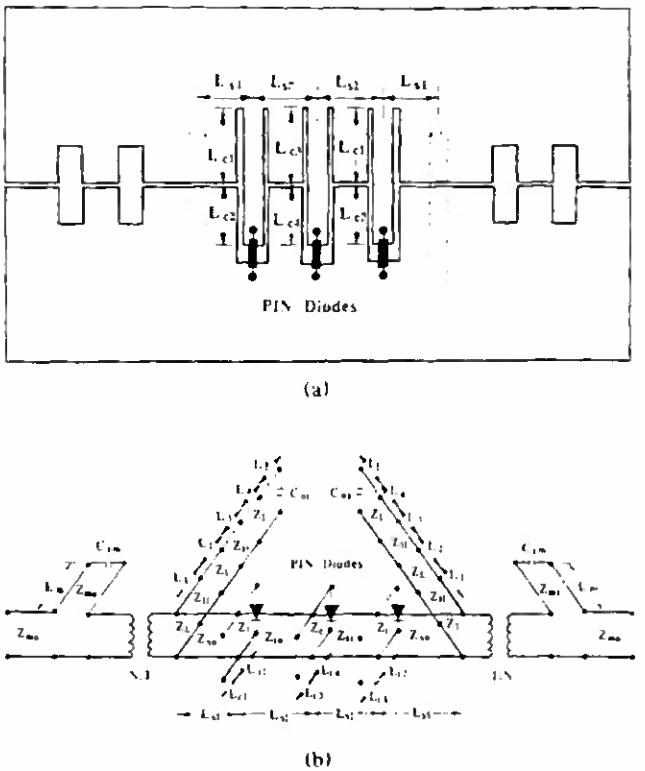


Fig. 7. The p-i-n diode switchable CPW–slotline band-pass filter: (a) configuration; (b) equivalent circuit.

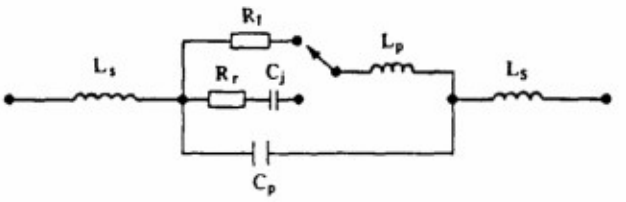


Fig. 8. The equivalent circuit of a p-i-n diode.

TABLE III
Optimized Lengths of the Three-Section, Three-p-i-n Diode Switchable CPW–Slotline Band-Pass Filter Shown in Fig. 7
$Z_H = 245\ \Omega$, $Z_L = 60\ \Omega$, $Z_{m0} = 50\ \Omega$, $Z_{s0} = 60\ \Omega$, $Z_c = 50\ \Omega$

| Variable | $L_{c1}$ | $L_{c2}$ | $L_{c3}$ | $L_{c4}$ | $L_{s1}$ | $L_{s2}$ |
|---|---|---|---|---|---|---|
| mm | 19.99 | 15.45 | 19.93 | 12.19 | 3.18 | 9.23 |

interconnecting lines are optimized to provide low insertion loss in the passband and high rejection in the stopbands. The p-i-n diodes are then forward-biased (ON state) to determine if the circuit meets the isolation specification across the whole band. The circuit was optimized for minimum insertion loss in the passband when the p-i-n diodes are reversed-biased and maximum isolation when the p-i-n diodes are forward-biased.

Table III shows the circuit dimensions for the switchable filter. The switchable filter was fabricated on a 50-mil-thick RT-Duroid 6010.5 substrate and the $S$ parameters were tested using standard SMA connectors with an HP-8510 network analyzer. Fig. 9 shows the theoretical and experi-

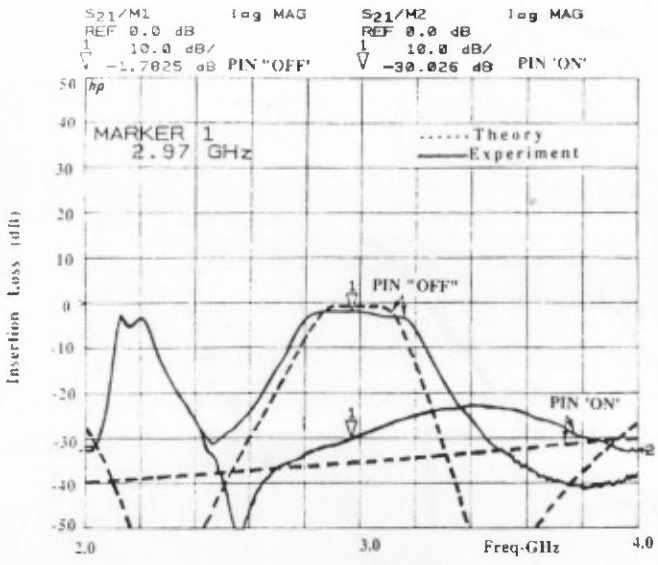


Fig. 9. The theoretical and experimental results of the p-i-n diode switchable band-pass filter.

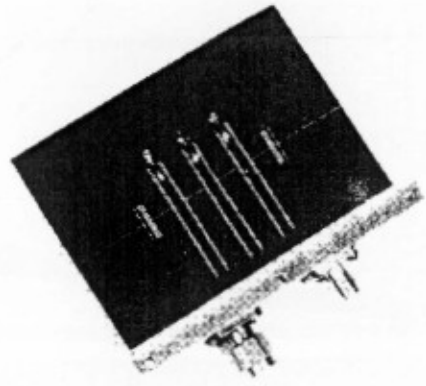

Fig. 10. A photograph of the varactor-tunable CPW–slotline band-pass filter.

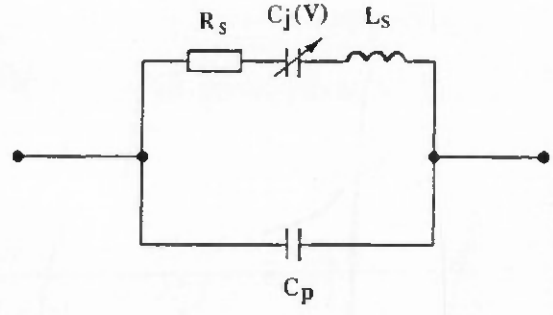


Fig. 11. The equivalent circuit of a varactor diode.

mental results of the switchable filter. From the theoretical results, the center frequency is 3.0 GHz with an insertion loss (including the transition loss) of 1.0 dB when the p-i-n diodes are OFF. When the p-i-n diodes are ON, the isolation is at least 30.0 dB across the 2.0 to 4.0 GHz range. The experimental results indicated an insertion loss of 1.7 dB in the passband and over 25.0 dB isolation except for a spike at 2.1 GHz. The reasons for the spike are explained in Section III. This loss includes the 1.0 dB loss caused by the two transitions; therefore, the actual filter loss is only 0.7 dB.

This planar integrated circuit can be easily assembled at very low cost. The good switching performance has many system applications. Because of the planar nature, this circuit is amenable to monolithic implementation.

## V. Varactor-Tunable CPW–Slotline Band-Pass Filters

Electronically tunable microwave filters have many applications in a wide range of microwave systems which require broad tuning ranges and fast tuning speed. Although YIG-tuned filters offer very wide tuning ranges, they are limited in tuning speed. Varactors can provide wide tuning ranges with high tuning speed for frequency agile systems. Hunter and Rhodes [20] have developed varactor-tunable combline filters, while Makimoto and Sagawa [21] have developed varactor-tunable microstrip ring filters. This section describes the integration of three varactors with the CPW–slotline filter to create a varactor-tunable band-pass filter. The varactors are mounted over the open end of the CPW resonator in the same manner as the p-i-n diodes of the switchable filter. Fig. 10 shows a photograph of the varactor-tunable CPW–slotline filter. The circuit configuration and equivalent circuit are the same as in Fig. 7, except that the p-i-n diodes are replaced by varactor diodes. The varactor equivalent circuit used in the circuit model is shown in Fig. 11. $R_s$ is the series resistance of the diode while $C_p$ represents the package capacitance. $L_s$ accounts for the inductance of the bonding wire to the package. The junction capacitance, $C_j(V)$, varies as a function of bias voltage from 0 to 30 V. The varactor diodes used are from M/A COM (model 46600) with $L_s = 0.2$ nH, $C_p = 0.25$ pF, and $R_s = 8\ \Omega$. $C_j$ varies from 0.5 to 2.5 pF. These approximate values were used to optimize the circuit parameters in the model. The junction capacitance used in the circuit optimization was 1.0 pF. The center frequency for the design optimization was set at 3.0 GHz with a $\pm 200$ MHz bandwidth. The circuit model optimized the passband to less than 1.5 dB insertion loss with more than 30.0 dB isolation in the stopbands.

Table IV shows the optimized circuit dimensions for the varactor-tunable filter. The varactor-tunable filter was fabricated on a 50-mil-thick RT-Duroid 6010.5 substrate. Parts (a) and (b) of Fig. 12 show the theoretical and experimental results of the varactor-tunable filter. The frequency tuning range agrees well but there is a discrepancy in the bandwidth. The theoretical bandwidth increases at the lower end while the experiment shows an increase at the higher end. This discrepancy could be due to the simplified model used in the analysis. The model does not account for discontinuities of the CPW to slotline junctions, the variation of the $Q$ factor of the varactor as a function of voltage, and the variation of the device parasitics.

A tuning bandwidth of 600 MHz was achieved for varactor bias voltages of 0 to 25 V. The maximum insertion loss of 2.15 dB (excluding the 1.0 dB transition loss) occurs at the low-end frequency of 2.7 GHz and decreases to 0.7 dB at the high-end frequency of 3.3 GHz. The passband varies from 250 MHz in the low end to 450 MHz in the high end.

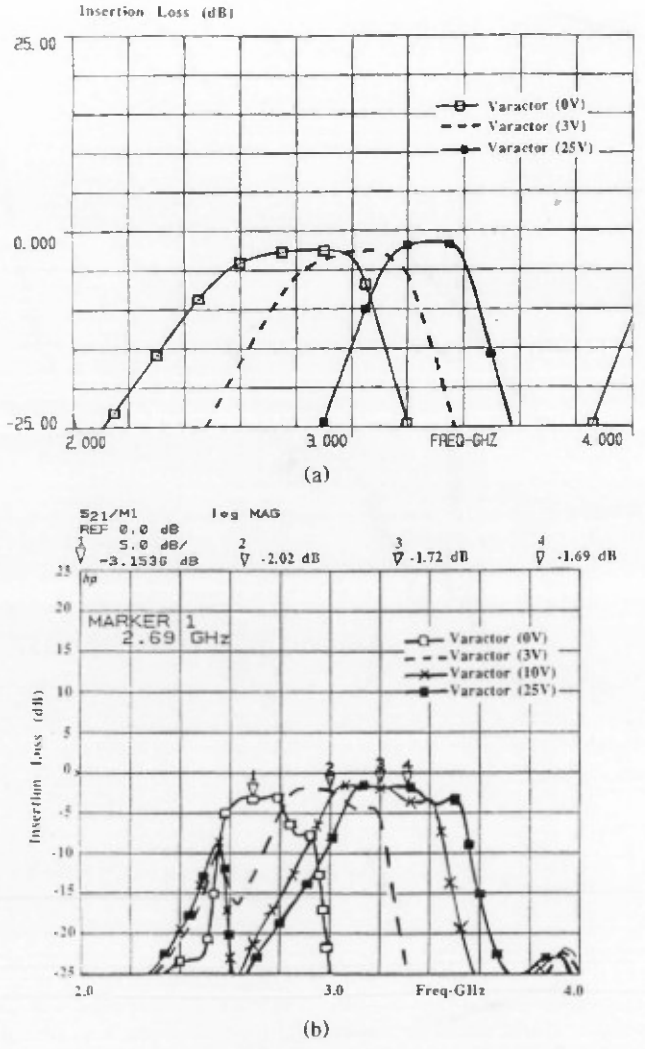


Fig. 12. The varactor-tunable CPW–slotline band-pass filter: (a) theoretical insertion loss; (b) experimental insertion loss.

TABLE IV
OPTIMIZED LENGTHS OF THE VARACTOR-TUNABLE CPW–SLOTLINE BAND-PASS FILTER SHOWN IN FIG. 7 WITH P-I-N DIODES REPLACED BY VARACTOR DIODES
$Z_H = 245\ \Omega$, $Z_L = 60\ \Omega$, $Z_{m0} = 50\ \Omega$, $Z_{s0} = 60\ \Omega$, $Z_c = 50\ \Omega$

| Variable | $L_{c1}$ | $L_{c2}$ | $L_{c3}$ | $L_{c4}$ | $L_{s1}$ | $L_{s2}$ |
|---|---|---|---|---|---|---|
| mm | 19.57 | 8.84 | 19.99 | 8.59 | 3.20 | 9.03 |

Unequal passbands have been reported before for other types of varactor-tuned filters [21].

## VI. CONCLUSIONS

Novel CPW–slotline band-pass filters and microstrip-to-slotline transitions have been developed. Two transitions incorporating dc blocks and three-section slotline low-pass filters were designed to achieve 1.0 dB insertion loss over the 2.0 to 4.0 GHz range. A novel band-pass filter was developed using three coplanar waveguide resonators cascaded by slotlines. The filters were made switchable and tunable by incorporating the p-i-n and varactor diodes in the resonators, respectively. Wide-band switching and tuning were achieved with low insertion loss in the passband and high isolation in the stophands.

A simple CAD model and a computer program have been developed to optimize the various parameters for the required filter design. These circuits offer many advantages, among them low cost, low loss, high isolation, and ease of series and shunt device integration. The filters have many applications in various microwave systems. The circuits are amenable to monolithic circuit integration and can be scaled to the millimeter-wave frequency range.

## ACKNOWLEDGMENT

The authors would like to thank R. C. Waits for his instruction and use of the fabrication facilities.

## REFERENCES

[1] M. Houdart, "Coplanar lines: Application to broadband microwave integrated circuits," in *Proc. Sixth European Microwave Conf.*, 1976, pp. 49–53.
[2] R. A. Pucel, "Design considerations for monolithic microwave circuits," *IEEE Trans. Microwave Theory Tech.*, vol. MTT-29, pp. 513–534, June 1981.
[3] D. R. Chen and D. R. Decker, "MMIC's—The next generation of microwave components," *Microwave J.*, pp. 67–68, May 1980.
[4] Y. Fujiki *et al.*, "Higher-order modes in coplanar-type transmission lines," *Electron. and Commun. Japan*, vol. 58-B, pp. 74–80, 1975.
[5] T. Hatsuda, "Computation of coplanar-type stripline characteristics by relaxation method and its application to microwave circuits," *IEEE Trans. Microwave Theory Tech.*, vol. MTT-23, pp. 795–802, Oct. 1975.
[6] J. B. Knorr and B. Kuchler, "Analysis of coupled slots and coplanar strips on dielectric substrates," *IEEE Trans. Microwave Theory Tech.*, vol. MTT-23, pp. 541–548, July 1975.
[7] C. P. Wen, "Coplanar-waveguide directional couplers," *IEEE Trans. Microwave Theory Tech.*, vol. MTT-18, pp. 318–332, June 1970.
[8] D. F. Williams and S. E. Schwarz, "A planar subharmonically-pumped 71 GHz receiver with integral feed antenna," *Int. J. Infrared and Millimeter Waves*, vol. 7, no. 2, pp. 183–195, 1986.
[9] L. Yuan, J. Paul, and P. Yen, "140 GHz quasi-optical planar mixer," in *IEEE MTT-S Int. Microwave Symp.*, 1982, pp. 374–375.
[10] Y. C. Shih, L. Q. Bui, and T. Itoh, "Millimeter-wave diplexers with printed circuit elements," *IEEE Trans. Microwave Theory Tech.*, vol. MTT-33, pp. 1465–1469, Dec. 1985.
[11] D. F. Williams and S. E. Schwarz, "Design and performance of coplanar waveguide bandpass filters," *IEEE Trans. Microwave Theory Tech.*, vol. MTT-31, pp. 558–566, July 1983.
[12] K. C. Gupta, R. Garg, and I. J. Bahl, *Microstrip Lines and Slotlines*. Dedham, MA: Artech House, 1979, ch. 6.
[13] B. Schuppert, "Microstrip/slotline transitions—Modeling and experimental investigation," *IEEE Trans. Microwave Theory Tech.*, vol. 36, pp. 1272–1282, Aug. 1988.
[14] J. B. Knorr, "Slotline transitions," *IEEE Trans. Microwave Theory Tech.*, vol. MTT-22, pp. 548–554, 1974.
[15] S. B. Cohn, "Slotline field components," *IEEE Trans. Microwave Theory Tech.*, vol. MTT-20, pp. 172–174, 1972.
[16] E. Hammerstad and O. Jensen, "Accurate models for microstrip computer-aided design," in *IEEE MTT-S Int. Microwave Symp. Dig.*, 1980, pp. 407–409.
[17] R. Garg and K. C. Gupta, "Expressions for wavelength and impedance of slotline," *IEEE Trans. Microwave Theory Tech.*, vol. MTT-24, p. 532, 1976.
[18] G. Ghinoe and C. Naldi, "Analytical formulas for coplanar lines in hybrid and monolithic MIC's," *Electron. Lett.*, vol. 20, no. 4, pp. 179–187, 16 Feb. 1984.
[19] T. S. Martin, F. Wang, and K. Chang, "Theoretical and experimental investigation of varactor-tuned switchable microstrip

ring resonator circuits," *IEEE Trans. Microwave Theory Tech.*, vol. 36, pp. 1733–1740, Dec. 1988.
[20] I. C. Hunter and J. D. Rhodes, "Electrically tunable microwave bandpass filters," *IEEE Trans. Microwave Theory Tech.*, vol. MTT-30, pp. 1354–1360, Sept. 1982.
[21] M. Makimoto and M. Sagawa, "Varactor tuned bandpass filters using microstrip-line ring resonators," in *IEEE MTT-S Int. Microwave Symp. Dig.*, 1986, pp. 411–414.

**Yong-Hui Shu** [redacted]. He received the B.S. and M.S. degrees in electrical engineering from the Nanjing Institute of Technology, Nanjing, China in 1982 and 1985, respectively.

From March 1985 to July 1989, he was with the Department of Radio Engineering of Nanjing Institute of Technology (current name, Southeast University) as a Lecturer. From August 1989 to July 1990, he was with the Department of Electrical Engineering of Texas A&M University as a Research Associate. In August 1990, he joined Epsilon Lambda Electronics Corporation, Geneva, IL, as a Microwave Design Engineer. His current interests are in microwave and millimeter-wave devices, circuits, and subsystems.

Mr. Shu has published 20 technical papers in microwave and millimeter-wave areas.

**Julio A. Navarro** [redacted] He received the B.S.E.E. degree from Texas A&M University in May 1988. He has been a cooperative education student with General Dynamics-Fort Worth since May 1985.

He has worked in avionic systems design, advanced technology and systems engineering, field engineering, antenna systems, and radar cross section research. As a master's candidate at Texas A&M University, he has initiated projects involved with active varactor tunable end-fire radiating elements, switchable and tunable CPW filters, and varactor-tuned CPW oscillators (patents pending). He has also developed K- and Ka-band aperture-coupled patch antennas for a NASA-Lewis–Texas Instruments project. He is currently completing the requirements for the M.S.E.E. degree and will pursue Ph.D. studies under the direction of Dr. Kai Chang.

**Kai Chang** (S'75–M'76–SM'85–F'91) received the BSEE degree from the National Taiwan University, Taipei, Taiwan, the MS degree from the State University of New York at Stony Brook, and the PhD degree from the University of Michigan, Ann Arbor, in 1970, 1972, and 1976, respectively.

From 1972 to 1976, he worked for the Microwave Solid-State Circuits Group, Cooley Electronics Laboratory of the University of Michigan as a Research Assistant. From 1976 to 1978, he was with Shared Applications, Inc., Ann Arbor, where he worked on computer simulation of microwave circuits and microwave tubes. From 1978 to 1981, he was with the Electron Dynamics Division, Hughes Aircraft Company, Torrance, CA, where he was involved in the research and development of millimeter-wave solid-state devices and circuits, power combiners, oscillators, and transmitters. From 1981 to 1985, he was with TRW Electronics and Defense, Redondo Beach, CA, as a Section Head developing state-of-the-art millimeter-wave integrated circuits and subsystems including mixers, VCO's, transmitters, amplifiers, modulators, up-converters, switches, multipliers, receivers, and transceivers. He joined the Electrical Engineering Department of Texas A&M University in August 1985 as an Associate Professor and was promoted to Professor in 1988. In January 1990, he was appointed E-Systems Endowed Professor of Electrical Engineering. His current interests are in microwave and millimeter-wave devices and circuits, microwave integrated circuits, microwave optical interactions, and antennas.

Dr. Chang served as the editor of the four-volume *Handbook of Microwave and Optical Components*, published by John Wiley & Sons, Inc., in 1989 and 1990. He is the editor of *Microwave and Optical Technology Letters* and of the Wiley Book Series on Microwave and Optical Engineering. He has published over 100 technical papers and several book chapters in the areas of microwave and millimeter-wave devices and circuits. Dr. Chang received the Special Achievement Award from TRW in 1984, the Halliburton Professor Award in 1988, and the Distinguished Teaching Award in 1989 from the Texas A&M University.

PII Redacted